Combined Linearization of both Analog and Digital Pre-Distortion for Broadband Radio over Fiber Transmission

Xiaoran Xie

A Thesis

in

The Department

of

Electrical and Computer Engineering

Presented in Partial Fulfillment of the Requirements

For the Degree of Master of Applied Science at

Concordia University

Montreal, Quebec, Canada

August, 2017

CONCORDIA UNIVERSITY
SCHOOL OF GRADUATE STUDIES

This is to certify that the thesis prepared

By: Xiaoran Xie

Entitled: Combined Linearization of both Analog and Digital Pre-Distortion for Broadband Radio over Fiber Transmission

and submitted in partial fulfillment of the requirements for the degree of

Master of Applied Science (Electrical and Computer Engineering)

complies with the regulations of this University and meets the accepted standards with respect to originality and quality.

Signed by the final examining committee:

_____ Chair
Dr. R. Raut

_____ External Examiner
Dr. Minyuan Chen

_____ Internal Examiner
Dr. Glenn Cowan

_____ Supervisor
Dr. John Xiupu Zhang

Approved by: _____
Dr. W.E. Lynch, Chair
Department of Electrical and Computer Engineering

_____ 20___ _____
Dr. Amir Asif, Dean,
Faculty of Engineering and Computer Science

ABSTRACT

Combined Linearization of both Analog and Digital Pre-Distortion

for Broadband Radio over Fiber Transmission

Xiaoran Xie

The benefits of rapid wireless communication development are continuously being enjoyed by people all over the world. However, the increasing number of wireless applications leads to surge in demand of spectrum resources which conflicts with the limited band resources. One solution is increasing the available band resources, but a more effective way is improving the utilization of the existing bandwidth. In the Fourth Generation (4G) wireless communication and Wi-Fi standard, the orthogonal frequency division multiplexing (OFDM) technique is introduced. As an OFDM signal is a non-constant envelope signal and usually has a high peak-to-average power ratio (PAPR), it is very sensitive to the distortion caused by the nonlinear response of inline components in transmission systems.

Within a system, the nonlinearity is basically due to two areas. First, RF power amplifier (PA) is a main contributor. For efficient operation, the PA is set to the saturation zone where a high amount of nonlinearity is present. Consequently, the nonlinearity in the power amplifier will be unbearably high. This nonlinearity is called quiescent nonlinearity. Moreover, with the increasing of signal bandwidth and transmission rate, the memory effect may occur. So, in the 4G and 5G wireless system, both phenomenon should be considered.

Second, when radio over fiber (RoF) transmission is incorporated into front-haul transmission systems, it is capable of simplifying the remote radio units (RRU) from complex signal processing, thus potentially cost-effect. However, optical sideband modulation is used in RoF, and nonlinear distortion is induced to the signals. Therefore, RoF is another contributor to high quiescent nonlinearity.

The nonlinearity from RF PA, RoF system, and other devices will cause out-of-band spectral regrowth and in-band distortion. These problems lead to performance degradation. Some techniques to overcome the limitation of the above nonlinearity were proposed such as feed-forward, feed-back, pre-distortion, and post-distortion. Among these techniques, pre-distortion methods have been widely adopted for its flexible and robust mechanism in the modern ultra-wideband communication systems.

Pre-distortion is divided into two branches: Analog Pre-distortion (APD) and Digital Pre-distortion (DPD). The basic idea of APD is using dedicated nonlinearity devices, like a diode or field effect transistor, to generate a certain nonlinearity that can compensate a PA or RoF system. With the APD method, the odd order of intermodulation distortion (IMD) is usually compensated, but APD devices cannot fix the memory effect induced by PA. Different from the APD method, the DPD linearizes a communication system by digital means. With some digital processing methods, DPD is capable of compensating both memory effect and quiescent nonlinearity. However, the baseband DPD cannot suppress out-of-band distortion, while RF DPD requires costly RF detectors and A/D converters with a high sampling rate

In view of the fact that both APD and DPD have their advantages and disadvantages, a new pre-distortion method of combined APD and DPD is proposed. This new method can both suppress the quiescent nonlinearity and memory effect in a transmission system or PA. Here, APD is used to compensate the third order Intermodulation Distortion (IMD3) induced by an RoF system and the DPD is used to suppress the memory effect that mainly comes from the PA, in addition to in-band nonlinear distortion.

The validity of proposed pre-distortion method is proved in both simulation and experiment. In the simulation, an RoF transmission system model is built to induce both quiescent nonlinearity and memory effect. The RoF model is based on measured data. The PA model is an evolved Wiener-Hammerstein model that can induce both long-term and short-term memory effect. The APD circuit is designed and simulated in software Advanced Design System (ADS). In the

simulation, the performance of the proposed pre-distortion method is evaluated by the improvement of Error Vector Magnitude (EVM) and IMD3. After determining the optimal memory depth and optimal RF input power in terms of EVM and IMD3, three cases are considered in the simulation. The first case is a general two-band LTE signal. Two LTE signals located at 800 MHz and 900 MHz pass through the simulation system. It is shown that an average 21.6-dB improvement of EVM, an average 4.6-dB improvement of IMD3, and a 23.8-dB improvement of Adjacent Channel Power Ratio (ACPR) are obtained. In the second case, a two-band LTE signal is located at 800 MHz and 840 MHz. It is shown that a 11.3 dB improvement of EVM, a 9.8 dB improvement of IMD3, and a 9.3 dB improvement of ACPR are achieved. For the third case that is a three-band test, three signals are set to 800 MHz, 850 MHz and 900 MHz. It is shown that a 16.7 dB improvement of EVM, a 21.8 dB improvement of IMD3, and a 18.4 dB improvement of ACPR are got. In the first two cases, 2D-DPD is used as DPD method, and for the third case the RF DPD method is used. The APD circuit used in all three cases is an anti-parallel Schottky diodes based circuit that was designed and fabricated by a former student. The results of the proposed pre-distortion method is compared to traditional DPD-only and APD-only. It is revealed that the proposed pre-distortion method results in higher improvement in EVM, ACPR, and IMD3. This means that the advantages of APD and DPD were combined successfully.

The experiments further verify the advantages of proposed linearization method. Like the simulation, three cases are also considered in experiments. For case one with two-band LTE signal located at 800 MHz and 900 MHz, it is shown that a 11.0 dB improvement of EVM, a 15.0 dB improvement of IMD3, and 19.4 dB improvement of ACPR are obtained. For case two with two-band LTE signal located at 800 MHz and 840 MHz, it is shown that an 8.2 dB improvement of EVM, a 16.8 dB improvement of IMD3, and a 4.6 dB improvement of ACPR are achieved. For case three with three LTE signals at 800 MHz, 850 MHz, and 900 MHz, it is shown that a 10.1 dB improvement in EVM, a 16.9 dB improvement in IMD3, and an 8.6 dB improvement in ACPR are achieved. Moreover, the proposed pre-distortion method leads to better performance in EVM, IMD3, and ACPR than APD-only or DPD-only method.

At the end of the thesis, another evolved 2D-DPD method is proposed based on the mathematical model of combined analog and digital pre-distortion method. The high order nonlinear memory effect is ignored in evolved 2D-DPD. Therefore, the number of coefficients is reduced while the performance remains almost the same. This relationship between the coefficients number and nonlinearity order is discussed. Finally, a simple simulation is done which proves the benefits of evolved 2D-DPD.

ACKNOWLEDGEMENTS

I would like to express my sincere gratitude to my supervisor Dr. John Xiupu Zhang, for his advice, help, and support for me to finish this thesis.

I would like to express my appreciation to my colleague Weijie Tang, for his endless help and advice in the simulation of DPD and experiment setups.

I would like to express my thank Dr. Ran Zhu for his help in usage of APD circuit during his busy working days, hoping that I did not interrupt any important works.

I am also deeply indebted to my colleague Lara A. Juras, who has gone through all the pain to help me review my thesis and made countless marks and comments.

I would like to thank Shuvasish Saha for his support in APD setups.

I would like to thank Hao Sun and Peijia Yan for their assistance in the lab.

I would like to thank my parents, Zhengyuan Gao and Shiwei Xie, for their infinitive love and support during my study in Canada. I also want to thank my grandmother, Shumin Jin, for her encourage during my research.

Table of Contents

List of Figures

List of Tables

List of Acronyms

ACPR	Adjacent Channel Power Ratio
ADC	Analog-to-Digital Converter
AMPS	Advanced Mobile Phone System
APD	Analog Pre-distortion
ASK	Amplitude Shift Keying
AWG	Arbitrary Waveform Generator
BBU	Baseband Unit
CDMA	Code Division Multiple Access
CPU	Central Processing Unit
CWDM	Coarse Wavelength-Division Multiplexing
D-AMPS	Digital AMPS
DBR	Distributed Bragg Reflector
DDR	Dynamic Deviation Reduction
DFB	Distributed-Feedback
DPD	Digital Pre-distortion
DSP	Digital Signal Processor
DWDM	Dense Wavelength-Division Multiplexing
DWL	Dual-Wavelength Linearization
EAM	Electro-Absorption Modulator
ET	Envelope Tracking
EVM	Error Vector Magnitude

FFT	Fast Fourier Transform
FIR	Finite Impulse Response filter
FPGA	Field-Programmable Gate Array
FSK	Frequency Shift Keying
FWM	Four-Wave Mixing
GaAs	Gallium Arsenide
GaN	Gallium Nitride
GMP	Generalized Memory Polynomial
GMSK	Gaussian Minimum Shift Keying
GSM	Global System for Mobile Communications
iFFT	Inverse Fast Fourier Transform
IFWM	Intra-channel Four-Wave Mixing
IIR	Infinite Impulse Response filter
IMD2	2nd Order Intermodulation Distortion
IMD3	3rd Order Intermodulation Distortion
IMD5	5th Order Intermodulation Distortion
IXPM	Intra-channel Cross-Phase Modulation
LDMOS	Laterally Diffused Metal Oxide Semiconductor
LNA	Low-Noise Amplifier
LS	Least Squares
LSM	Least Squared Method
LTE	Long-Term Evolution
LTE-A	Long-Term Evolution Advanced

MCF	Multi-Core Fiber
MDM	Mode-Division Multiplexing
MIMO	Multiple-Input and Multiple-Output
MMF	Multi-Mode Fiber
MP	Memory Polynomial
MSE	Mean Squared Error
MSTO	Mobile Switching Telephone Office
MZM	Mach-Zehnder Modulator
OFDMA	Orthogonal Frequency-Division Multiple Access
ORx	Optical Receiver
OTN	Optical Transport Network
OTx	Optical Transmitter
PD	Photodetector
PSK	Phase Shift Keying
QAM	Quadrature Amplitude Modulation
QPSK	Quadrature Phase Shift Keying
RAN	Radio Access Network
RF	Radio Frequency
RoF	Radio-over-Fiber
RRH	Remote Radio Head
RRU	Remote Radio Unit
SC-FDMA	Single-Carrier Frequency-Division Multiple Access
SFDR	Spur-Free Dynamic Range

SLM	Single-Longitudinal-Mode
SMF	Single Mode Fiber
SOA	Semiconductor Optical Amplifier
SPM	Self-Phase Modulation
SSPA	Solid-State Power Amplifier
TD-CDMA	Time-Division Code-Division Multiple Access
TDMA	Time-Division Multiple Access
TD-SCDMA	Time-Division Synchronous Code-Division Multiple Access
W-CDMA	Wideband Code-Division Multiple Access
WPD	Wilkinson Power Divider
XPM	Cross-Phase Modulation

Chapter 1 Introduction

1.1 The History of Wireless Communication

Ever since 1895, when a young college student, Guglielmo Marconi, conducted the first wireless communication experiment in the backyard, wireless communication has gone through 122 years of history. Engineer moved all the wired service, like telegraph, radio, telephone and television, into wireless means. Among them, the 'wireless telephone' or mobile phone brought greatest changes to human society. Back to 1980's, many cellular systems were launched. Among them, Bell Labs launched the most famous mobile phone system, Advanced Mobile Phone System (AMPS). AMPS is an analog wireless system with a low band utilization rate and transmission rate. As AMPS is a virtual circuit switching network, only voice service is supported. In addition, according to the signaling system used in AMPS, roaming service is not supported [1].

1990s is the decade of Internet. The internet has undergone an explosive development. Naturally, people hope to access to Internet with their cell phones. But an analog system could not afford such a high transmission rate. Therefore, the Second-Generation (2G) mobile system was established. Many standards were adopted in 2G, such as Global System for Mobile Communication (GSM), IS-95 and Digital AMPS (D-AMPS). All these 2G standards used digital communication technologies. Several advanced digital modulation methods are used in these systems, like Quadrature Phase Shift Keying (QPSK), π/4-QPSK, and n-QAM etc. The multiplexing methods like Time Division Multiple Access (TDMA) and Code Division Multiple Access (CDMA) were also employed in the 2G system. In GSM networks, the Internet service is not supported initially. The Internet service is provided by General Packet Radio Service (GPRS), an evolution of GSM. So, in most of the GSM systems, voice and Internet data transmitted in different ways. On the other hand, IS-95 supported both data and voice in the same structure. Therefore, Third Generation (3G) mobile system is mostly based on CDMA method used in IS-

95. [1]

The 3G mobile system has changed everything. Several advanced CDMA based multiplexing techniques are used in 3G communications. According to IMT-2000 standard published in 2000, CDMA2000, WCDMA and, TD-SCDMA were established as international standards by International Telecommunication Union (ITU) [2]. The transfer rate is increased from 64 Kbps in 2G to 2 Mbps in 3G, which makes the broadband service possible. Besides, the All-IP network is also proposed and tested in the 3G system, which means that both voice service and Internet data service are transmitted following package switching in IP networks. Therefore, the network architecture is simplified while the transmission rate is further increased.

Human has infinite desire in high speed Internet access, and soon people are not satisfied with 3G networks for its low speed. So, the Fourth Generation (4G) standard is proposed, which is called Long-Term Evolution (LTE). In LTE standard, the improvement happens in two domains. First, the band utilization rate is further increased by Orthogonal Frequency-Division Multiple (OFDM) access and Single-Carrier Frequency-Division Multiple Access (SC-FDMA) in the air interface. Second, the network structure of 4G standard is totally changed. In Figure 1-1, it is shown that the whole system uses a single gateway SGi to communicate with IP Network. Compared with the traditional 2G/3G structure which needs three gateways. One is for signaling system for controlling, one is for circuit switching system for voice service, and the other is for packet switch system for data service. 4G structure significantly simplified the whole system. All these improvements increase the transmission rate of 4G standard.

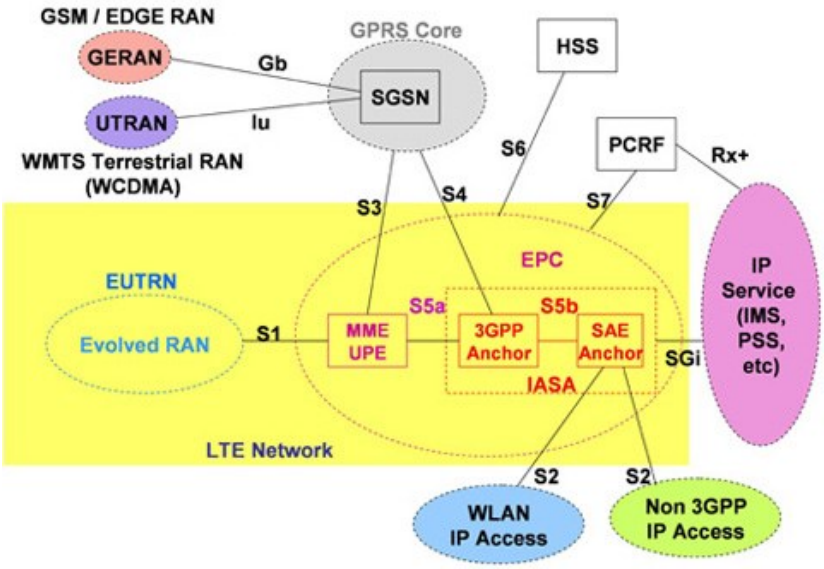

Figure 1-1 The structure of LTE network [3]

However, the LTE standard is not a 'real' 4G system as its transmission rate cannot meet what is claimed in IMT-Advanced standard. With the help of Multiple-input and Multiple-output (MIMO) technique, the LTE standard can achieve a 299.6 Mbps (64QAM, 20 MHz, 4*4 MIMO) transmission rate. But this is still too low for a 4G system. So, a new technique named additional carrier aggregation is proposed, which can support almost 3.3 Gbps peak download rate (128 QAM, 100 MHz, 8*8 MIMO).

Nowadays Fifth Generation (5G) standard is already in sight. In the new standard, the wireless band utilization rate will be further increased. The structure of the core system will be flatter, smarter, and plainer than ever before. Therefore a 100 Gbps download rate should be achieved.

Table 1-1 shows the comparison of different mobile communication standards. It is found that the transmission rate is increasing.

Table 1-1 Definitions of Parameter of the mobile communication generations

Feature	1G	2G	3G	4G	5G
Developed In	1980	1990	2001	2010	~2020
Spectral Located	900MHz	1800MHz	2100MHz	2600MHz	2.4~90GHz
Rate	2 Kbps	64 Kbps	2 Mbps	1 Gbps	100 Gbps
Standard	AMPS	GSM IS-95	W-CDMA TD-SCDMA CDMA2000	LTE-A	To Be Defined

1.2 Radio-over-Fiber System

First developed for analog applications, Radio-over-Fiber (RoF) system was proposed by A. J. Cooper in 1990 [4]. In an RoF system, the modulated signal is transmitted directly in the optical fiber. The base station will receive a modulated signal from the RoF link and then feed the signal into the antenna directly. Therefore, the procedures like up-conversion, down-conversion, modulation and demodulation can be done in Central Processing Unit (CPU), instead of Baseband Unit (BBU) and Remote Radio Head (RRH) at each base station [5]. Just like Figure 1-2 shows, a centralized CPU replaced dispersed remote processing unit. Therefore, the complexity of each base station is reduced. The only work that base stations should do is to receive the modulated optical signal and feed it to antenna. This will greatly reduce the cost of infrastructure construction in each base station.

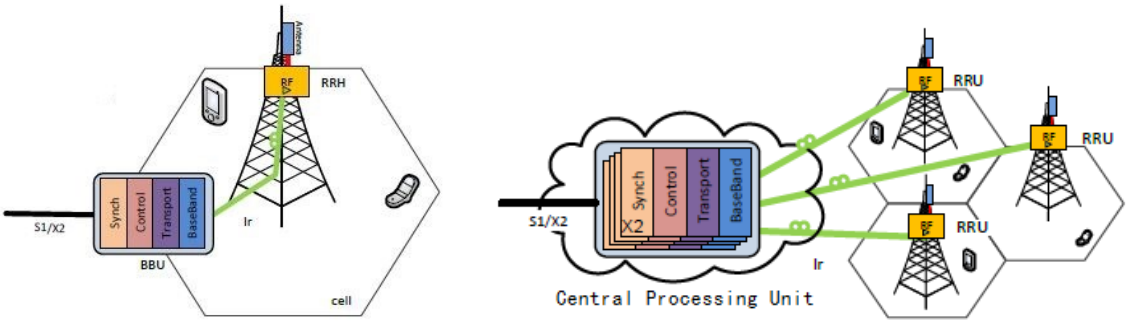

Figure 1-2 Traditional architecture (a) and RoF transmission architecture (b)

Figure 1-3 shows the detail of an RoF system. The signal is processed in a CPU. After the original signal is modulated and up-converted to a proper RF frequency. The RF signal is transmit to Optical Transmitter (OTx). The OTx will modulate the RF signal into optical signal. In the OTx, the signal can be either direct or external modulated. For direct modulation, the output optical signal is directly changed by the driving current of the laser. For external modulation, either Electro-Absorption modulator (EAM) or Mach-Zehnder modulator (MZM) is adopted following a continuous wave (CW) laser. A higher modulation bandwidth can be achieved using an external modulator, while direct modulation has a simple structure. After transmitted through optical fiber, the signal is received by Optical Receiver (ORx). The receiver demodulates the optical signal back to RF signal. This RF signal is amplified by an RF power amplifier (PA) and fed into antennas. A reverse process is applied to uplink.

RoF system has many advantages. Firstly, RoF system centralizes the whole communication system. With all the signal processing units centralized, the complexity of remote base stations is reduced, which leads to a lower power consumption and lower maintenance cost in commercial applications. Besides, the price of traditional coaxial cable itself is much more expensive than optical fiber. And the optical fiber has small dimensional size which occupies less space.

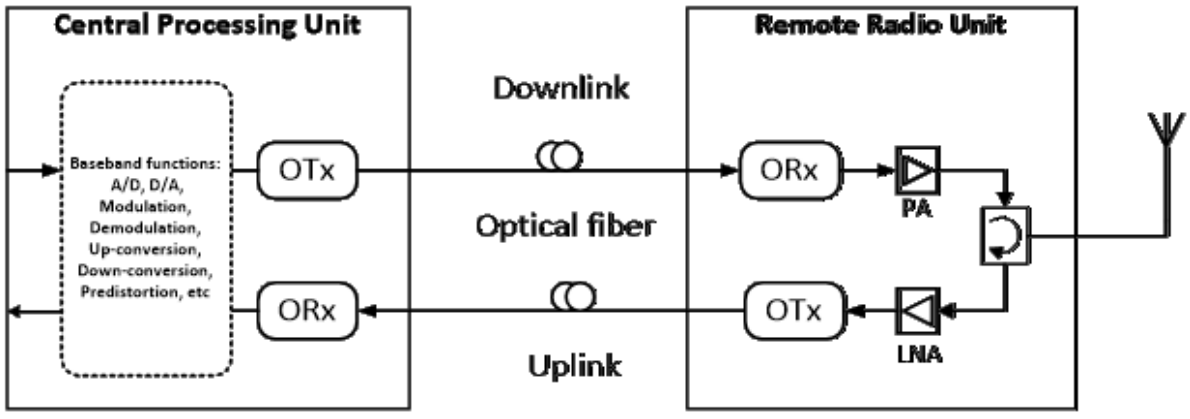

Figure 1-3 Schematic of an RoF link

Secondly, as a basic property of optical fiber, the attenuation loss of optical fiber is lower

than traditional coaxial cable. The attenuation loss of a widely used single mode fiber (SMF) is below 0.2 dB/km at 1550 nm and 0.4 dB/km at 1310nm [6]. For medium-distance transmission between CPU and RRU, the coaxial cable will induce huge attenuation loss, which needs several RF amplifiers, and leads to higher power consumption. As the attenuation loss of optical fiber is considerably low, the centralization of signal processing can only be achieved with the help of RoF systems.

Thirdly, optical fiber can support ultra-wideband signal. The bandwidth of a standard SMF can be several THz, while the coaxial cable can only support several GHz. Only one SMF can transmit all the signals for MIMO system in 5G mobile systems. Instead, much more coaxial cables are required to support the same bandwidth.

Furthermore, the RoF system can well support Software Defined Radio (SDR) devices. The ordinary digital communication systems need a complex controlling component at each base station for SDR. But for RoF system, simply changing some settings at CPU results in the same goal.

In the future, even CPUs may not be needed anymore, and all the processing can be done at local exchanges. As the All-IP networks have been well developed, all the gateways or signaling systems can be virtualized and centralized. With the help of some state-of-art networking techniques like Software Defined Network (SDN), a flexible, simple, flat, and fusion wireless communication network may be achieved.

However, besides all these great advantages, RoF system has a major disadvantage. As RoF systems are an analog communication links, it is very sensitive to distortion caused by nonlinearity. Compared with traditional coaxial cable links, RoF systems contain much more nonlinearity devices. All the TOx, SMF, ROx, and PA may generate nonlinear distortion. Therefore, linearization techniques are highly required to compensate for nonlinear distortion in an RoF transmission system.

1.3 Motivation and Contribution

Two main factors are used to measure the nonlinear distortion. They are Error Vector Magnitude (EVM) and Adjacent Channel Power Ratio (ACPR). A high EVM may cause the received signal totally unreadable, while a high ACPR may interfere signals located nearby. What is more, if the RoF system transmits more than one signal simultaneously, Third Order Intermodulation Distortion (IMD3) and Fifth Order Intermodulation Distortion (IMD5) may be generated. Both IMD3 and IMD5 may interfere the signal nearby.

There are several methods of linearization [7]. Besides those out-of-date methods like feed-forward and feed-backward, the other methods can be divided into two major groups. First is optical method. The second is electrical method. In this thesis, the electrical domain linearization is only considered. The electrical methods can also be divided into two branches, analog pre-distortion (APD) and digital pre-distortion (DPD). Each of them has its own advantages and disadvantages. APD can be used to reduce out-of-band distortion like IMD3 and IMD5. The power efficiency of APD is much better than that of DPD. Moreover, the APD circuits are much simpler and smaller than the DPD. But the APD has some disadvantages. Although the APD can be used to improve the EVM and ACPR, the improvement is unbearably low. In addition, the APD cannot be used for suppressing the impact of memory effect, which is the main cause of the EVM degradation. On the other hand, DPD can be used to suppress in-band distortion, and the improvement of EVM and ACPR by using the DPD is significantly high. The DPD has two categories: baseband DPD and RF DPD. A baseband DPD like 2D-DPD cannot be used to suppress the out-of-band distortion like IMD3 and IMD5. RF DPD can be used to reduce the IMD3 and IMD5, however, it requires a high sampling rate detector and A/D convertor.

In this thesis, a new pre-distortion (PD) method which is called combined linearization of both analog and digital pre-distortion for broadband radio over fiber transmission is proposed, analyzed, and demonstrated. For this combined APD and DPD method, the APD circuit is used to compensate for the out-of-band and in-band nonlinearity and the DPD is used to compensate for

the memory effect and in-band distortion. The proposed linearization method can improve the IMD3, EVM, and ACPR simultaneously. Two-band and three-band simulations and experiments show and demonstrate the improvements in EVM, ACPR, and IMD3.

1.4 Thesis Outline

The rest of the thesis is organized as follows:

Chapter 2 is the literature review about the details of RoF system, nonlinearity theory, and linearization techniques.

Chapter 3 gives the theoretical analysis of the proposed linearization technique and demonstrates how APD and DPD work together. Nonlinearity models used in analyze and simulation is introduced. Both APD and DPD is discussed in detail. Then, a mathematical model is established to describe the proposed linearization technique. The advantages of proposed linearization technique are proved mathematically.

Chapter 4 contains the simulation of the proposed linearization method. It is built with MATLAB and Advanced Design System (ADS). The detail of the simulation procedure is given. In the simulation, the optimal memory depth is found. Two-band and three-band tests have been run to evaluate the performance of the proposed linearization method. In the first case, two 20 MHz LTE signals are located at 800 MHz and 900 MHz. In the second case, two 20 MHz LTE signals are located at 800 MHz and 840 MHz, very close to each other. In the three-band test case, three 20 MHz LTE signals are located at 800 MHz, 850 MHz and 900 MHz. In the first and second cases, 2D-DPD is applied. In the third case, RF DPD is adopted as 2D-DPD can only process two-band signal. Comparisons has been made between the proposed combined linearization model and conventional DPD-only or APD-only model. Simulation results show that the proposed linearization is capable of suppressing with in-band, out-of-band quiescent nonlinearities, and memory effects of the RoF transmission system simultaneously.

Chapter 5 present the experiment setup and procedures. Optimal memory depth and RF input power of the proposed linearization model applied in the real RoF link have been decided by experiments. Two-band and three-band tests have been conducted to evaluate the performance of the proposed linearization method in the real RoF link. In the first case, two 20 MHz LTE signals are located at 800 MHz and 900 MHz. In the second case, two 20 MHz LTE signals are located at 800 MHz and 840 MHz. In the third case, three 20 MHz LTE signals are located at 800 MHz, 850 MHz and 900 MHz. In the first and second cases, 2D-DPD is applied. In the third case, RF DPD is adopted as 2D-DPD can only process two-band signal. Comparisons to conventional DPD-only or APD-only methods have also been made. Experiment results almost agree with the simulation results.

Chapter 6 introduce an evolved 2D-DPD method which is based on mathematical model of proposed linearization method. By ignore high order memory effect, the complexity of 2D-DPD can be significantly reduced. Simulation of a two-band 20 MHz LTE signal located at 800 MHz and 900 MHz is done. Comparisons to conventional 2D-DPD method have been made. In the simulation evolved 2D-DPD method can achieve similar improvement with less coefficients.

Chapter 6 make the conclusion of this thesis and give suggestions for the future work to achieve better improvement in IMD3.

Chapter 2 Background and Literature Review

2.1 Introduction

Chapter 2 first introduces several important techniques used in RoF link. These include lasers, optical modulators, optical receivers, and power amplifiers. Next, the nonlinearity characteristics of the RoF link are discussed in Section 2.3 and Section 2.4. In Section 2.6, various linearization technologies are discussed.

2.2 Radio-over-Fiber system

2.2.1 Lasers

An optical signal is initially generated by lasers. The laser which is widely used is called distributed-feedback (DFB) laser. Compared with the classic Fabry-Perot laser and the distributed Bragg reflector (DBR) laser, the DFB laser does not contain multi-longitudinal-mode and has a better power efficiency then DBR laser. Figure 2-1 shows the structure of these lasers [6]. Figure 2-2 shows the spectrum of Fabry-Perot laser which contains several huge side modes.

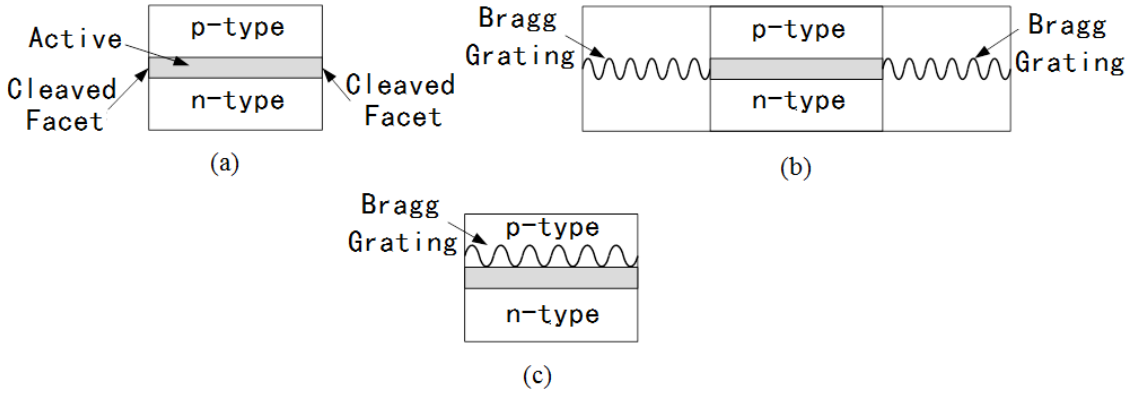

Figure 2-1 Structure of Fabry-Perot laser (a), structure of DBR laser (b), and structure of DFB laser (c) [6]

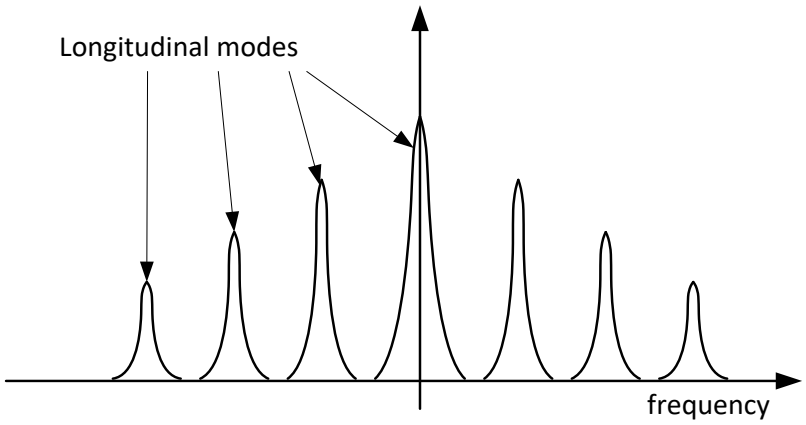

Figure 2-2 Output spectrum of Fabry-Perot laser

2.2.2 Optical Subcarrier Modulation

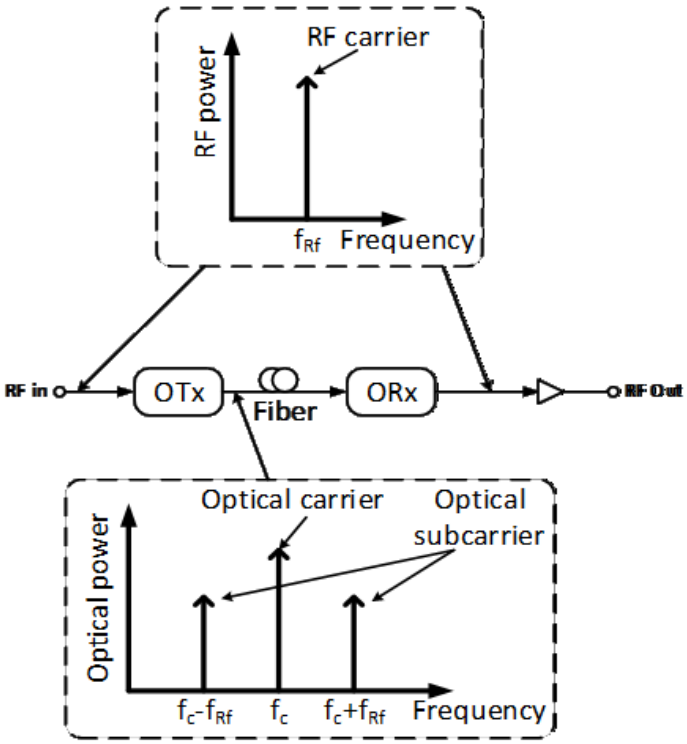

Figure 2-3 Schematic of optical subcarrier modulation

Figure 2-3 shows the schematic of double sideband optical subcarrier modulation and demodulation. The original RF signal is located at f_{RF} and is upconverted by the OTx. In the

frequency domain, the RF signal is directly transferred to carrier frequency. In the digital optical modulation, the carrier frequency f_c is directly modulated. But in analog system, the modulated signal is located at subcarrier which is f_{RF} away from f_c. Therefore, the analog modulation system will occupy more bandwidth than digital system. As the three signals, located at f_c-f_{RF}, f_c, and f_c+$f_{RF,}$ are transmitted simultaneously, the RoF system is more sensitive to nonlinearity in the optical link.

Optical subcarrier modulation methods can be divided into two groups: direct and external modulation. In a direct modulator, the intensity of a laser is directly modulated by the input electrical current. Figure 2-4 shows a direct modulation model. Direct modulation devices are usually very simple and small, but they are very sensitive to the chirp [6]. The Figure 2-5 shows the mechanism of direct modulation. If the input power of an electrical wave is lower than the threshold, there will be a high distortion in the system.

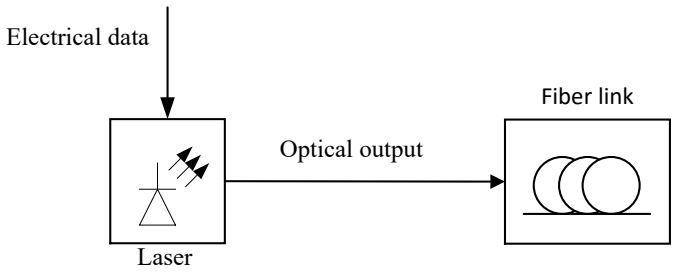

Figure 2-4 Direct modulation method

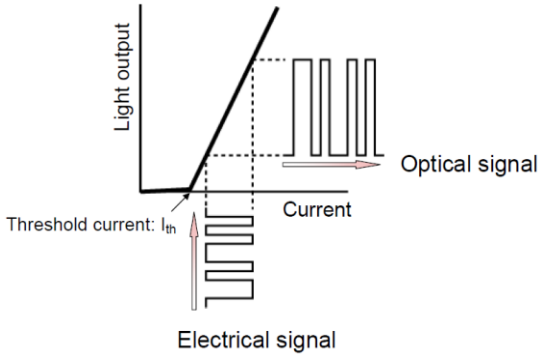

Figure 2-5 Mechanism of direct modulation method [8]

Another characteristic of the direct modulation devices is a strong nonlinearity, Figure 2-6 shows that the nonlinearity of direct modulation devices is related with input current and the temperature. Moreover, the direct modulation cannot modulate the phase of an optical carrier. Only the amplitude of optical carrier can be changed by direct modulator.

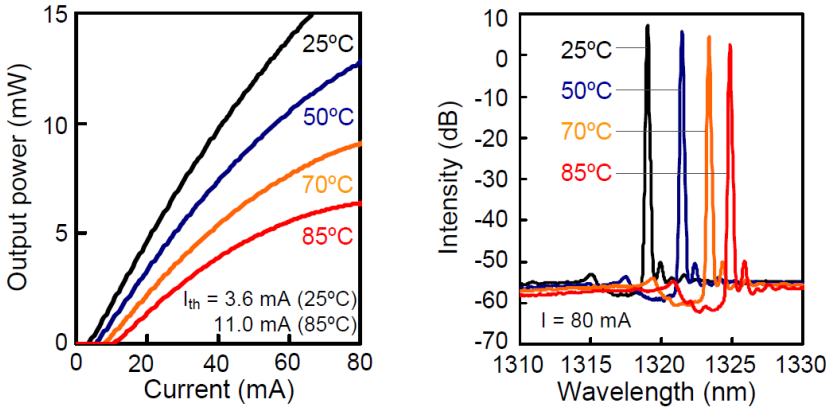

Figure 2-6 Transmission characteristic of a directly modulated laser [8]

In an external modulator, the optical signal is modulated by an independent component. The external modulators include Electro-Absorption Modulator (EAM) and Mach-Zehnder Modulator (MZM). The general structure of an external modulation system is shown in Figure 2-7.

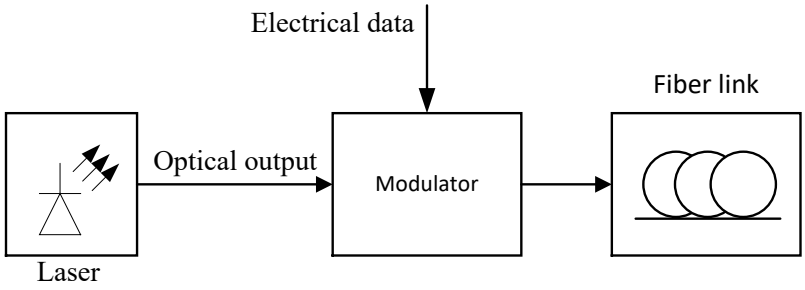

Figure 2-7 Structure of external modulator

EAM use a semiconductor waveguide to modulate the optical signal. The structure of a typical EAM is shown in Figure 2-8. The advantages of EAM are small size, low bias voltage, and no threshold. Most of the EAM is combined with laser diode in one chip. This combined device is usually called an Electro-Absorption Modulated Laser (EML). The size of an EML is similar to a

direct modulator, but an EML can support a higher bandwidth with a lower chirp compared with that of direct modulator. Also, the absorption recovery time of EAM is very low, usually less than 10 ps with high reverse bias voltage [9]. The characteristics of EAM are well researched by other researchers [10], [11]. The absorption of semiconductor is controlled by the bias voltage. Thus, the modulated signal is related with reverse bias voltage. A typical transmission characteristic of an EAM is shown in Figure 2-9. The nonlinearity of the EAM visible in Figure 2-9 is mainly induced by the intrinsic nonlinear absorption of semiconductor waveguide.

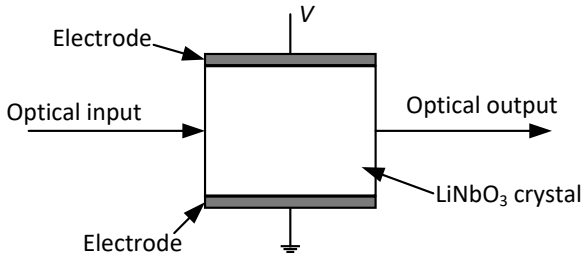

Figure 2-8 Phase modulation in a LiNbO3 crystal

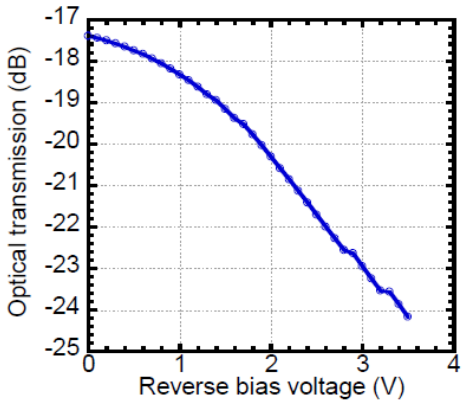

Figure 2-9 A typical transmission characteristic of EAM [12]

MZM is another widely used external modulator. In fact, the MZM is more popular than EAM. Thanks to the advantages of MZM like multi modulation schemes and zero chirp, researchers usually ignore its large size. The structure of an MZM is shown in Figure 2-10. The input power is divided into two arms of the same length. In each arm, the electrode will modulate the optical carrier by phase. After the signal is modulated separately in two arms, they are

combined together by another power divider. The electric field output of the MZM is given as follows:

$$E_{out}(t) = \frac{1}{2}E_{in}(t)\left[e^{j\frac{\pi}{V_\pi}V_1(t)} + e^{j\frac{\pi}{V_\pi}V_2(t)}\right] \quad (2.1)$$

where $E_{out}(t)$ is the electric field of the output signal, $E_{in}(t)$ is the electric field of the input frequency carrier, V_π is the half-wave voltage and $V_1(t)$ and $V_2(t)$ are two applied voltages. The electric field of the output signal is the sum of two phase modulated signal. So, two applied voltages should be:

$$V_1(t) = V_{RF}\, cos(\omega_{RF}\, t) + V_{bias} \quad (2.2)$$

$$V_2(t) = V_{RF}\, cos(\omega_{RF}\, t + \theta) \quad (2.3)$$

where V_{RF} and θ are the amplitude and phase of the input RF signal and the V_{bias} is the bias voltage applied to the MZM. To realize different modulation methods, V_{bias} and θ should be carefully adjusted.

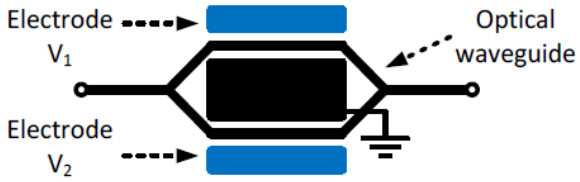

Figure 2-10 Structure of an MZM

2.2.3 Optical Receivers

An optical receiver is used to convert the optical signals into electronic signals. The core of the receiver is a photo-diode. A single photodiode can be considered as an optical receiver, such as PN photodiodes or PIN photodiodes, but most of the optical receivers also contain pre-amplifier and some signal processing component within it. Figure 2-11 shows a typical and simple sample of optical receiver. The signal processing circuit can be an analog filter or other devices.

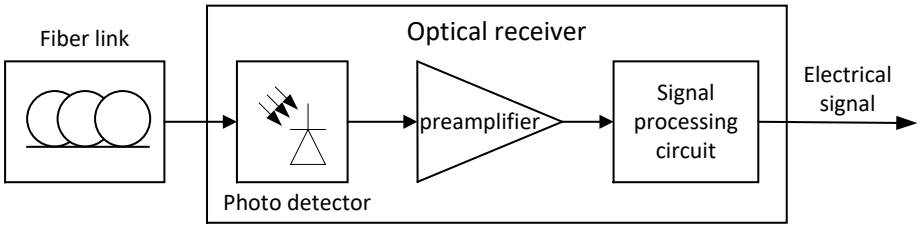

Figure 2-11 A sample of optical receiver [6]

In the RoF system, the direct receiver shown in Figure 2-11 acts as an amplitude demodulator. However, in some digital optical transmission system, the optical signal is modulated by phase. A simple direct receiver or incoherent receiver cannot detect the phase or frequency changes of the optical signal. So, the coherent receiver is developed. As presented in Figure 2-12, the optical I/Q coherent receiver has a similar structure with microwave I/Q demodulator. With a coherent receiver, a phase modulated signal, such as a n-QAM signal, can be detected and demodulated. Therefore, coherent receivers are widely used in digital optical systems.

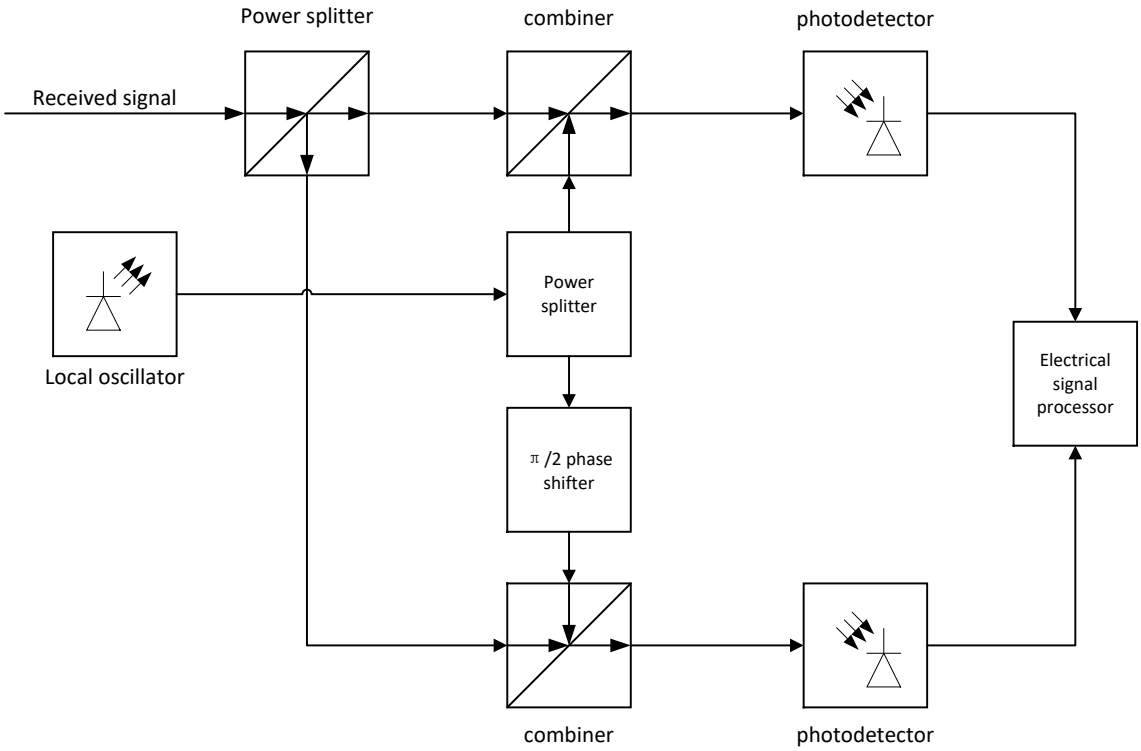

Figure 2-12 Structure of I/Q coherent receiver

2.2.4 RF Power Amplifier

The power amplifier (PA) is another main cause of distortion in RoF systems. As the output signal of the optical receiver is very low and needs to be amplified to feed the antenna, one or more amplifiers are often connected in series after the optical receiver.

PA quality is measured by efficiency and linearity, but these two words are contradictory. As the PA is the highest power consumption device in the RoF system, the efficiency of a PA is the most important property. In a high efficiency PA, more DC power is converted to output RF power. This means achieving the same output power with lower electrical power input and in turn, reducing the operating cost of base stations.

Therefore, the PA is always operated near the saturation point that achieves the best efficiency. However, the nonlinearity is very strong near the saturation point due to the transistors being used in the PA. The V-I characteristic of all transistors are similar no matter how it is fabricated. Figure 2-13 shows the V-I characteristic curve of a typical 3DG4A NPN silicon transistor [13].

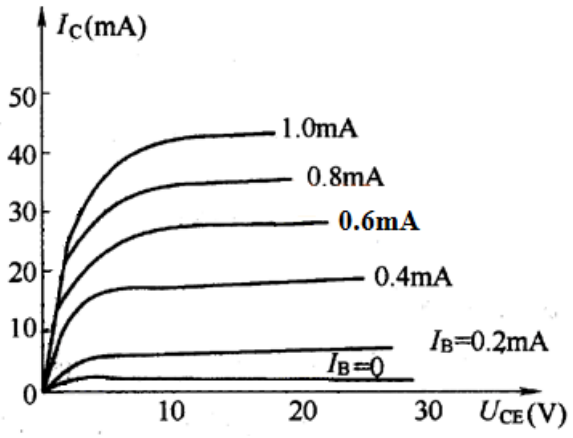

Figure 2-13 V-I characteristic curve of 3DG4A transistor [13]

Nowadays, many new types of PA are being developed. Among them, the Envelope Track (ET) Power Amplifier is the most popular technique [14], [15], [16]. ET PA adopts some idea from

feed forward linearization. The DC bias of the power amplifier is controlled by the envelope of the input signal. The structure of a newly designed ET power amplifier is presented in Figure 2-14 [17]. With the help of the envelope, the RF PA can always work in the maximum efficiency zone and the nonlinearity of the PA is suppressed [18]. With the ET PA, a higher efficiency and better linearity are achieved simultaneously. Thus, many other researches also focus on this domain [19], [20].

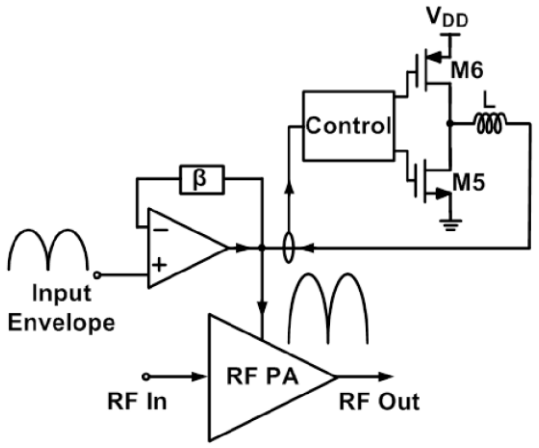

Figure 2-14 Linear assisted ET envelope amplifier architecture [17]

2.3 Nonlinearity Characteristics in Radio-over-Fiber Systems

2.3.1 Harmonics

In nonlinearity devices like transistors or photodiodes, the relationship between the input power and the output current should be $i_c = f(v)$, where $v = v_i + V_Q$, V_Q is the value of bias point and v_i is the input signal. When using power series to approximate, the Taylor series at the bias point will be:

$$I_c = a_0 + a_1 (v - V_Q) + a_2 (v - V_Q)^2 + a_3 (v-V_Q)^3 + \ldots \quad (2.4)$$

Substituting $v = v_i + V_Q$ into the above formula, then:

$$I_c = a_0 + a_1 v_1 + a_2 v_2^2 + a_3 v_3^3 + \ldots + a_N v_i^N + \ldots \quad (2.5)$$

where the parameters $a_N = \frac{1}{N!} \times \frac{\partial^N i_c}{\partial v^N}\Big|_{v=V_Q}$ are related with bias point.

Assuming the input signal is $v_i(t) = V_i \cos \omega_1 t$, the output of the system should be:

$$i_c = \left(a_0 + \frac{a_2 V_i^2}{2}\right) + \left(a_1 V_i + \frac{3}{4} a_3 V_i^3\right) \cos(\omega_1 t) + \frac{1}{2} a_2 V_i^2 \cos(2\omega_1 t) + \frac{1}{4} a_3 V_i^3 \cos(3\omega_1 t) + \cdots \quad (2.6)$$

In the real system, an ideal linear system does not exist. This means the output response is not strictly proportional to the input excitation. When a tone signal passes through a nonlinear device, the output will not be a tone signal anymore. Other than the fundamental component at ω_1, the output signal also contains the DC component and other harmonic components at $N\omega_1$. The magnitude of N[th] order harmonic component is inversely proportional with N, so the magnitude of high order harmonic will be lower than noise [21]. Therefore, high order harmonics can be ignored.

2.3.2 1dB Gain Compression Point

From the Formula (2.6), the gain of the fundamental signal is:

$$\left(a_1 V_i + \frac{3}{4} a_3 V_i^3\right) \quad (2.7)$$

In most of the systems, the a_1 has opposite sign of a_3. Therefore, the system gain will reduce with the increasing of V_i. By using dB to calculate the amplitude of the I/O signal, it can be found that the output power deviates from ideal linear line with the increasing of the input power. When the deviation of output power reaches the 1 dB in the system, the value of input power is called 1dB gain compression point (P_{1dB}). This relationship of input and output power is shown in Figure 2-15.

P_{1dB} is an important performance parameter [21]. A higher P_{1dB} means a higher linear

output power. When the input is small, the system works in the linear zone which has a better linearity. The whole system gradually enters the non-linear area as the input power increases. At this stage, the nonlinearity effect occurs in the system. When the input power increases to a certain point, the system will be saturated. In the saturation zone, the output power cannot increase anymore. Even the input power continuously increasing, the output power remains the same. At this stage, the system will induce enormous nonlinearity distortion and phase distortion.

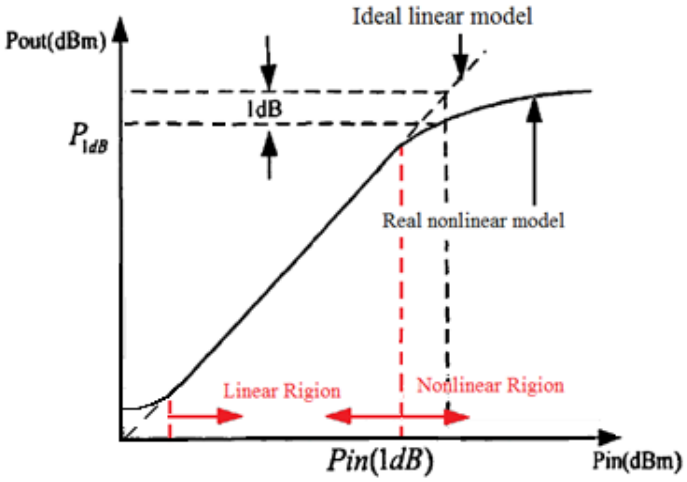

Figure 2-15 The nonlinearity of RoF system

2.3.3 Intermodulation Distortion

When more than one signal are transmitted in the system simultaneously, the output power will contain noises at other frequency generated by the fundamental signal. This phenomenon is also ascribed to nonlinearity of the system. The sub-signals generated from the fundamental input signal are called intermodulation components. Some of the components located very close to the original signal making the system harder to filter. This is called intermodulation distortion [21].

Assuming the input signal is $\mathrm{v} = V_{1m}\cos\omega_1 t + V_{2m}\cos\omega_2 t$ and the input signals have same amplitude, that is $V_m = V_{1m} = V_{2m}$, then $\mathrm{v} = V_m(\cos\omega_1 t + \cos\omega_2 t)$.

The output signal of system will be:

$$i = f(v) = (a_0 + a_2 V_m^2) + \left(a_1 V_m + \frac{9}{4} a_3 V_m^3\right)(\cos(\omega_1 t) + \cos(\omega_2 t))$$
$$+ \frac{1}{2} a_2 V_m^2 (\cos(2\omega_1 t) + \cos(2\omega_2 t)) + a_2 V_m^2 \cos(\omega_1 \pm \omega_2) t$$
$$+ \frac{3}{4} a_3 V_m^3 (\cos(2\omega_2 \pm \omega_1) t + \cos(2\omega_1 \pm \omega_2) t) + \cdots \quad (2.8)$$

Formula (2.8) shows that other than fundamental signals and the harmonic signals, the system also induce second order intermodulation distortion (IMD2) at $\omega_1 \pm \omega_2$, and third order intermodulation distortion (IMD3) at $2\omega_1 \pm \omega_2$ and $2\omega_2 \pm \omega_1$. The output spectrum of a nonlinear system is shown in Figure 2-16. Generally, the even order IMD and harmonic can be removed by filter easily, but some of the odd order IMD is located quite near the origin signal and cannot be removed by filter. Figure 2-17 shows the spectrum around two fundamental signals. Expanding the spectrum, the IMD3 and IMD5 are found very close to the signal.

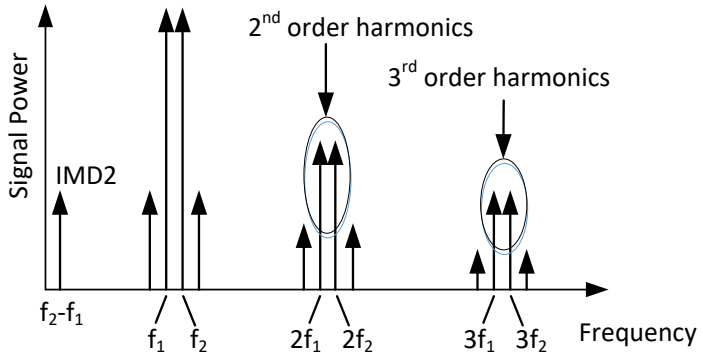

Figure 2-16 Output spectrum

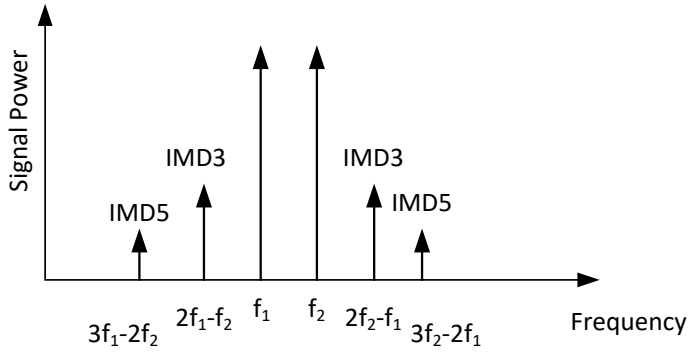

Figure 2-17 Output Spectrum around two signals

In engineering applications, engineers usually use Third-Order Intercept Point (IP3) to measure the IMD. The IP3 is defined in logarithmic coordinates. As shown in Figure 2-18, extending the linear region of the fundamental signal and the IMD3 signal has their extension lines converge at one point. This particular point is IP3 point. The input power at IP3 point is called IIP3, while the output power is called OIP3. The definition of IP2 and OIP2 is same as IP3 and OIP3.

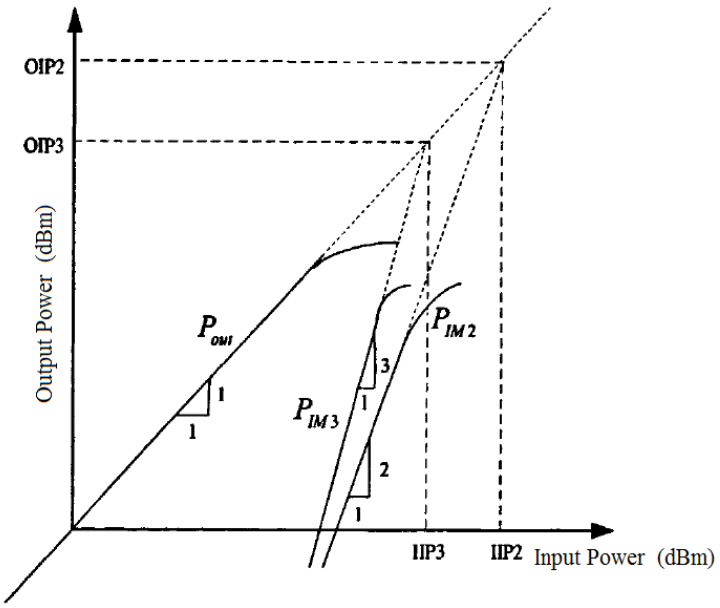

Figure 2-18 The IP3 and IP2 of a nonlinearity system

2.3.4 Memory Effect

The wireless communication systems were considered as memoryless systems during the past few decades. In the 1G and 2G, both the transmission rate and carrier frequency are low. The effect of the memory effect can be safely ignored. At that time, researchers simplified the system as a fixed mechanism and never affected by history signals. Many models without memory effect are described in Section 2.6.3.

The 3G system significantly increases the band utilization rate [2]. Therefore, the memory effect cannot be ignored in the transmission system anymore. In the recent model, the past signals

remain affects to the current signal. This is the memory effect in nonlinear systems. With this new change, researchers began to investigate linearization techniques along with the memory effect. Figure 2-19 shows the mechanism of the memory effect.

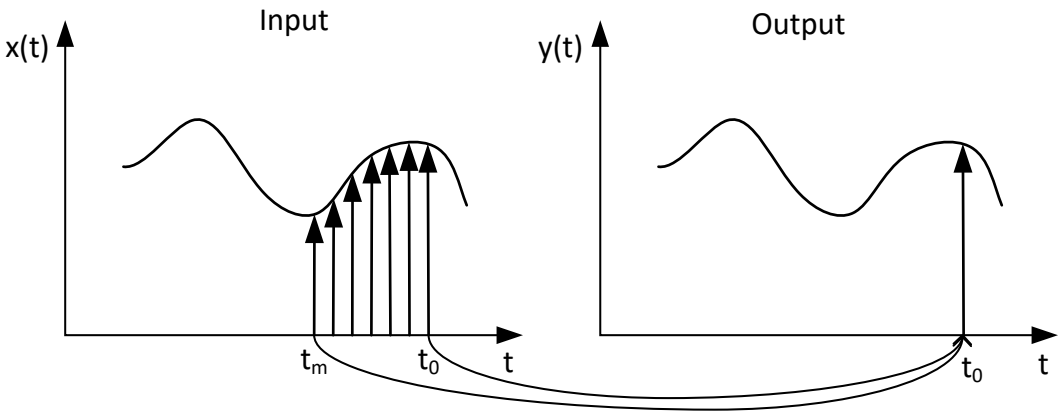

Figure 2-19 The memory effect of the input signal on the output signal

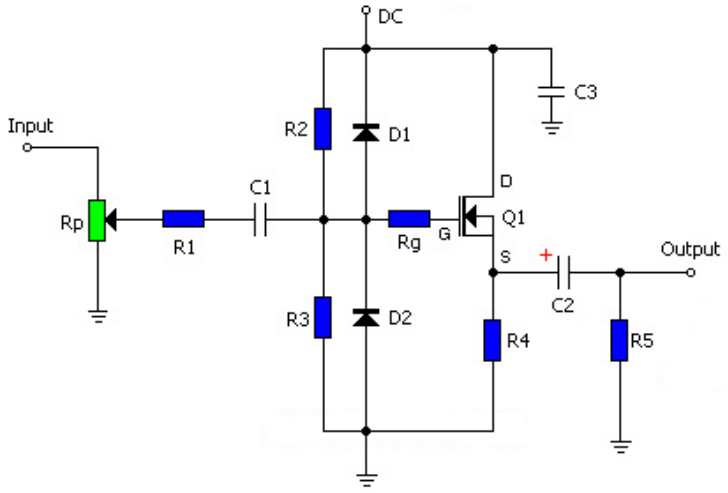

Figure 2-20 A simple Class-A PA

The memory effect can be induced by any device in the system, such as laser, fiber, A/D converter, etc., but it is mainly induced by the PA. The memory effect could be divided into two branches, the long-term memory effect and the short-term memory effect.

The long-term memory effect is mainly induced by memory components within electrical

devices. Figure 2-20 presents a traditional Class-A amplifier. Several capacitors are used in the circuit. Combined with the parasitic capacitance and parasitic inductance, these induce the short-term memory effect in the PA. Similar mechanisms also happen in all the electrical devices in RoF systems but can be ignored.

The long-term memory effect is caused by thermal effects, charge trapping, bias circuit effects, and control circuitry [21]. Compared with short-term memory effect, the long-term memory effect lasts for a much longer time. Therefore, long-term memory effect plays a very important role in nonlinear systems and is more serious than short-term effect.

2.4 The Measurement of Nonlinearity on Communication System

When the communication system upgrades to a wideband or even ultra-wideband system from narrowband system, the modulation technique is also improved with them. The simple amplitude, frequency or phase modulation has died out in modern highspeed data transmission systems. Those state-of-the-art techniques require much more complex modulation and multiplexing methods to support wideband transmission. The QAM technique is widely used in the cable TV service and the Coded Orthogonal Frequency Division Multiplexing (COFDM) is used in wireless digital TV service. These wideband services need some parameters to measure their performance. Thus, some new nonlinearity parameters, like ACPR and EVM, is proposed for wideband signal.

2.4.1 Adjacent Channel Power Ratio

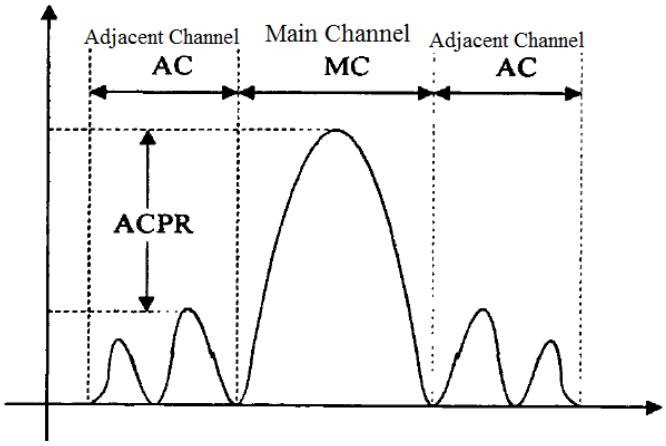

Figure 2-21 The ACPR of the output signal

ACPR is defined as the power ratio between main channel and adjacent channel [21]. In 2G, 3G, and 4G wireless communication system, the ACPR is a main indicator of the nonlinearity degree, which is clearly stipulated by ITU as a standard [22]. Figure 2-21 shows the ACPR of the output signal.

2.4.2 Error Vector Magnitude

The non-linear distortion in RoF systems directly affects the non-constant envelope signal modulated by linear modulation scheme. These modulation techniques modulate the phase and amplitude simultaneously. Therefore, they are more sensitive to the nonlinearity in the communication system. The distortion caused by the nonlinearity includes both phase and amplitude distortion leading to changes in the constellation [21]. Thus, some of the constellation points may locate in nearby decision areas and lead to bit error. This kind of distortion is usually measured by EVM. The EVM is the vector error between the ideal signal and measured signal. The EVM shows the degree of how far the point on the constellation deviating from its ideal place, as shown in Figure 2-22.

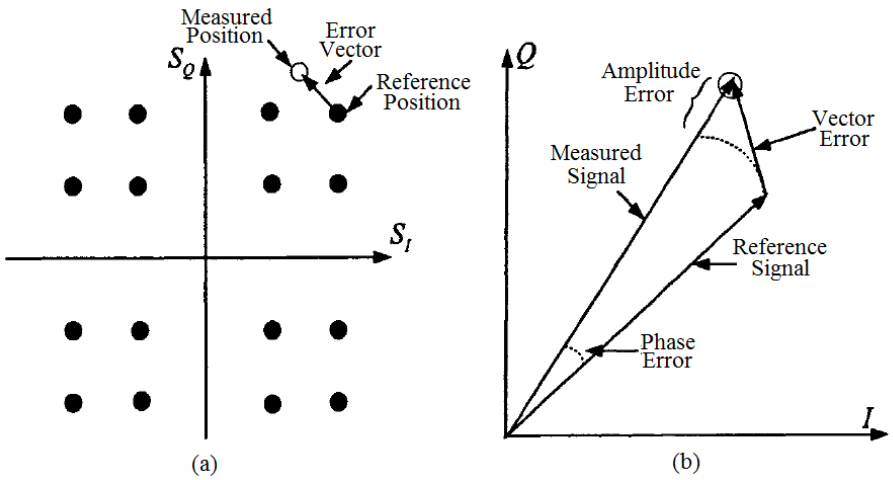

Figure 2-22 The principle of EVM

The mathematic definition of EVM is:

$$EVM = \sqrt{\frac{\frac{1}{N}\sum_{i=1}^{N}\left|S_{ideal,i}-S_{meas,i}\right|^2}{\frac{1}{N}\sum_{i=1}^{N}\left|S_{ideal,i}\right|^2}} \tag{2.9}$$

The communication systems need to ensure its EVM performance. Thus, the signal can be demodulated correctly. In engineering practice, the EVM can be measured by Vector Signal Analyzer (VSA). However, in this paper, the EVM is calculated from a recorded signal by MATLAB. In the ETSI 25.123 standard, it is stipulated that the EVM should be less than 17.5% with QPSK modulation, and less than 12.5% with 16QAM modulation [22].

2.5 Behavior Model of Nonlinearity System

When nonlinearity devices are being designed in a communication system, a nonlinearity model needs to be built for both circuit simulation and system simulation. This model should exactly demonstrate the nonlinearity characteristic. Consequently, the nonlinearity model is very important for the research in distortion and the design of pre-distortion system.

Researchers use two ways to build up a nonlinearity model: the circuit model and the behavior model.

The circuit model uses several models of active components and passive components to build up a relationship between the input and output signal. It is an accurate copy of a real circuit. All the models are combined just as the real circuit. Sometimes a multi-field simulation is also applied to the model.

The advantage of circuit model is its accuracy, but the complexity is the main disadvantage [23]. With almost a 'real' device in the simulation, the computing consumption is extremely high. The circuit model achieves high accuracy by sacrificing designing and computing time. In the proposed linearization method, the APD circuit is simulated with a circuit model which will be discussed later.

As the circuit model is hard to design, researchers proposed behavior model. The behavior model uses the black-box concept [23]. After importing several testing signals into the nonlinearity system, the output of the system is measured and modeled. The accuracy of the behavior model is related with the model structure and the measurement method. In general, researchers use the determined test signal to test the nonlinearity system. Thus, the model between the input and output signal is built up. In the simulation of the proposed linearization method, the PA and RoF model is built up with behavior model.

The behavior model is divided into several branches. Two main branches are the model with memory effect and the model without memory effect. The behavior model with memory effect can also be divided into the linear memory effect model and the nonlinear memory effect model. All these models will be discussed in detail in Section 2.6.3.

2.6 Linearization Techniques for Radio-over-Fiber System

Ever since H. S. Black proposed the first feedforward linearization technique in 1923 [24], lots of linearization techniques have been proposed to compensate the nonlinearity [7]. The basic idea of linearization is simple but robust: generating an opposite nonlinearity to compensate the nonlinearity system.

Among all the linearization techniques, some of them can be used in a RoF system. These techniques can be divided into several kinds. Figure 2-23 shows the classification of linearization that can be used in RoF system.

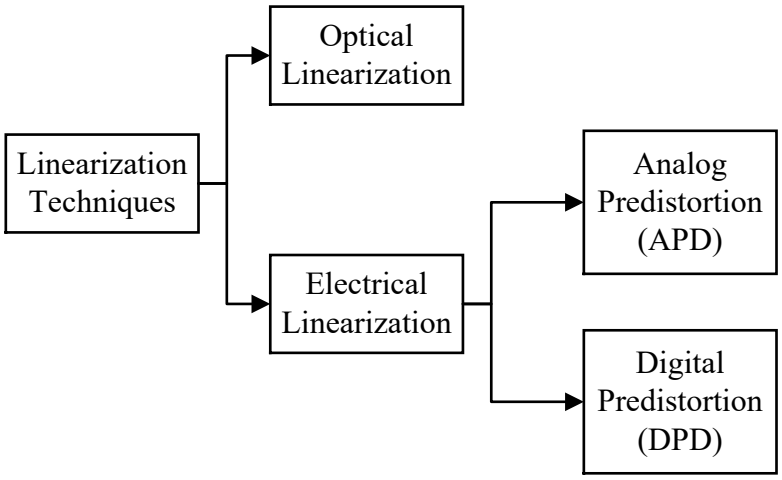

Figure 2-23 Classification of linearization techniques

2.6.1 Optical Linearization Techniques

Optical linearization contains two nonlinearity optical devices that can compensate the nonlinearity for each other. Therefore, the final output is a linearized signal. As the bandwidth of optical signal can be extremely wide, the optical linearization is much more fitful to compensate a wideband signal like OFDM. Unfortunately, all the optical linearization techniques can only deal with the quiescent distortion, like IMD3 and IMD5, induced by the OTx. Other nonlinearity devices in the RoF system cannot be linearized by optical linearization techniques. Two main optical linearization techniques are proposed for RoF system: mixed-polarization and dual-wavelength linearization.

The mixed-polarization approach uses two polarizers to suppress the IMD3 induced by EAM based RoF system [25]. The structure is shown in Figure 2-24 . The EAM is set between two polarizers. The optical signal is first polarized by the first polarizer. Next, the polarized signal is modulated by EAM. Thus, the IMD3 generated by the EAM is also a polarized signal but has a

different angle than the fundamental signal. Afterwards, the modulated signal passes through another polarizer filtering out the IMD3. For a certain signal, the angle of two polarizers α and β should be calculated carefully to match the system requirements. With this technique, the spur-free dynamic range (SFDR) has 12.5dB improvement [25]. Another evolved method is also proposed which replaces the second polarizer with a semiconductor optical amplifier (SOA) [26].

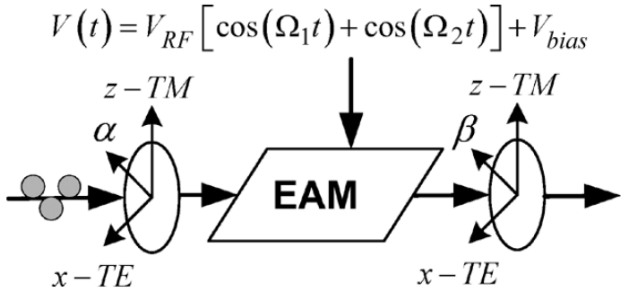

Figure 2-24 Schematic of mixed-polarization linearization

In [27], K. K. Loi, *et al*. proposed a dual-wavelength linearization technique. The dual-wavelength technique requires two input optical carriers at λ_1 and λ_2. They are coupled together and modulated after the coupler. With this process, they can cancel the nonlinearity for each other. In the experiment, two input lasers are set to 1552.6 nm and 1510 nm. By changing the optical power ratio between two lasers, the IMD3 can be reduce by 30 dB with EAM [27] and 26 dB with MZM [28]. In other experiment, same procedure can compensate the second-order nonlinearity by 23 dB with EAM [12]. Figure 2-25 shows the schematic of dual-wavelength linearization.

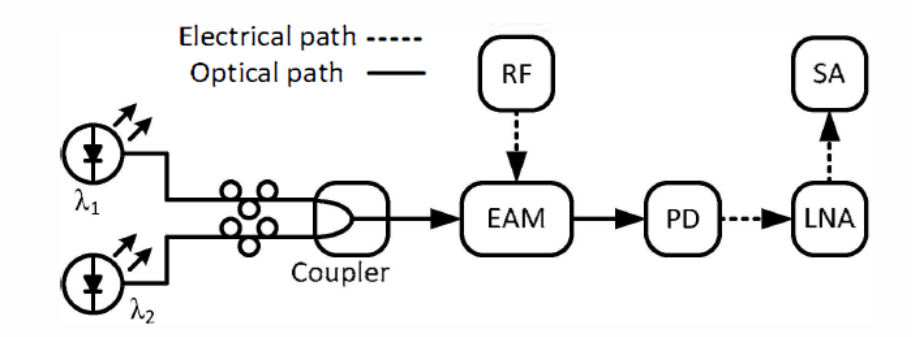

Figure 2-25 Schematic of dual-wavelength linearization

2.6.2 Analog Pre-distortion

The basic idea of APD is simple. Another nonlinear device is adopted in the APD circuit to generate certain IMD3 and/or IMD5. These IMDs have the same amplitude and reverse phase with the IMDs generated by OTx or PA [29]. The added nonlinear device can either be a diode, transistor or field effect tube. The principle of the APD is shown in Figure 2-26. The IMD3 generated by APD circuit has an opposite phase with the IMD3 generated by optical modulator, they could compensate each other. After the transmission, these two IMDs compensate each other. Thus, the system is linearized.

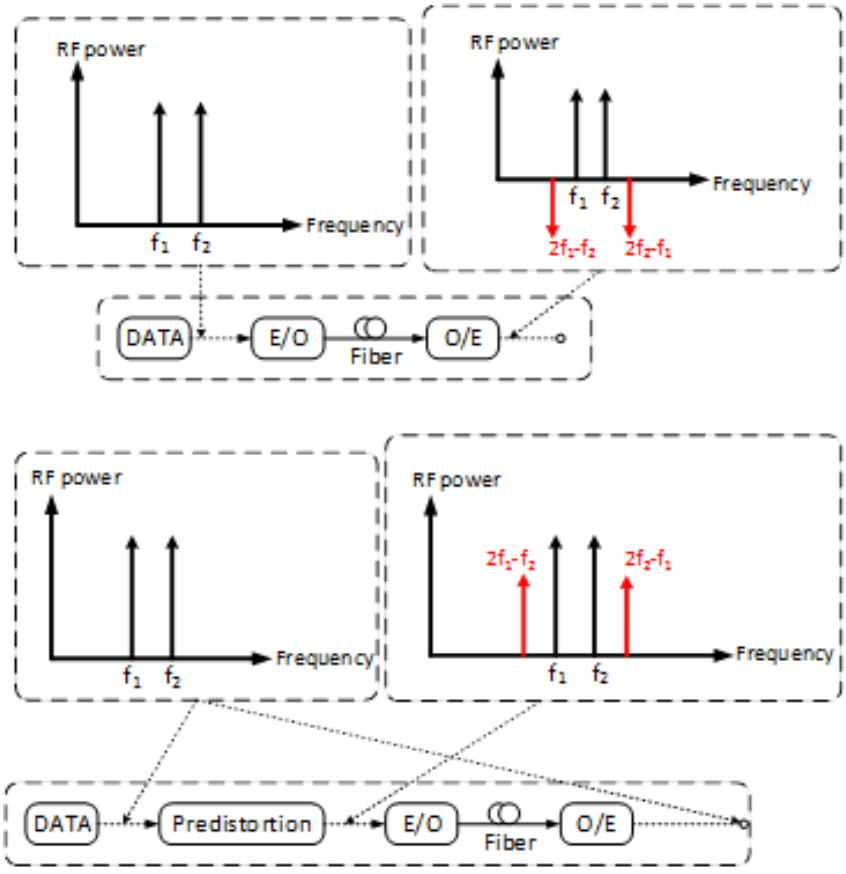

Figure 2-26 Analog pre-distortion principle [29]

The APD has several benefits and weaknesses. It can provide ultra-wideband linearization and can support a high bandwidth signal with a small size and low power consumption. Compared

with the DPD device which is usually processed by field-programmable gate array (FPGA), the complexity of APD is extremely lower than DPD. However, the APD also has the same disadvantage with the optical linearization techniques. It cannot compensate the memory effect.

As the diode is the smallest nonlinear component, many APD circuit is designed based on diodes. Figure 2-27 presents several reported APD circuit [30-32]. They all use a diode-based circuit that has a serial or anti-parallel setup. These diodes can generate in-phase IMD3 with the RF signal. Generally, these APDs can improve the SFDR for about 10 dB within a limited bandwidth up to few hundreds of MHz. Other APD circuits can afford a wider bandwidth like [34] which is 3.1 GHz to 4.8 GHz.

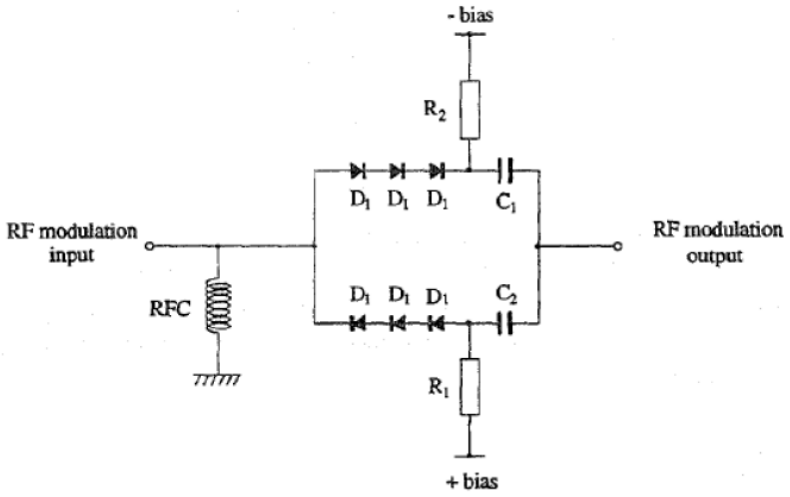

(a)

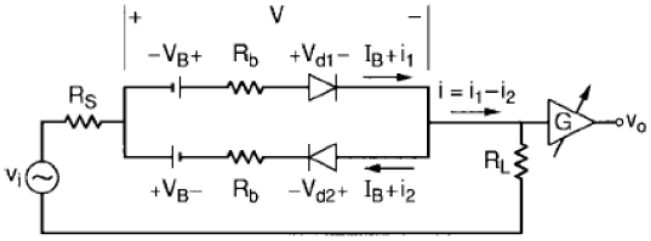

(b)

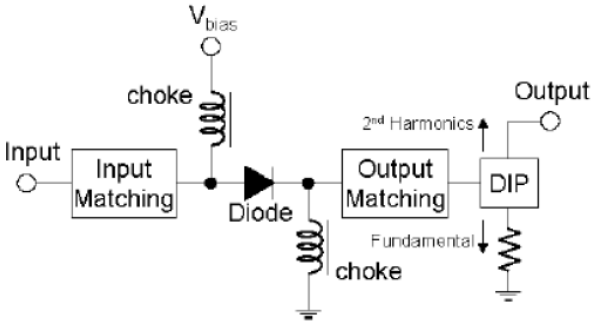

(c)

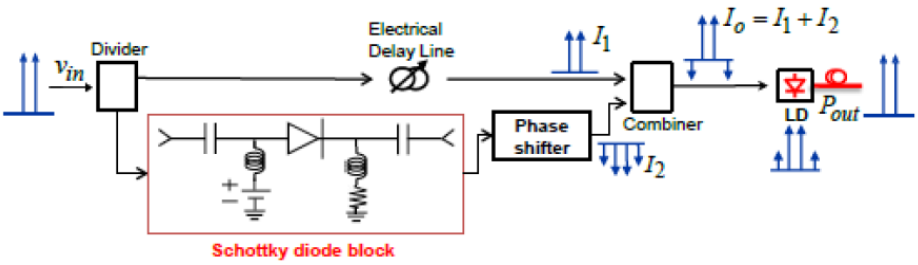

(d)

Figure 2-27 Schematics of the analog APDs [30-33]

The schematic of [34] is shown in Figure 2-28. In this design, the input RF signal is first divided by power splitter. Afterwards, two signals are matched by the λ/4 transformers. Two diodes are used to generate in-phase IMD. The output signal is feed into a EAM. This APD circuit can suppress the IMD3 by 7 dB and the SFDR by 11 dB.

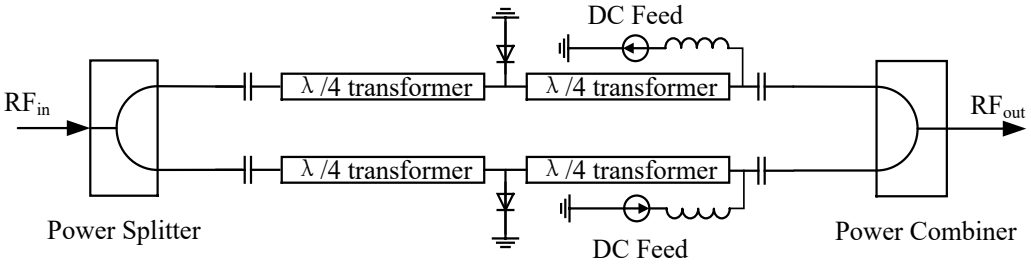

Figure 2-28 Schematic of the APD circuit reported in [34]

The size of [34] is too large due to λ/4 transformers. In order to decrease the size of the APD circuit, some new circuit is proposed [12]. The schematic of [12] is shown in Figure 2-29. Since the series resistance of the zero bias diodes used in [12] is high enough, the λ/4 transformers

and power splitters are removed. The power consumption is also reduced for same reason. The two diodes are set to anti-parallel and the bias current is carefully adjusted to achieve certain nonlinearity. In the experiment, the proposed APD in [12] can improve SFDR by 10 dB from 7 GHz to 14 GHz and 6 dB from 15 GHz to 18GHz.

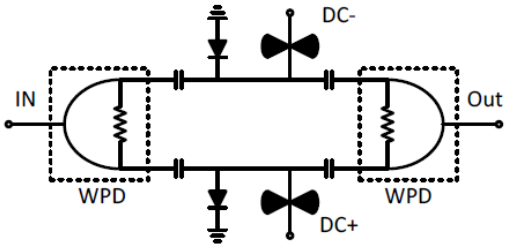

Figure 2-29 Schematic of the APD circuit reported in [12]

Further evolution of APD is reported in [29]. The WPD is removed from the circuit as shown in Figure 2-30. Thus, the size of the circuit is further reduced and as the Wilkinson power divider (WPD) is removed from the circuit, the bandwidth is extremely increased to from 10 MHz to 40 GHz. The experiment shows a 5dB improvement in SFDR and 1 dB improvement in EVM from 1 to 30 GHz. This APD circuit is adopted in this thesis as the APD method. The details of this APD circuit will be discussed in next chapter.

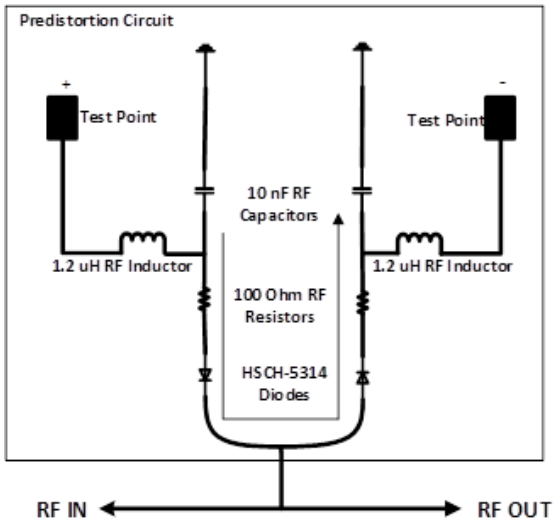

Figure 2-30 Schematic of the APD circuit reported in [29]

2.6.3 Digital Pre-Distortion

Digital pre-distortion techniques have been developed for years. Several models were reported to describe and compensate the nonlinearity of a system or device. With the increasing of transmission rate in communication systems, the requirement of accuracy is also increased. In this section, a brief introduction of DPD history is presented.

At the very early stage of the DPD technique, memory effect is not important among all nonlinearity effect [21]. At that time, several models are reported without memory effect. Within a DPD model without memory effect, the main nonlinearity characteristics are quiescent AM-AM distortion and AM-PM distortion. These models can be described as an algebraic functions of instantaneous envelope amplitude.

First model is the traditional polynomial model. It is the simplest way to approximate the AM-AM and AM-PM characteristic curve. The function is:

$$y(n) = \sum_{k=0}^{K} a_k x(n)|x(n)|^k \tag{2.10}$$

where $x(n)$ and $y(n)$ are the input and output signal, *K* is the order of the polynomial, and a_k is the complex parameter of the polynomial. The polynomial model is simple, but the accuracy of the polynomial model is poor.

Second option is the Seleh model. It uses two algebraic functions to describe the AM-AM and AM-PM distortion. Under the polar coordinates, the characteristic function of AM-AM and AM-PM is written as $A(\cdot)$ and $\Phi(\cdot)$,

$$A(|x(n)|) = \frac{\alpha_\alpha |x(n)|}{1+\beta_\alpha |x(n)|^2} \tag{2.11}$$

$$\Phi(|x(n)|) = \frac{\alpha_\varphi |x(n)|^2}{1+\beta_\varphi |x(n)|^2} \tag{2.12}$$

where α_α, β_α, α_φ, and β_φ are constant.

The Seleh model is a more accurate description of the nonlinearity characteristic of traveling wave tube amplifier. With only four sets of parameters, the Seleh model is still very simple. The least squared method (LSM) can be used to calculate the parameter. The solid-state power amplifier (SSPA) or other nonlinear devices have a different AM-PM characteristic with the traveling wave tube amplifier. [35]. Therefore, the Seleh model is not a good choice to describe the SSPA or other nonlinear devices.

With the increasing of the transmission rate, signal bandwidth, and carrier frequency, the memory effect is more and more obvious in the communication system [36]. As the behavior model without memory effect only considers the quiescent nonlinearity, it is not fit for 3G or other wideband communication systems. So, several DPD models with linear memory effect are proposed.

First DPD model is the Wiener model [37]. The wiener model contains a linear time invariant (LTI) model followed by a nonlinear model. The structure is shown in Figure 2-31.

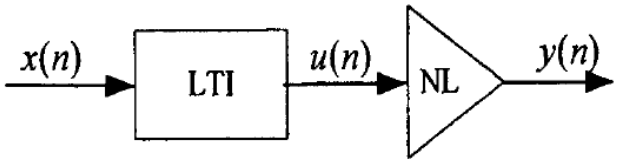

Figure 2-31 Wiener model

where the LTI model can be express as:

$$u(n) = \sum_{l=0}^{L-1} a_l x(n-l) \tag{2.13}$$

The nonlinear model can be express as:

$$y(n) = \sum_{k=2n-1}^{K} b_k u(n)|u(n)|^{k-1} \tag{2.14}$$

Substituting equation (2.13) into equation (2.14) leads to:

$$y(n) = \sum_{k=2n-1}^{K} b_k \left[\sum_{l=0}^{L-1} a_l x(n-l)\right]\left|\sum_{l=0}^{L-1} a_l x(n-l)\right|^{k-1} \tag{2.15}$$

where a_l are the coefficients of LTI model, b_k are odd order coefficients of none memory effect polynomial, L is the memory depth of the model, and K is the order of the nonlinearity.

Second model is the Hammerstein model [38]. This model has the inverse property of the Wiener model which contains a nonlinear model followed by a LTI. The structure of Hammerstein model is shown in Figure 2-32.

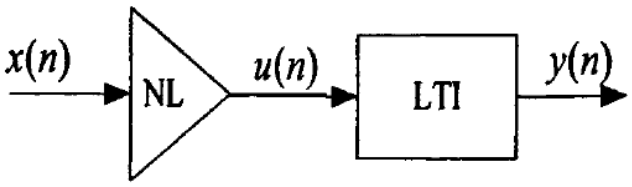

Figure 2-32 Hammerstein model

The two modules can express as:

$$u(n) = \sum_{k=2n-1}^{K} b_k x(n)|x(n)|^{k-1} \tag{2.16}$$

$$y(n) = \sum_{l=0}^{L-1} c_l u(n-l) \tag{2.17}$$

Substituting equation (2.16) into equation (2.17) yields

$$y(n) = \sum_{l=0}^{L-1} c_l \sum_{k=2n-1}^{K} b_k x(n-l)|x(n-l)|^{k-1} \tag{2.18}$$

where c_l are the coefficients of LTI model, b_k are odd order coefficients of no memory effect polynomial, L is the memory depth of the model, and K is the order of the nonlinearity.

The Hammerstein model is more suitable for DPD technique. As all the coefficients have a linear relationship, they can be simply calculated with least squared method (LSM) while the Wiener model needs other method like Newton Method to calculate high order coefficients.

Another linear memory effect DPD model is Wiener-Hammerstein model [38]. Two models are combined in series. The structure is shown in Figure 2-33.

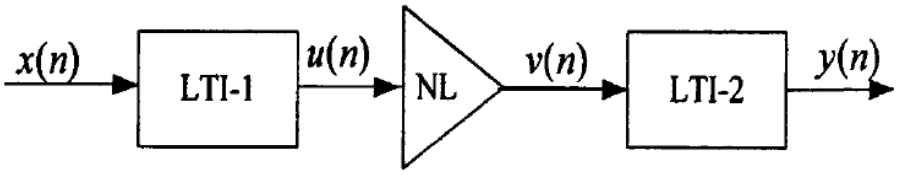

Figure 2-33 Wiener-Hammerstein model

The expression of the system should be:

$$y(n) = \sum_{l_1=0}^{L_c-1} c_{l_1} \sum_{k=2n-1}^{K} b_k \left[\sum_{l_2=0}^{L_a-1} a_{l_2} x(n-l_1-l_2)\right]^k \tag{2.19}$$

The advantage of this model is that it reaches the balance of the accuracy and the complexity, but it is still very difficult to calculate the coefficients. Therefore, it is never used in DPD method. However, it has been studied as a good model and analysis tool of nonlinear systems. In the simulation of the proposed linearization method in this thesis, a Wiener-Hammerstein model is used to describe a PA.

The linear memory effect DPD models can compensate the AM-AM and AM-PM noise caused by memory effect. But they cannot deal with the complex nonlinear memory effect that is affected by the input signal and each instantaneous frequency signal. This phenomenon becomes obvious when the feeding signal is a complex digital modulated wideband signal like 4G or Wi-Fi. Therefore, the researchers use Volterra series to build up the model.

The Volterra series was first developed as an extension of Taylor series with varying time effects. Actually, the Volterra series is so complex, complete, and accurate that all the time-related nonlinear system can be described by it. All the models discussed in this section are just special cases of Volterra series. The classical discrete-time expression for Volterra series is shown in Formula (2.20) [21].

$$
\begin{aligned}
y(t) \;=\; & \sum_{m_1=0}^{M} h_1(m_1)u(t-m_1) \\
& + \sum_{m_1=0}^{M}\sum_{m_2=0}^{M} h_2(m_1,m_2)u(t-m_1)u(t-m_2) \\
& + \sum_{m_1=0}^{M} \dots \sum_{m_n=0}^{M} h_{\mathrm{n}}(m_1,\dots,m_n)u(t-m_1)\dots u(t-m_{\mathrm{n}}) \\
= & \sum_{n=1}^{N}\sum_{m_1=0}^{M} \dots \sum_{m_n=0}^{M} h_{\mathrm{n}}(m_1,\dots,m_n)\prod_{j=1}^{n} u\left(t-m_{\mathrm{j}}\right) \qquad (2.20)
\end{aligned}
$$

where $h_n(m_1,\dots,m_n)$ are the kernels of the Volterra series, M is the memory depth, and N is the order of the nonlinearity.

As shown in (2.20), the Volterra model contains huge number of kernels and the calculation of these kernels is even more difficult as they are not linear parameters. The complexity is the main setback of the Volterra series.

There are lots of mathematic researches about the Volterra series [39] that help engineers further evolve the Volterra series. One of the most important simplified Volterra models is the memory polynomial (MP) or parallel Wiener model [40].

As only the diagonal terms of the Volterra series are considered, the memory polynomial is quiet brief and clear. The function (2.21) is the express of memory polynomial:

$$y(t) = \sum_{n=1}^{N}\sum_{m=0}^{M} a_{nm}x(t-m)|x(t-m)|^{n-1} \qquad (2.21)$$

where a_{nm} are the coefficients of the memory polynomial.

The memory polynomial model can also be expressed as a parallel Wiener model [38]. As shown in Figure 2-34, the parallel Wiener model is de-facto same with memory polynomial.

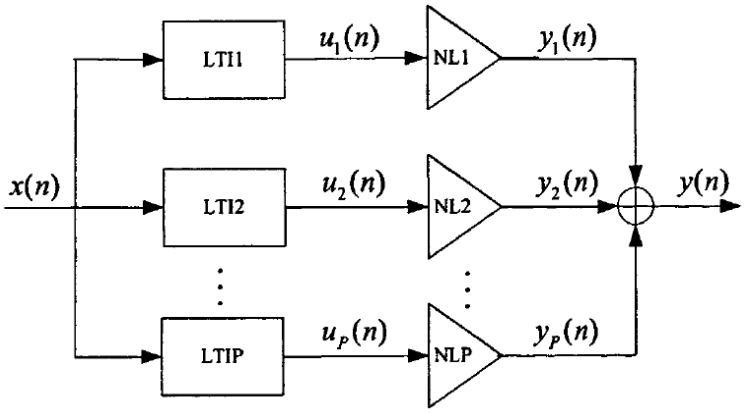

Figure 2-34 Parallel Wiener model

Compared with the classical Volterra series, the memory polynomial model is much more clear and simple. It can be used in most of the nonlinear devices in communication systems. Some memory polynomial based evolvement is also proposed by researchers, like generalized memory polynomial (GMP) [38] and 2D-DPD [41].

GMP adds cross terms adjacent with the diagonal terms. This means the relationship between past signal and its effect on the new signal is not a point-to-point mapping. The effect from a small period of time is also taken into consideration. Figure 2-35 is an illustration of GMP. The mathematical expression of GMP is:

$$\begin{aligned} y(n) = & \sum_{k=0}^{K_a-1}\sum_{l=0}^{L_a-1} a_{kl}x(n-l)|x(n-l)|^k \\ & + \sum_{k=1}^{K_b}\sum_{l=0}^{L_b-1}\sum_{m=1}^{M_b} b_{klm}x(n-l)|x(n-l-m)|^k \\ & + \sum_{k=1}^{K_c}\sum_{l=0}^{L_c-1}\sum_{m=1}^{M_c} c_{klm}x(n-l)|x(n-l+m)|^k \end{aligned} \tag{2.22}$$

where K_aL_a is the number of coefficients of diagonal terms, $K_bL_bM_b$ is the number of coefficients of cross terms between the signal and the lagging envelope, and $K_cL_cM_c$ is the number of coefficients of cross terms between the signal and the leading envelope.

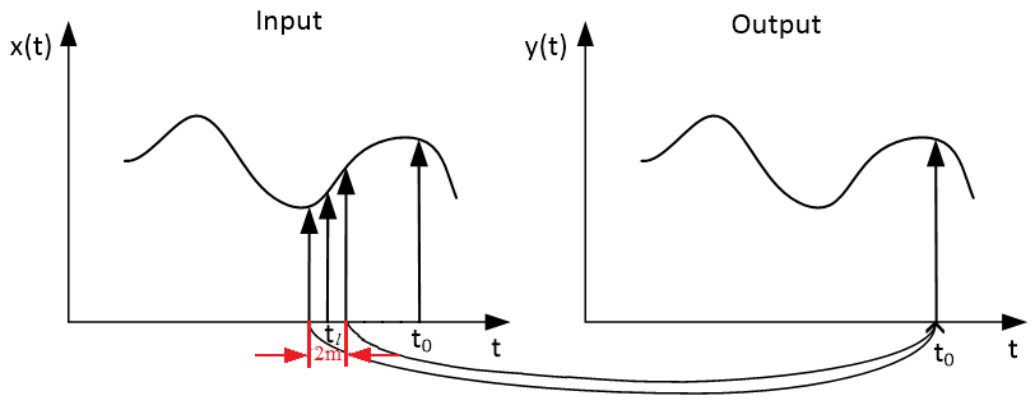

Figure 2-35 the mechanism of GMP

The experiment in [38] shows the GMP is better than MP in eliminating the power leakage in adjacent channels and a 60 dB of dynamic range is achieved.

2D-DPD is a DPD model used in a two-band signal [41]. Compared with other MP based DPD models, 2D-DPD also considers the effect of cross modulation between two signal bands. In 2D-DPD method, two bands of signal are sampled separately as baseband signals, because the gap between two bands is usually more than 100MHz. If sampled together, the signal cannot be considered as a baseband signal anymore. The model of 2D-DPD is expressed as:

$$y_1(n) = \sum_{m=0}^{M-1}\sum_{k=0}^{N}\sum_{j=0}^{k} c_{k,j,m}^{(1)} x_1(n-m) * |x_1(n-m)|^{k-j}|x_2(n-m)|^j$$

$$y_2(n) = \sum_{m=0}^{M-1}\sum_{k=0}^{N}\sum_{j=0}^{k} c_{k,j,m}^{(2)} x_2(n-m) * |x_1(n-m)|^{k-j}|x_2(n-m)|^j \qquad (2.23)$$

where $y_1(n), y_2(n)$ are the complex envelope of the output signals, $x_1(n), x_2(n)$ are the complex envelope of the input signals, and $c_{k,j,m}^{(1)}, c_{k,j,m}^{(2)}$ are the coefficients of this model.

The 2D-DPD is very good at improving the in-band linearity in the two-band scenario. Experiment results show an adjacent channel power ratio of less than -50 dB and a normalized mean square error of less than -40 dB [41].

The DPD can also be divided into baseband DPD and RF DPD according to the operation frequency. Most of the models discussed above, except 2D-DPD, can be used in both baseband DPD and RF DPD. The block diagram of both DPD models are shown in Figure 2-36.

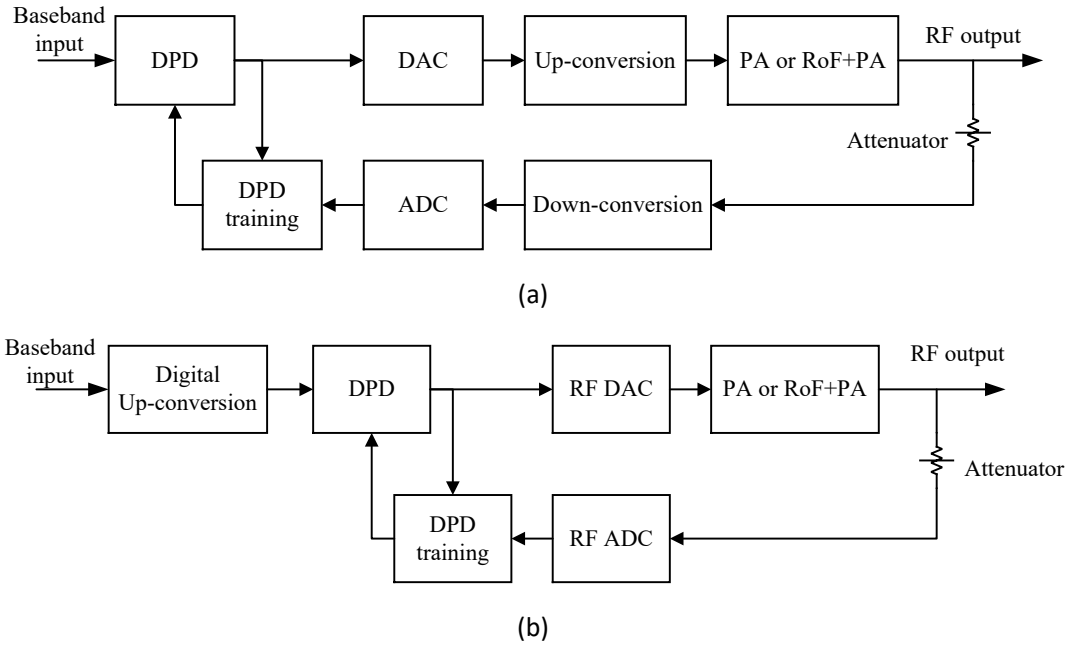

Figure 2-36 Block diagram of baseband DPD (a) and RF DPD (b)

The benefit of RF DPD is that it can compensate IMDs and have a better improvement of ACPR. However, the EVM improvement has a slightly worse performance for the RF DPD. As shown in Figure 2-37 the RF DPD needs a higher memory depth to suppress the long-term memory effect.

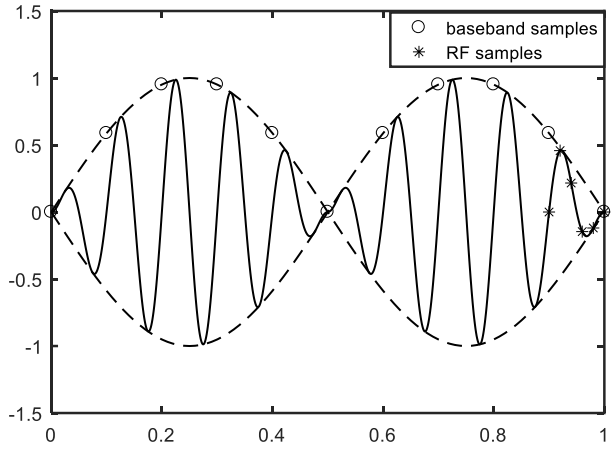

Figure 2-37 Baseband samples and RF samples

So, a novel DPD technique is proposed by W. Tang in [42] which combined baseband DPD and RF DPD together that is called envelope assisted RF DPD. The expression of proposed DPD is:

$$z(n) = \sum_{j=1}^{J}\sum_{p=0}^{P} a_{jp}x(n-p)|x(n-p)|^{j-1} + \sum_{k=1}^{K}\sum_{q=1}^{Q} b_{kq}x(n)|w(n-q)|^{k-1} \quad (2.24)$$

where $z(n)$ is the output of the proposed DPD model, $x(n)$ is the complex value of the RF signal in time domain, $w(n)$ is the sum of the absolute values of the baseband envelopes of each modulating signal, J is the highest nonlinear order of the RF signal, P is the memory depth in RF domain, K is the highest nonlinear order of the baseband signals, Q is the memory depth in baseband domain, and a_{jp} and b_{kq} are the coefficients of the DPD model.

This envelope assisted RF DPD can eliminate IMDs and ACPR. The EVM improvement is also good. In the experiment, the IMD3 is reduced by 12.2 dB, ACPR is reduced by 14.8 dB, and EVM is improved by 6.9 dB [42].

2.6.4 The Indirect Learning

The indirect learning is first developed by [43] to train a multilayered neural network and soon

it is used to calculate coefficients for MP [40]. But it can also be used in modeling nonlinear systems or other circumstances.

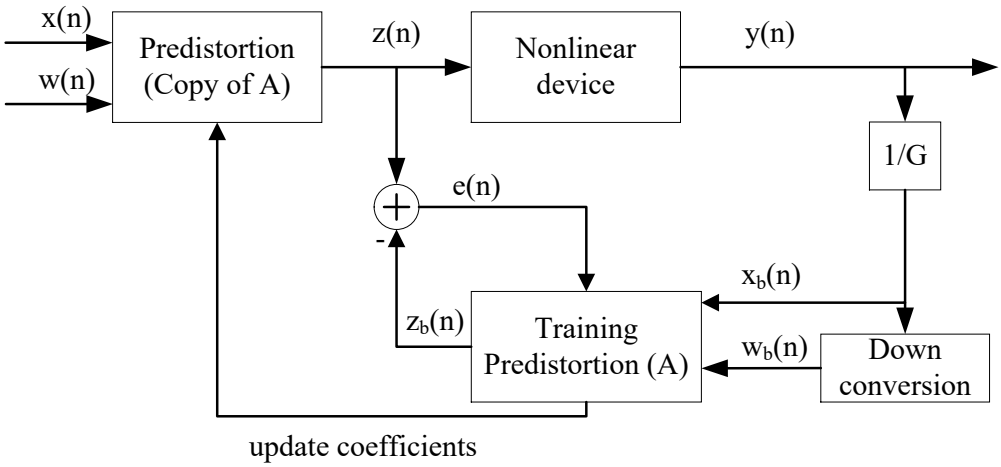

Figure 2-38 Indirect learning structure for DPD

The schematic of indirect learning is shown in Figure 2-38. The RF signal x(n) and baseband envelope w(n) pass through the pre-distortion module. Then the pre-distorted output signal z(n) is fed into the nonlinear device such as the RoF link or power amplifier. The output signal of nonlinear device is sampled by a detector where the G represents the gain of the nonlinear device. After attenuation, the RF signal $x_b(n)$ and baseband envelope $w_b(n)$ pass through the training pre-distortion module (A) in the feedback loop. It is identical to the pre-distortion module in the forward loop. The output signal $z_b(n)$ is expected to be equal with z(n). The error between $z_b(n)$ and z(n) is recorded as e(n). With the help of e(n), the training pre-distortion could calculate the coefficients of the DPD model and copy them to pre-distortion model. After several loops, the $z_b(n)$ should equal to z(n). Therefore, the system is linearized.

Chapter 3 Theoretical Analysis of Proposed Linearization Method

In this chapter, the theoretical analysis is presented. The block diagram of the system is shown in Figure 3-1. Fist the model of RoF system and PA used in design and simulation are introduced. Then, the combination of APD and DPD technique is also introduced and proved mathematically in this chapter.

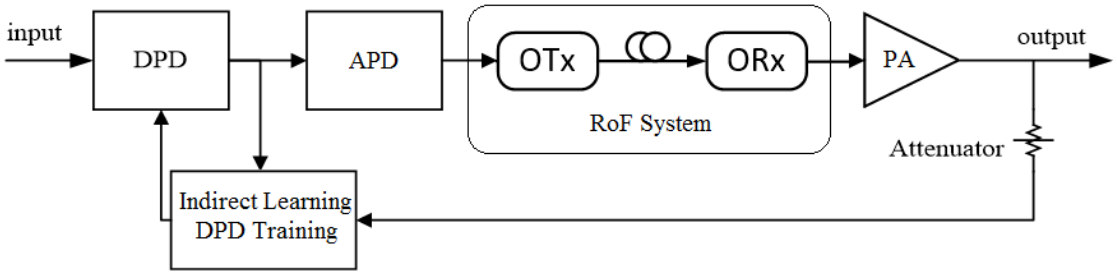

Figure 3-1 Brief block diagram of the test system

In Figure 3-1, the DPD represent the digital pre-distortion module, APD represent analog pre-distortion circuit. OTx is the optical transmitter. ORx is the optical receiver. The PA is the radio-frequency power amplifier.

3.1 Model of Radio-over-Fiber System

Building up a model is always the first step to analyze a system. In the original system without linearization devices, there are two nonlinearity generators, one is RoF system and the other is PA. In this section, the model of RoF system is described.

Both circuit model and behavior model can be used for RoF systems. However, the circuits of OTx and ORx are too complex. Therefore, the behavior model was applied to describe the real devices. As discussed in Chapter 2, the DPD model can be used in both describing and linearizing the system. Therefore, in the simulation, the envelope assisted RF DPD model is used to describe

the RoF system. Although in [42] the envelope assisted RF DPD is proposed for PA, it can still be used in most of the nonlinear systems including RoF system.

As described in chapter 2.6.3, the mathematical expression of the envelope assisted RF DPD is shown in formula (2.24). If we rewrite the formula with:

$$u_{jp}(n) = x(n-p)|x(n-p)|^{j-1} \tag{3.1}$$

and

$$v_{kq}(n) = x(n)|w(n-q)|^{k-1} \tag{3.2}$$

The new expression will be:

$$z(n) = \sum_{j=1}^{J}\sum_{p=0}^{P} a_{jp}u_{jp}(n) + \sum_{k=1}^{K}\sum_{q=1}^{Q} b_{kq}v_{kq}(n) \tag{3.3}$$

which can also be transformed into vectors as:

$$z(n) = \left[u_{10}(n), \dots, u_{1P}(n), \dots, u_{J0}(n), \dots, u_{JP}(n), v_{11}(n), \dots, v_{1Q}(n), \dots, v_{K1}(n), \dots, v_{KQ}(n)\right]\alpha \tag{3.4}$$

where $\alpha = \left[a_{10}, \dots, a_{1P}, \dots, a_{J0}, \dots, a_{JP}, b_{11}, \dots b_{1Q}, \dots, b_{KQ}\right]^T$.

In a transmitted signal, enormous points are sampled from the signal depending on the length of the signal. Assuming the number of samples is N, the (3.4) is a matrix as：

$$\begin{bmatrix} z(1) \\ z(2) \\ \vdots \\ z(N) \end{bmatrix} = \begin{bmatrix} u_{10}(1) & \cdots & u_{JP}(1) & v_{11}(1) & \cdots & v_{KQ}(1) \\ u_{10}(2) & \cdots & u_{JP}(2) & v_{11}(2) & \cdots & v_{KQ}(2) \\ \vdots & \ddots & \vdots & \vdots & \ddots & \vdots \\ u_{10}(N) & \cdots & u_{JP}(N) & v_{11}(N) & \cdots & v_{KQ}(N) \end{bmatrix}\alpha \tag{3.5}$$

which can be simplified as:

$$Z = U\alpha \tag{3.6}$$

For the backward DPD, the input is the attenuated output signal $x_b(n)$ and the output signal is $z_b(n)$. We can derive a similar expression between $x_b(n)$ and $z_b(n)$:

$$Z_b = U_b\alpha \tag{3.7}$$

To calculate the difference between the output signal Z_b and original signal Z, LSM is used for estimating the coefficients. The formula of LSM is shown as:

$$\hat{\alpha} = \left({U_b}^H U_b\right)^{-1} {U_b}^H Z \tag{3.8}$$

Therefore, the coefficients of the RoF model is calculated.

In this procedure, a random LTE (64QAM-OFDM) signal, which is the same to the signal used in the simulation and experiment, is the input of the RoF system as U. The output signal is recorded and processed as Z. The input power of RF signal is set to -17.6 dBm same to the simulation and experiment. The carrier frequency of RF signal is 850 MHz which is the average carrier frequency of simulation and experiment. The bandwidth of input signal is 20MHz. The sampling rate is 10.32192 Gs/s, which is high enough to cover the signal and its distortion components like IMD3 and Harmonics. The model coefficients α is calculated with (3.8).

3.2 Model of Power Amplifier

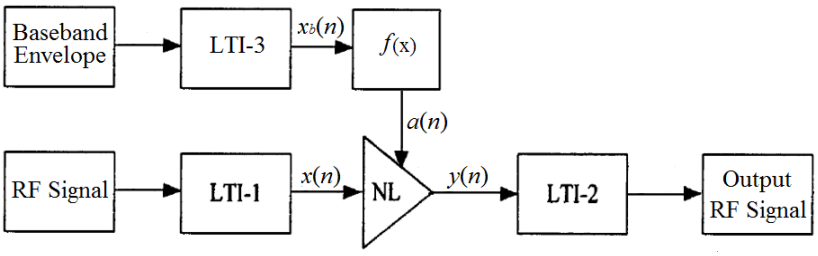

Figure 3-2 Evolved Wiener-Hammerstein PA model

As mentioned in Chapter 2.6.3, a Wiener-Hammerstein model is used in PA model. But a traditional Wiener-Hammerstein model cannot generate short-term or long-term memory effect simultaneously. So an evolved Wiener-Hammerstein model is proposed in [42] by W. Tang. The

Figure 3-2 shows the block diagram of proposed PA model.

The LTI-1, NL and, LTI-2 form the traditional Wiener-Hammerstein model. In the real devices, the LTI-1 and LTI-2 can be considered as a matching network. They will introduce short-term distortion. In this model, the LTI-1 and LTI-2 are finite impulse response filter (FIR). The impulse response of the LTI-1 and LTI-2 is:

$$H(z) = 0.1 + 0.4z^{-1} + 0.25z^{-2} + 0.15z^{-3} + 0.1z^{-4} \tag{3.9}$$

Figure 3-3 is the magnitude-frequency and phase-frequency characteristic curve of LTI-1 and LTI-2.

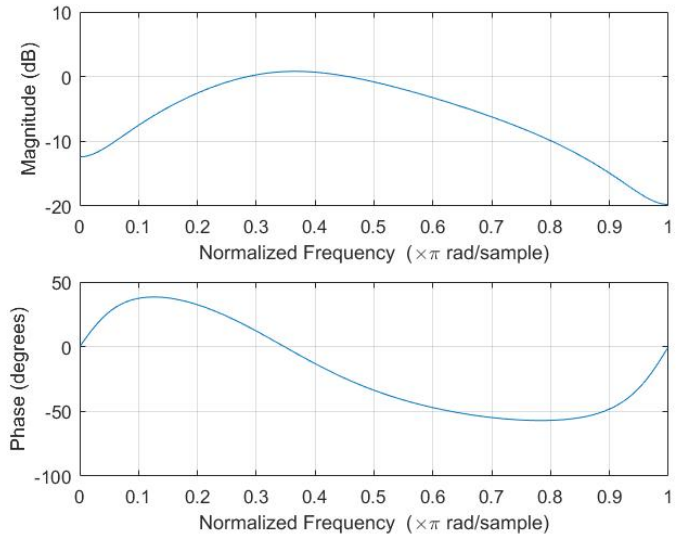

Figure 3-3 Magnitude-frequency and phase-frequency characteristic curve of LTI-1 and LTI-2

The NL will generate quiescent nonlinearity with the expression:

$$y(n) = b\left(1 - exp\left(-x(n)/a\,(n)\right)\right) \tag{3.10}$$

where $a(n)$ is the control signal generated by mapping function $f(x)$ from $x_b(n)$, b is a constant to adjust the power level.

The LTI-3 is used to generate long-term distortion, which is built up with an infinite impulse response filters (IIR). The impulse response of LTI-3 is:

$$H(z) = \frac{1-0.5z^{-1}+0.25z^{-2}}{0.5-0.32z^{-2}} \tag{3.11}$$

Figure 3-4 is the magnitude-frequency and phase-frequency characteristic curve of LTI-3.

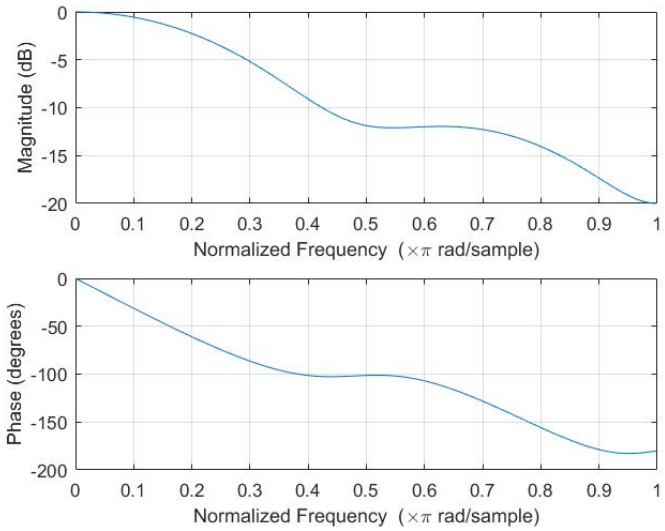

Figure 3-4 Magnitude-frequency and phase-frequency characteristic curve of LTI-3

The output of the LTI-3 is mapped into a control signal $a(n)$ by function:

$$a(n) = 10 - 2\exp(-x_b(n)/c) \tag{3.12}$$

where 'c' is a constant to change the shape of the curve. The $a(n)$ is used to adjust the characteristic of NL by function (3.10). Therefore, long-term memory effect is merged into the RF signal.

The overall input-output curve of the quiescent nonlinearity is shown in Figure 3-5.

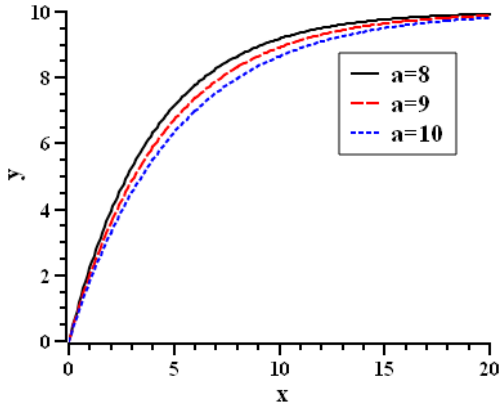

Figure 3-5 Overall input-output curve of the quiescent nonlinearity [42]

3.3 Combination of Analog and Digital Pre-Distortion Technique

As discussed before, the APD can only compensate the quiescent nonlinearity in the RoF system. The APD method has a great advantage in eliminating the IMDs, but can do nothing with memory effect. On the other hand, the baseband DPD can only deal with the in-band distortion caused by memory effect and quiescent nonlinearity. But baseband DPD cannot compensate out-of-band distortions like IMDs or harmonics. RF DPD can improve EVM, ACPR, and IMDs simultaneously, but requires a costly detector with ultra-high sampling rate. So, in the proposed combined linearization of both analog and digital pre-distortion, two advanced PD methods are combined together to compensate both in-band and out-of-band distortion caused by quiescent nonlinearity and memory effect simultaneously.

In this section, an APD [29] used in the proposed linearization method is introduced firstly. Next, the 2D-DPD method is also introduced. In the end, the benefits of combined PD method are analyzed.

3.3.1 Principle of Analog Pre-distortion

In [29] an advanced APD circuit is proposed, manufactured, and tested by S. Saha. The schematic of APD is already presented in Figure 2-30.

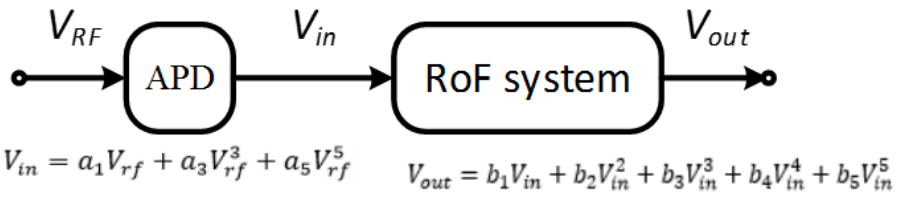

Figure 3-6 Relationship between PDC and RoF System [29]

The Figure 3-6 shows the details of expressions in the APD and RoF system. The output of APD circuit is directly fed into RoF system. In the APD, the anti-parallel structure of the diodes eliminated the even order distortions, only the odd orders are transmitted into the RoF system. The overall expression of V_{out} is:

$$V_{out} = a_1b_1V_{rf} + a_1^2b_2V_{rf}^2 + (a_3b_1 + a_1^3b_3)V_{rf}^3 + (a_1^4b_4 + 2a_1a_3b_2)V_{rf}^4$$

$$+ (a_5b_1 + 3a_1^2a_3b_3 + a_1^5b_5)V_{rf}^5 \quad (3.13)$$

the coefficient of IMD3 is $(a_3b_1 + a_1^3b_3)$, the coefficient of IMD5 is $(a_5b_1 + 3a_1^2a_3b_3 + a_1^5b_5)$. Then, in order to suppress the IMD3 and IMD5, their coefficients should be zero, which is:

$$\frac{a_1^3}{a_3} = -\frac{b_1}{b_3} \quad (3.14)$$

$$b_1 + 3a_1^2a_3b_3 + a_1^5b_5 = 0 \quad (3.15)$$

The coefficients of RoF is measured by the author of [29]. Therefore, the value of b_1, b_3 and b_5 is determined, and the a_1 and a_3 can be calculated from them. Thus, the settings of APD circuit can be calculated and simulated as a_1 and a_3 are known. The Figure 3-7 shows the overall equivalent circuit of proposed APD.

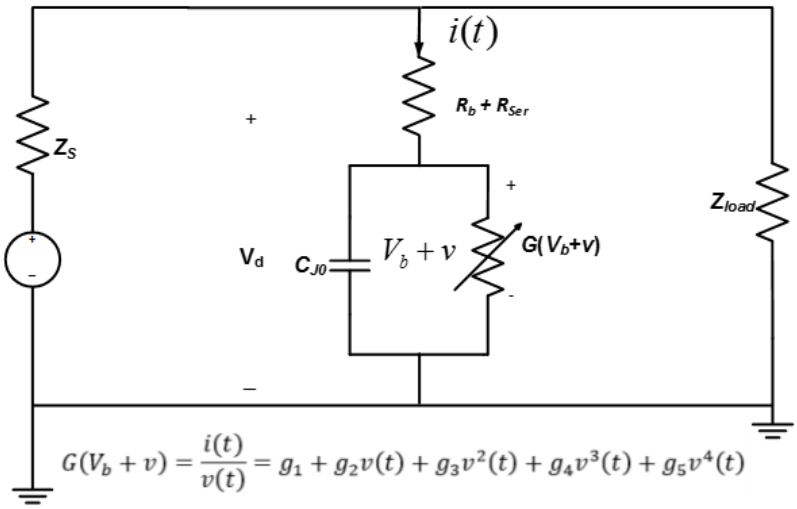

Figure 3-7 The diode equivalent circuit along with series resistance in the pre-distortion circuit

The diode used in the APD circuit is HSCH-5314 [44]. The data sheet of HSCH-5314 is shown in Table 3-1:

Table 3-1 Data sheet of HSCH-5314 [44]

B_V (V)	I_{BV} (A)	I_S(A)	C_{j0}(pF)	E_G(eV)	N	R_s(Ω)	P_B (V)	P_T	M
5	10E-5	3x10E-10	0.13	0.69	1.08	9	0.65	2	0.5

As all the parameter is known, the author of [29] carefully calculated and simulated the circuit, to achieve equation (3.12) and (3.13).

The experiment shows a 7.5 dB improvement in SFDR and 1.7 dB improvement in EVM [29].

3.3.2 Principle of Digital Pre-distortion

The 2D-DPD and RF DPD are adopted in the proposed pre-distortion method. The RF DPD is a memory polynomial based DPD function and requires a detector and A/D convertor with high sampling rate. The 2D-DPD is an evolved memory polynomial function specifically designed for two-band scenarios. Both 2D-DPD and RF DPD is analyzed and simulated during the research.

They share similar properties. So, in this section, 2D-DPD is explained in detail as example. Same procedure is also applicable to RF DPD.

The 2D-DPD is an evolvement of memory polynomial especially designed for two-band signal [41]. The traditional memory polynomial cannot deal with cross effects between two bands. But in the real system, two bands affect each other in both quiescent nonlinearity and memory effect. So 2D-DPD is a more accurate technique to suppress the nonlinearity. The mathematic expression of 2D-DPD is:

$$y_1(n) = \sum_{m=0}^{M-1} \sum_{k=0}^{N} \sum_{j=0}^{k} c_{k,j,m}^{(1)} x_1(n-m) * |x_1(n-m)|^{k-j} |x_2(n-m)|^j$$

$$y_2(n) = \sum_{m=0}^{M-1} \sum_{k=0}^{N} \sum_{j=0}^{k} c_{k,j,m}^{(2)} x_2(n-m) * |x_1(n-m)|^{k-j} |x_2(n-m)|^j \qquad (3.16)$$

where $y_1(n), y_2(n)$ are the complex envelopes of the output signals, $x_1(n), x_2(n)$ are the complex envelopes of the input signals, and $c_{k,j,m}^{(1)}, c_{k,j,m}^{(2)}$ are the coefficients of this model. As shown in (3.16), all the coefficients are linear, so they can be calculated by indirect learning procedure with LSM.

The 2D-DPD can significantly improve the EVM performance in a two-band signal, in some cases the ACPR is also improved.

3.3.3 Combination of Analog and Digital Pre-distortion

The APD and DPD both have advantages and disadvantages which are complementary. It must be a good idea to combine them together. So, in this thesis a new linearization method is proposed, which is called: combined linearization of both analog and digital pre-distortion. As shown in Figure 3-1, the DPD and APD is applicated in series. An enlarged block diagram is shown in Figure 3-8.

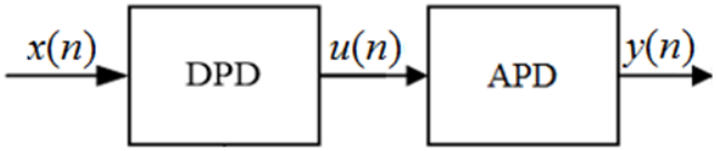

Figure 3-8 Relationship between DPD and APD

The APD is a nonlinear memoryless circuit. So, it can be expressed by a polynomial model as formula (2.10). The DPD model can be any model that can compensate memory effect. In this case, it is 2D-DPD. So, the relationship between $u(n)$, $x(n)$, and $y(n)$ should be:

$$u(n) = f\big(x(n)\big) \tag{3.17}$$

$$y(n) = h\big(u(n)\big) = \sum_{k=0}^{K} a_k u(n)|u(n)|^k \tag{3.18}$$

substitute Formula (3.17) into Formula (3.18):

$$y(n) = \sum_{k=0}^{K} a_k f\big(x(n)\big)\big|f\big(x(n)\big)\big|^k \tag{3.19}$$

where $f(x)$ is a DPD function containing both quiescent nonlinearity and memory effect. As the expression of $y(n)$ is too complex, no useful properties can be found from it. Therefore, it is needed to simplify the expressions with an engineering method.

First, we defined that the nonlinearity part of $f(n)$ is $e(n)$. Therefore, $u(n)$ can be expressed as:

$$u(n) = bx(n) + e\big(x(n)\big) \tag{3.20}$$

where b is a constant and $e\big(x(n)\big)$ contains all the quiescent nonlinearity and memory effect of DPD model.

Then, substituting (3.20) into (3.18) leads to:

$$y(n) = h\big(bx(n) + e(n)\big) = \sum_{k=0}^{K} a_k (bx(n) + e(n))|bx(n) + e(n)|^k \tag{3.21}$$

As $y(n)$ is a nonlinear time invariant formula, we can use distributive law and add the error

caused by the nonlinearity of $y(n)$, then $y(n)$ will be:

$$y(n) = h\big(bx(n)\big) + h\big(e(n)\big) + e'(n)$$
$$= b^{K+1}\sum_{k=0}^{K} a_k x(n)|x(n)|^k + \sum_{k=0}^{K} a_k e(n)|e(n)|^k + e'(n) \quad (3.22)$$

where $e'(n)$ is the error caused by the linear distributive law.

As b is a constant and approximately one, the first term of $y(n)$ is exactly the APD model. The second and third term of $y(n)$ is a nonlinearity polynomial with memory effect, which can be expressed by a DPD model, like MP, GMP, or 2D-DPD. Therefore, the whole system with both APD and DPD can be written in a parallel form. As the DPD technique used in this thesis is 2D-DPD, the model of proposed linearization method is:

$$y_1(n) = \sum_{m=0}^{M-1}\sum_{k=0}^{N_1}\sum_{j=0}^{k} c_{k,j,m}^{(1)} x_1(n-m) * |x_1(n-m)|^{k-j}|x_2(n-m)|^j$$
$$+ \sum_{k=0}^{N_2}\sum_{j=0}^{k} d_{k,j}^{(1)} x_1(n) * |x_1(n)|^{k-j}|x_2(n)|^j$$

$$y_2(n) = \sum_{m=0}^{M-1}\sum_{k=0}^{N_1}\sum_{j=0}^{k} c_{k,j,m}^{(2)} x_2(n-m) * |x_1(n-m)|^{k-j}|x_2(n-m)|^j$$
$$+ \sum_{k=0}^{N_2}\sum_{j=0}^{k} d_{k,j}^{(2)} x_2(n) * |x_1(n)|^{k-j}|x_2(n)|^j \quad (3.23)$$

where $d_{k,j}$ are coefficients which is decided by the APD circuit.

Within Formula (3.23), the first term is the original 2D-DPD model. The second term is a memoryless polynomial which is used to describe the APD circuit with the cross effect between two bands. As two parts are parallel, they are simply added together.

From Formula (3.23), it is obvious that the expression of APD is the same to DPD formula when the memory depth is set to zero. The coefficients of APD is carefully designed that can compensate quiescent nonlinearity. And the DPD coefficients are calculated to eliminated both

memory effect and quiescent nonlinearity. If the coefficients of DPD is calculated after the APD is added to the system, the $c_{k,j,0}$ should have the same sign with $d_{k,j}$. Then the APD and DPD can work together to further reduce the EVM.

In the frequency domain, the overall effect of the system can also be considered as a sum of affects generated by the APD and DPD. As the DPD method is a baseband 2D-DPD, it can compensate ACPR in some cases. The APD can deal with the out-of-band distortions like IMD3. These effects can be combined to further suppress the signal leaking.

It is proved mathematically that the proposed linearization method can combine the benefit of DPD and APD together.

Chapter 4 Simulation with Combined Analog and Digital Pre-Distortion Method

The proposed linearization method is simulated in MATLAB and ADS. The MATLAB is used to generate LTE signals, build up nonlinearity models, operate DPD procedures, and measure the results. The APD is simulated in ADS with parameters determined by a fabricated APD circuit. The optimal memory depth is found firstly. The simulation is operated with two-band and three-band LTE signals, with a bandwidth of 20MHz for each band.

4.1 Overview of Simulation System

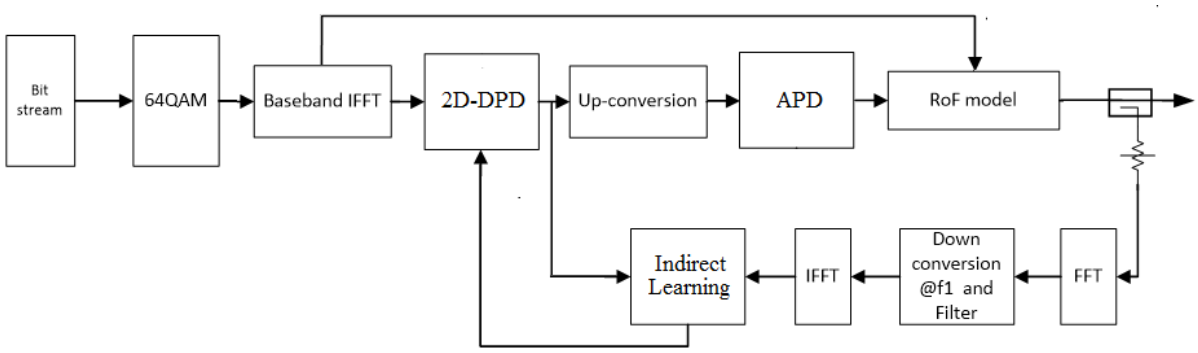

Figure 4-1 The structure of proposed linearization method with 2D-DPD

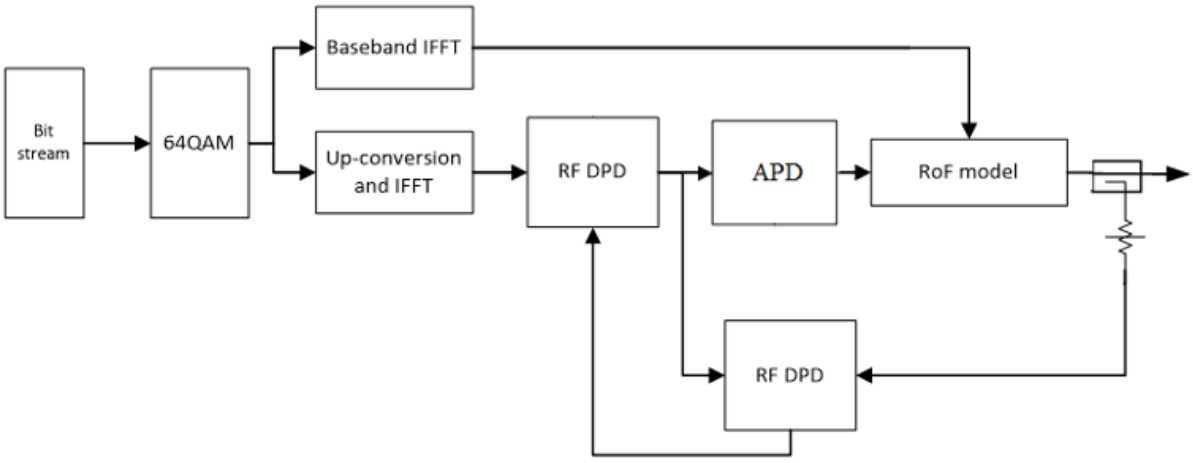

Figure 4-2 The structure of proposed linearization method with RF DPD

In two-band simulations, the 2D-DPD is adopted as DPD method, the structure is shown in Figure 4-1. The output of a random bit stream generator is directly modulated by 64QAM. The output of 64QAM is a standard 20 MHz LTE signal. The output of 64QAM is a frequency-domain signal and is transformed into time-domain by iFFT. Then the time-domain base-band signal is processed by 2D-DPD model and up-converted to RF band. This RF band time-domain signal is then pass through a APD circuit and RoF system. The output signal is sampled by an RF detector. The detected signal is transformed back to time-domain and down-converted. The base-band signal is transformed back to frequency-domain which is used in indirect learning structure to calculate the coefficients of 2D-DPD.

But the 2D-DPD is proposed specifically for two-band signals, it cannot be used in the three-band simulations or experiments. So, in three-band simulations and experiments, the RF DPD is adopted as DPD method. The structure of RF DPD is similar with base-band DPD. The only difference is that all the DPD and indirect learning structure is operated in RF band. Therefore, in Figure 4-2, the RF DPD module is located after up-conversion and the indirect learning structure does not contain down-conversion procedures.

The model of APD is designed by S. Saha in [29]. The fabricated APD circuit of [29] is also used in the experiment.

In each simulation and experiment case, four circumstances are considered. The original system without neither APD nor DPD, the system with APD-only or DPD-only, and the system with proposed APD and DPD method. These circumstances compared with each other according to the EVM, ACPR, and IMD3 improvement.

In the simulation, a 64QAM-OFDM LTE signal is used. A random bit stream is feed in to the system and is modulated by 64QAM modulators. After modulation, bits are modulated to 64 constellation symbols. Each symbol represents a complex value of the subcarrier which has a bandwidth of 15 kHz. Therefore, these digital symbols are allocated onto the subcarriers in

frequency domain. One inverse fast Fourier transform (iFFT) is used to converts the signal from frequency domain to time domain. For a 20 MHz LTE signal, there are 100 resource blocks allocated for transmitting control signals and data. Each resource block contains 12 subcarriers occupying a bandwidth of 180 KHz. Therefore, 1200 subcarriers are used to transfer a 20 MHz LTE signal. The iFFT size is 2048, corresponding to a baseband sampling frequency of 30.72 MHz. The size of the RF iFFT is 262144, corresponding to a RF sampling frequency of 3.93216 GHz. Cyclic prefix has been added to the baseband and RF signals in time domain. The length of the cyclic prefix is 4.7 μs for each OFDM symbol, as defined in the LTE standard, corresponding to 143 samples of the baseband signal and 18304 samples of the RF signal.

4.2 The Optimal Memory Depth in Simulation

All the DPD functions have two important parameters: the order number and the memory depth. In a general communication system, sixth order distortion is always below the noise level. So, the Order number is set to five in the simulation and experiment. The memory depth is the property decided by nonlinear systems. The optimal memory depth of the DPD should be found to achieve best performance.

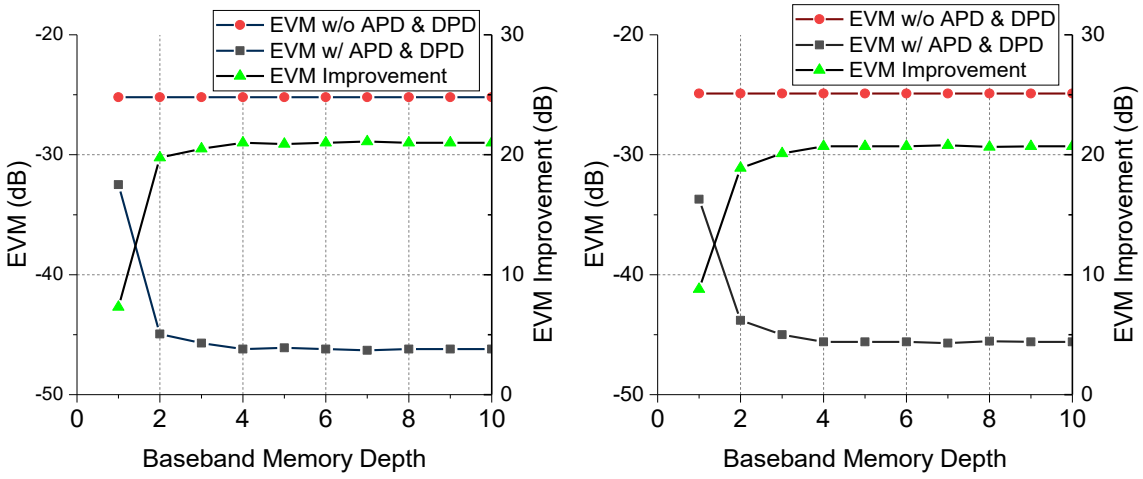

Figure 4-3 The relationship between EVM improvement and memory depth in 2D-DPD

As shown in Figure 4-3, the EVM improvement stops increasing after memory depth larger

than 4 in both bands. So, the memory depth of 2D-DPD is set to four.

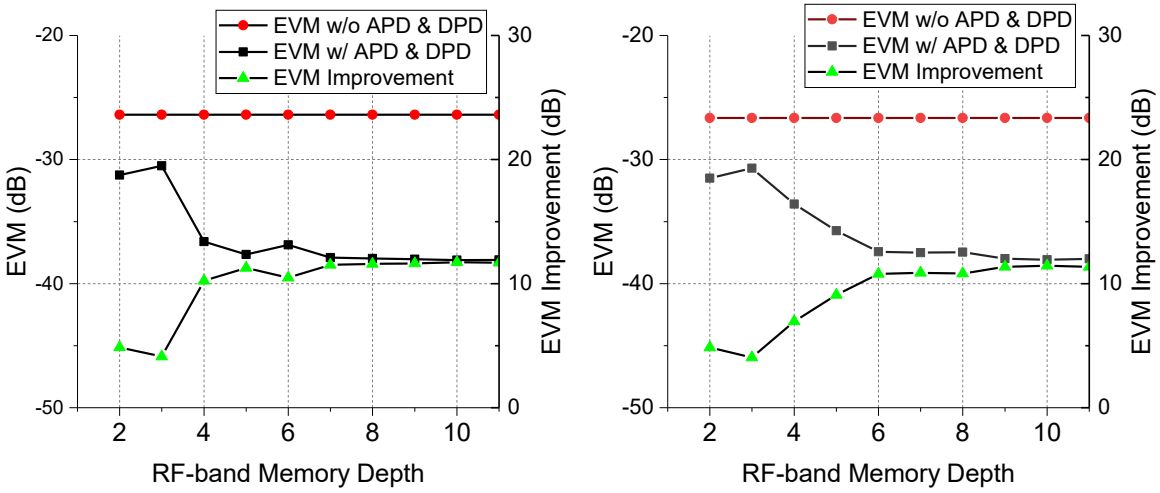

Figure 4-4 The relationship between EVM improvement and memory depth in RF DPD

Same test is also applicated to RF DPD in order to find the memory depth used in three-band case. The Figure 4-4 shows that the memory depth saturate at nine. So, the memory depth of RF DPD is set to nine.

4.2.1 Case one: LTE 1 @800MHz and LTE 2 @900MHz

In case one, two 20MHz bandwidth LTE signals located at 800MHz and 900MHz are transmitted through the simulation system. The performance is measured and calculate in four circumstances: without neither APD nor DPD, with APD only, with DPD only, and with both APD and DPD. Following are the results.

Figure 4-5 shows the output and input spectrum of the system in different settings. The black line is the original signal which is the input of the system. The red line represents the output signal without linearization techniques applicated. The blue and green line represent the output of DPD only or APD only. The purple line shows the output of the proposed PD method, which used a combined APD and DPD technique.

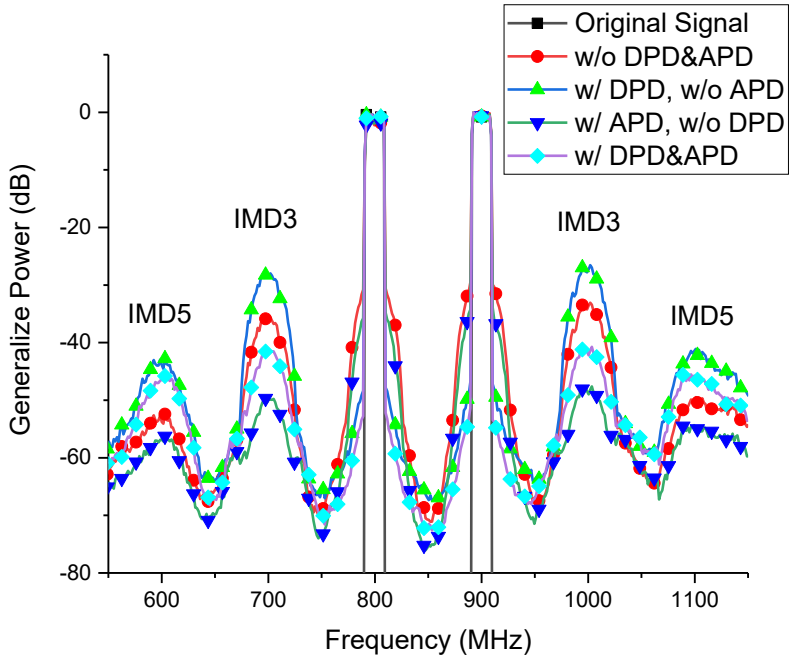

Figure 4-5 Output spectrum from 500MHz to 1200 MHz (case one)

From Figure 4-5, it is obvious that if only 2D-DPD technique is applicated, the IMD3 and IMD5 is increased. As the nonlinearity in the simulated PA model is too severe, the signal power is reduced higher than IMD3 power. This phenomenon will not occur in the experiment, because the nonlinearity of devices is slitter than simulation models. This phenomenon also happens in other cases and will not be explained again.

The IMD3 located at 700 MHz and 1000 MHz is decreased when APD circuit is added to system. It can reduce 15.4 dB when only APD is added, and 4.6 dB when both APD and DPD is used. The IMD5 located at 600 MHz and 1100 MHz is also reduced by APD circuit. The IMD5 in the simulation system has two sources. It can be the IMD5 of RoF or PA model generated form two signal bands, and it also can be the IMD3 of PA model generated from the IMD3 of RoF system and one band. However, as the IMD5 is increased by the 2D-DPD, the overall IMD5 of the proposed PD is even higher than the original signal. So, the IMD5 is not discussed in the simulation.

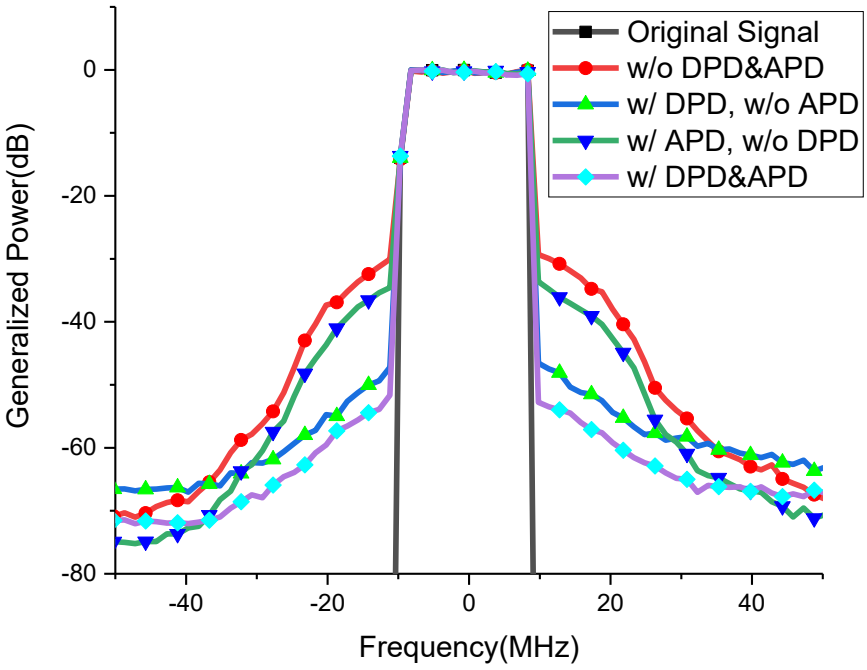

Figure 4-6 Spectrum around lower-band @800MHz in (case one)

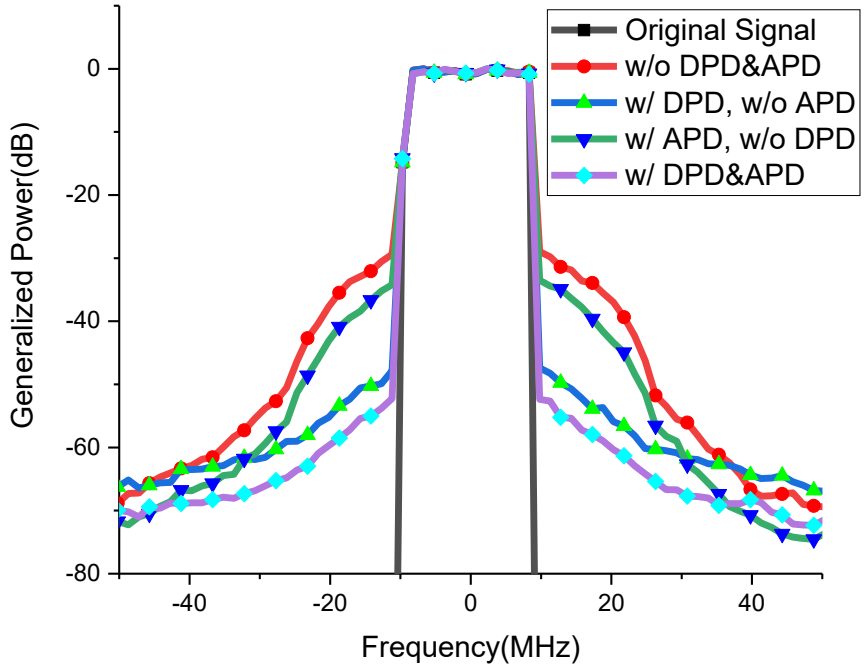

Figure 4-7 Spectrum around upper-band @900MHz in (case one)

The Figure 4-6 and Figure 4-7 shows the enlarged signal concentrated on the signal bands.

It is clear that both APD and 2D-DPD can reduce the ACPR. And they can make together to further reduce the ACPR. The result shows a 23.6 dB improvement with proposed linearization, 4.7 dB improvement with APD, and 19.4 dB improvement with 2D-DPD.

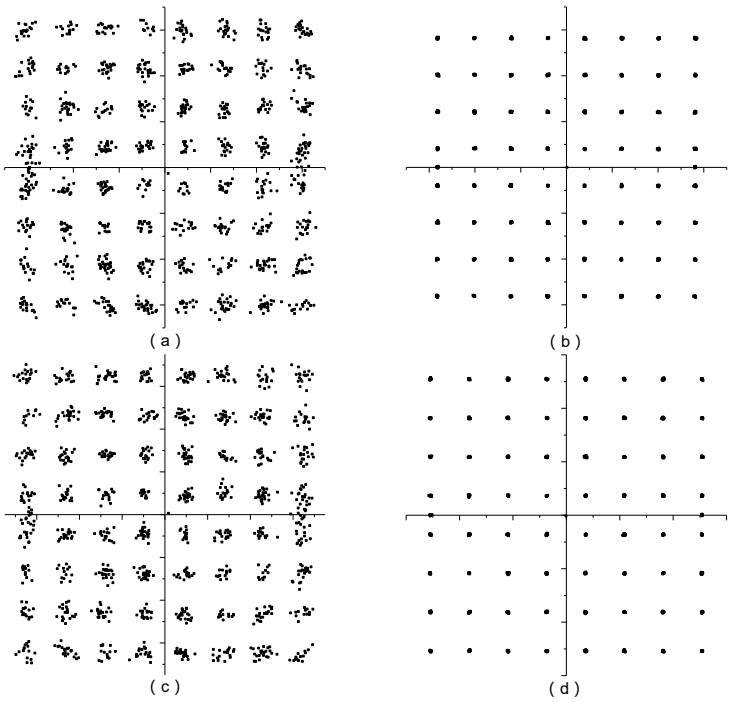

Figure 4-8 Constellation of signal in lower-band with (a) neither APD nor DPD, (b) with only 2D-DPD, (c) with only APD, (d) with both APD and DPD (case one)

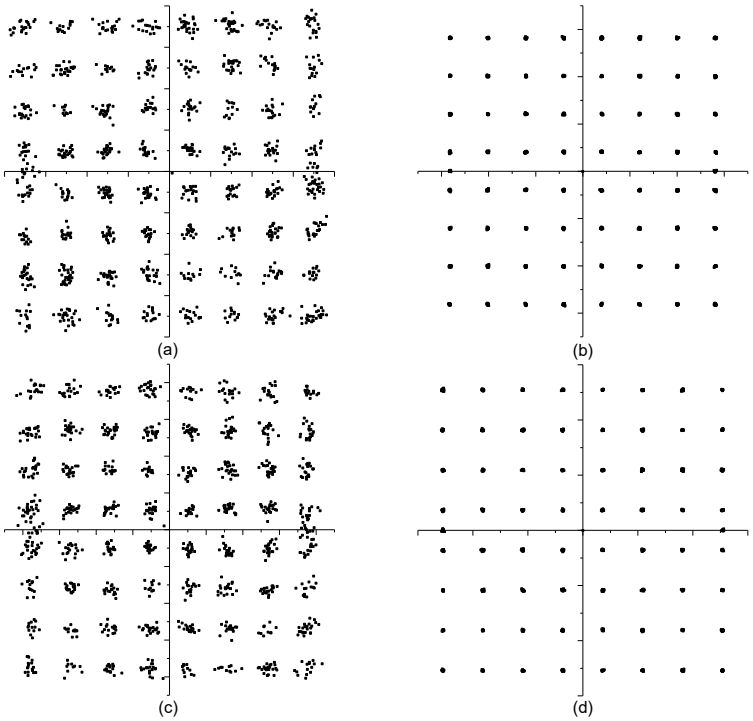

Figure 4-9 Constellation of signal in lower-band with (a) neither APD nor DPD, (b) with only 2D-DPD, (c) with only APD, (d) with both APD and DPD (case one)

The Figure 4-8 is the constellations of the LTE signal @800MHz. It shows the results with neither APD nor DPD, with only 2D-DPD, with only APD, and with proposed linearization separately. The EVM of these results are -25.2 dB, -46.2 dB, -26.3 dB, and -46.5 dB correspondingly.

Similar with lower-band, the upper-band shows the same results in Figure 4-9. The EVM of the output signals with neither APD nor DPD, with only 2D-DPD, with only APD, and with proposed linearization are -24.9 dB, -45.6 dB, -26.1 dB, and -45.7 dB correspondingly.

In these constellations, both APD and DPD can improve the EVM, but the performance of the 2D-DPD is much better. Besides, comparing the 2D-DPD with proposed combined PD, the improvement of EVM is almost the same because the improvement is almost saturated with 2D-DPD. Even the APD is added, the improvement is not obvious.

4.2.2 Case two: LTE 1 @800 MHz and LTE 2 @840 MHz

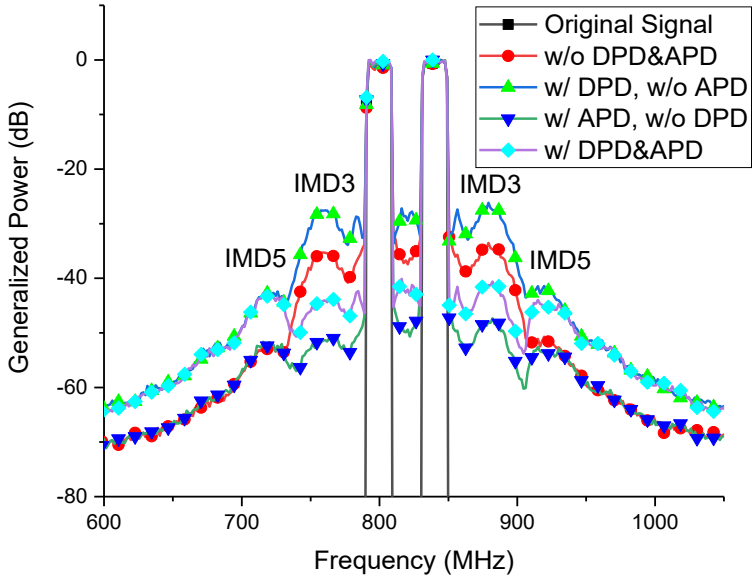

Figure 4-10 Output spectrum from 500MHz to 1050 MHz (case two)

In this case, two LTE signals are located much closer to each other, one is at 800 MHz, the other is at 840 MHz. the bandwidth of LTE signal is 20 MHz. The spectrum from 600 MHz to 1050 MHz is shown in Figure 4-10. Same to case one, the 2D-DPD used in this case still increases the IMD3, while the APD circuit can suppress it. Therefore, the overall improvement of IMD3 of proposed linearization is only 9.8 dB.

The enlarged spectrums around two LTE signals are shown in Figure 4-11 and Figure 4-12. The ACPR is increased by 5 dB with 2D-DPD, and is reduced by 13.9 dB with APD. The proposed linearization can improve ACPR by 9.5 dB.

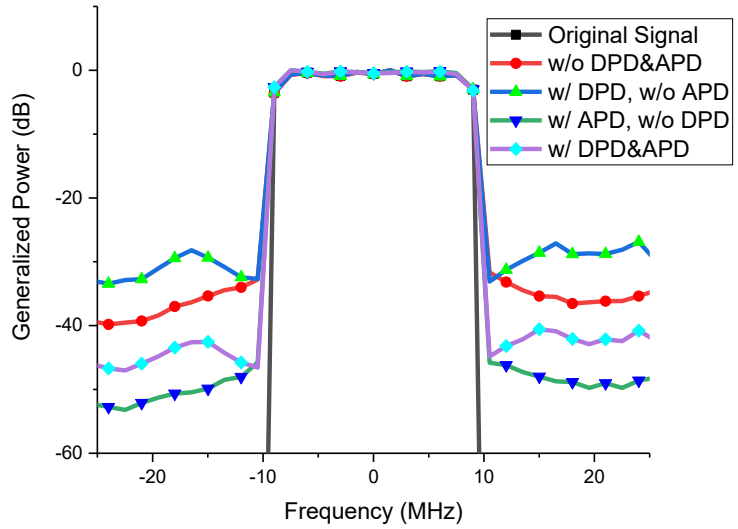

Figure 4-11 Spectrum around the lower-band in simulation (case two)

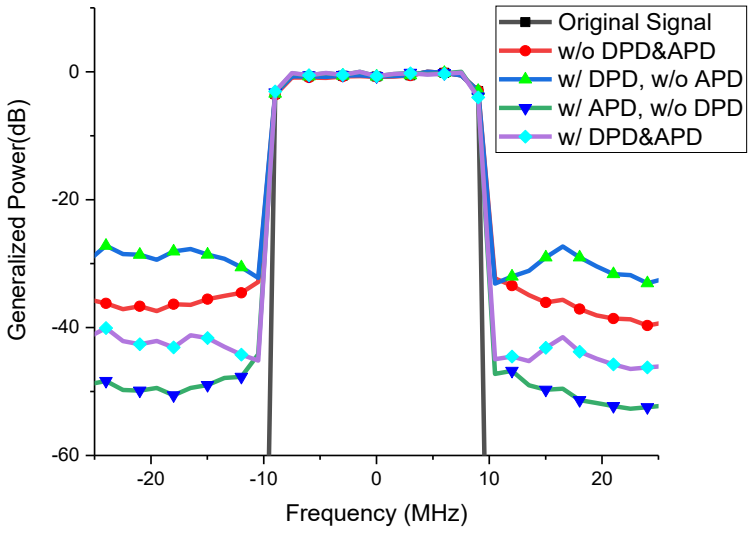

Figure 4-12 Spectrum around the upper-band in simulation (case two)

The constellations of case two is also calculated. As shown in Figure 4-13 and Figure 4-14, the EVM improvement in lower-band is 10.7 dB with 2D-DPD, 0.6 dB with APD, and 11.4 dB with proposed PD. The EVM improvement in upper-band is 10.9 dB with 2D-DPD, 0.3 dB with APD and 11.2 dB with proposed PD.

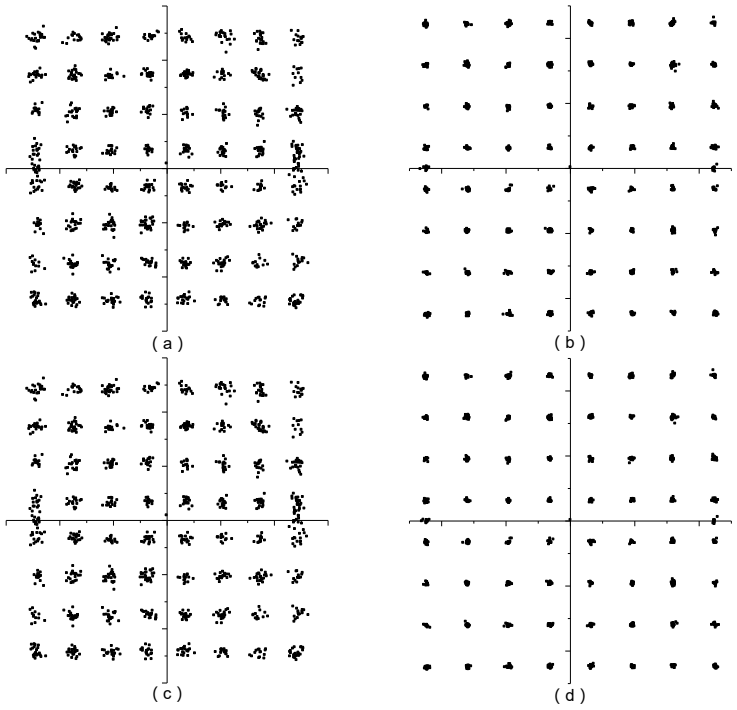

Figure 4-13 Constellation of signal in lower-band with (a) neither APD nor DPD, (b) with only 2D-DPD, (c) with only APD, (d) with both APD and DPD (case two)

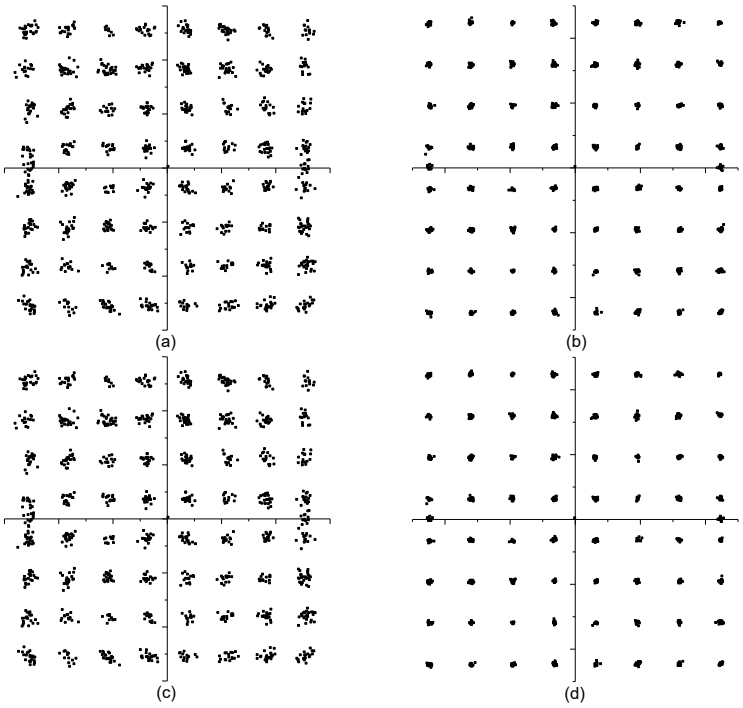

Figure 4-14 Constellation of signal in upper-band with (a) neither APD nor DPD, (b) with only 2D-DPD, (c) with only APD, (d) with both APD and DPD (case two)

4.2.3 Case Three: LTE 1 @800MHz, LTE 2 @850MHz, and LTE 3 @900MHz

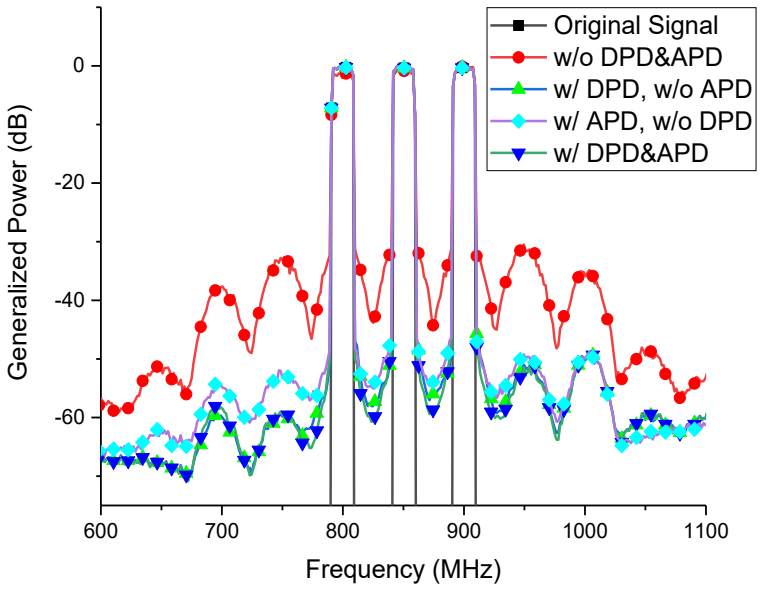

Figure 4-15 Output spectrum from 600MHz to 1100 MHz (case three)

In three-band test, as 2D-DPD is designed specifically for two-band scenario, RF DPD is applicated as DPD method. Figure 4-15 shows that the improvement of IMD3 is 26.1 dB at 750MHz, 21.9 dB at 700MHz, 21.2 dB at 950 MHz, and 18.1 at 1000MHz with proposed linearization function. As both RF DPD and APD can enormously reduce the IMD3, the improvement of IMD3 with proposed linearization is not significantly higher than the APD or RF DPD method.

The enlarged spectrum around each band are shown in Figure 4-16, Figure 4-17, and Figure 4-18. ACPR reduced 19.1 dB in lower-band, 17.5 dB in middle-band, and 18.3 dB in upper-band. The improvement in the middle-band is slightly smaller than the lower-band and upper-band. This is because the IMD3 of middle and upper band is located at the lower-band. The PDC can suppress the IMD3 around lower-band to further reduce ACPR. Similar phenomenon also happens in upper-band.

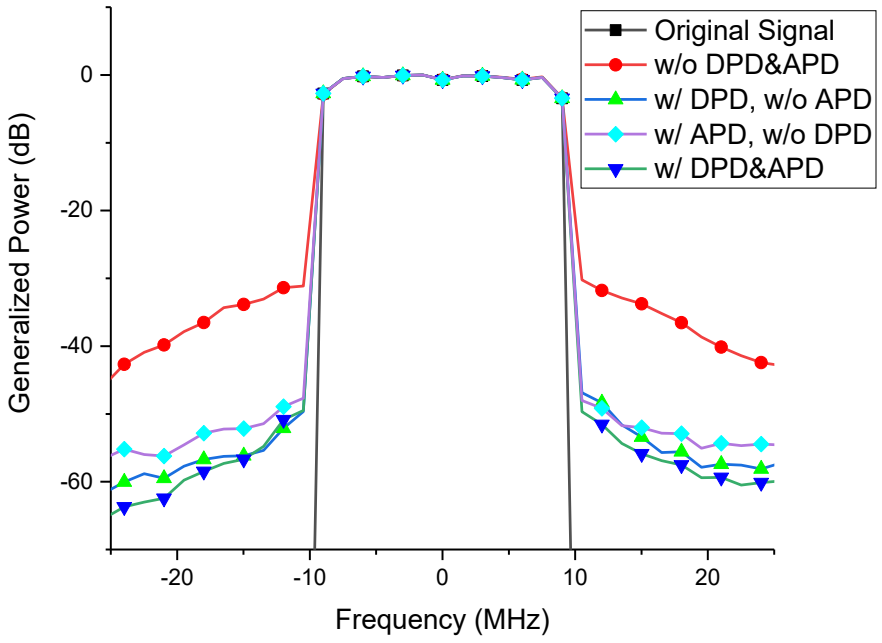

Figure 4-16 Spectrum around the lower-band in simulation (case three)

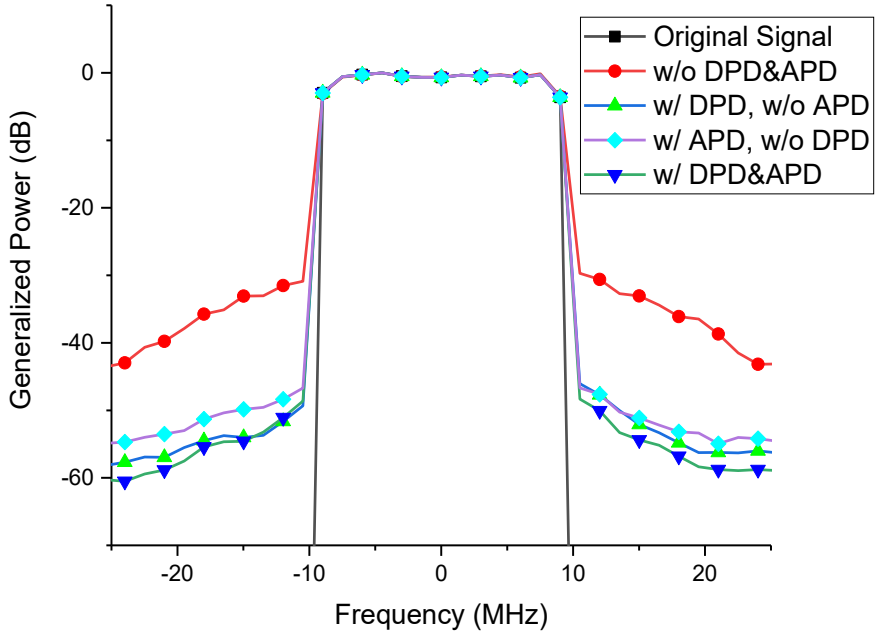

Figure 4-17 Spectrum around the middle-band in simulation (case three)

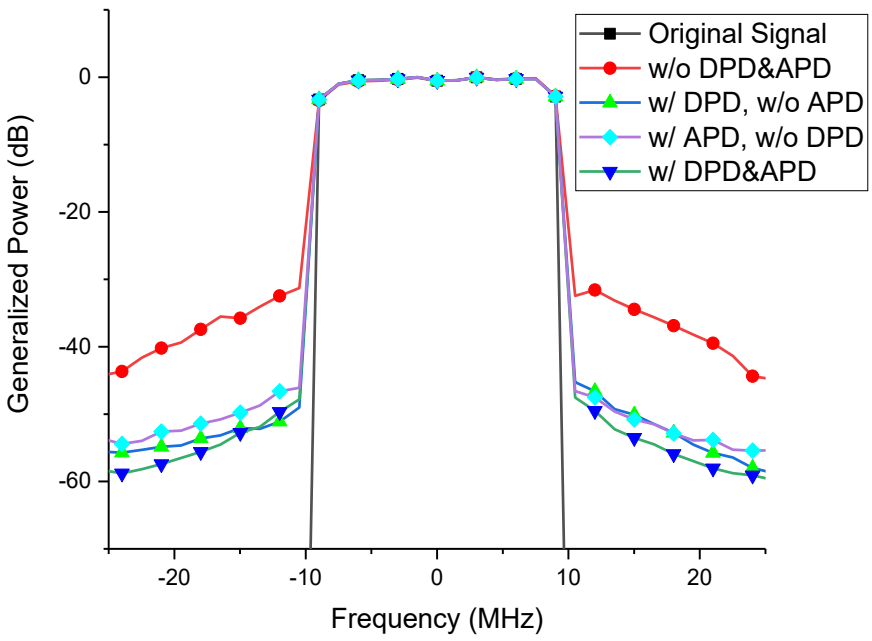

Figure 4-18 Spectrum around the upper-band in simulation (case three)

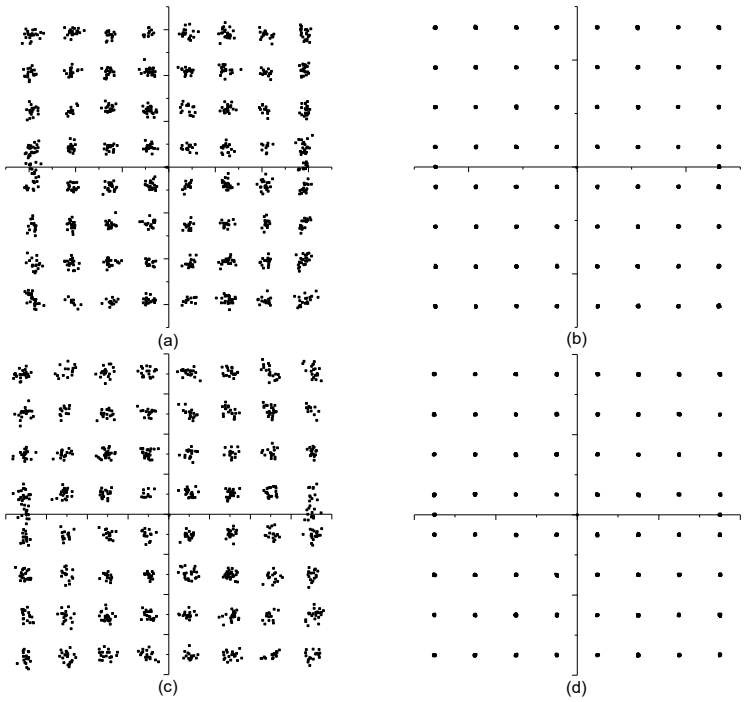

Figure 4-19 Constellation of signal in lower-band with (a) neither APD nor DPD, (b) with only 2D-DPD, (c) with only APD, (d) with both APD and DPD (case three)

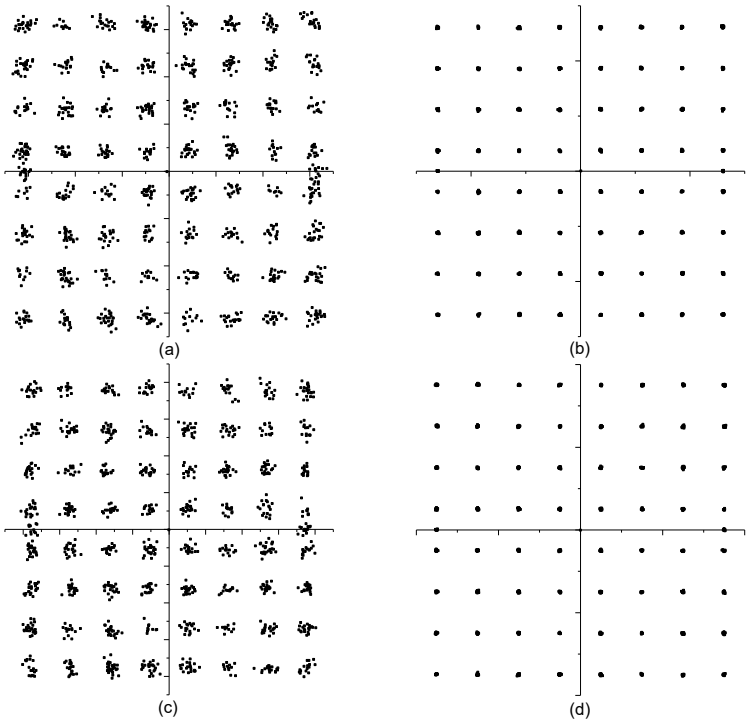

Figure 4-20 Constellation of signal in middle-band with (a) neither APD nor DPD, (b) with only 2D-DPD, (c) with only APD, (d) with both APD and DPD (case three)

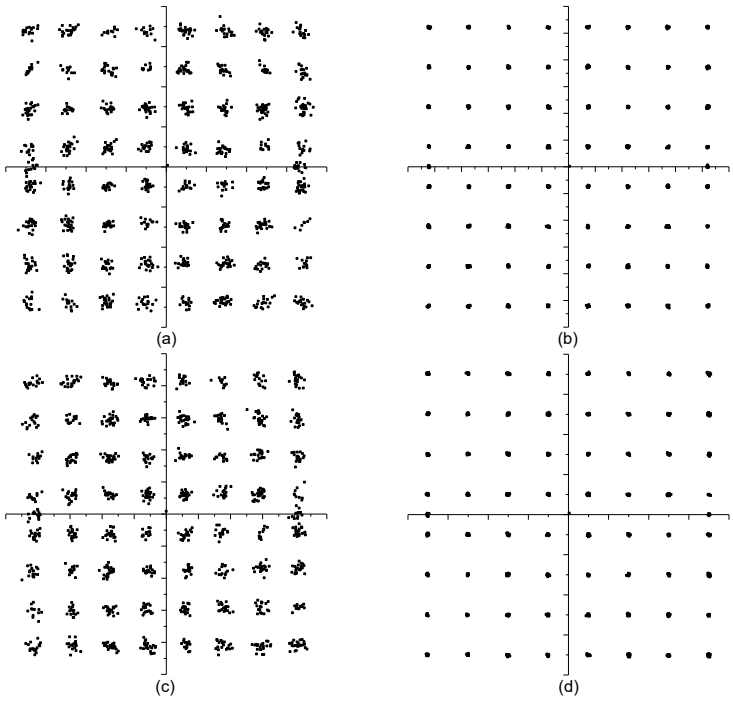

Figure 4-21 Constellation of signal in upper-band with (a) neither APD nor DPD, (b) with only 2D-DPD, (c) with only APD, (d) with both APD and DPD (case three)

As shown in Figure 4-19, Figure 4-20, and Figure 4-21, the proposed linearization can improve the EVM by 17.7 dB at lower-band, 16.5 dB at middle-band, and 15.8 dB at upper-band. The APD can improve the EVM by 3.1 dB at lower-band, 1.7 dB at middle-band, and 3.5 dB at upper-band. The RF DPD can improve the EVM by 17.1 dB at lower-band, 16.0 dB at middle-band, and 14.2 at upper-band. The improvement of EVM is higher in lower-band and upper-band. The reason is same to ACPR improvement as explained above. These results prove that the APD and RF DPD can work together to further reduce the EVM.

4.2.4 Simulation Summary

The performance of simulated linearization methods is summarized in Table 4-1, Table 4-2, and Table 4-3. The linearization methods compared with each other in three cases. In case one and two, the 2D-DPD is applicated as DPD method. But in case three, as the 2D-DPD cannot linearize a three-band signals, the RF DPD is adopted as DPD method.

Table 4-1 The simulation results in case one

PD Method	EVM Improvement	ACPR Improvement	IMD3 Improvement
w/ APD, w/o DPD	1.1 dB	4.9 dB	15.4 dB
w/o APD, w/ DPD	21.4 dB	19.4 dB	-8.2 dB
w/ APD & DPD	21.6 dB	23.8 dB	4.6 dB

Table 4-2 The simulation results in case two

PD Method	EVM Improvement	ACPR Improvement	IMD3 Improvement
w/ APD, w/o DPD	0.5 dB	13.9 dB	19.1 dB
w/o APD, w/ DPD	10.8 dB	-5.0 dB	-9.6 dB
w/ APD & DPD	11.3 dB	9.3 dB	9.8 dB

Table 4-3 The simulation results in case three

PD Method	EVM Improvement	ACPR Improvement	IMD3 Improvement
w/ APD, w/o DPD	2.8 dB	15.8 dB	19.3 dB
w/o APD, w/ DPD	15.8 dB	17.5 dB	17.6 dB
w/ APD & DPD	16.7 dB	18.4 dB	21.8 dB

As can be seen in the results. The proposed linearization combined the advantages of APD and DPD. In all three cases, proposed linearization achieved the best improvement. EVM, ACPR, and IMD3 is suppressed in these situations. What is more, the DPD method adopted in the proposed linearization is not limited, both baseband DPD like 2D-DPD and RF-band DPD like RF DPD can combine with APD circuit.

Chapter 5 Experiments with Combined Analog and Digital Pre-Distortion Method

In Chapter 4, the advantage of proposed linearization is verified in simulation. In this chapter, the proposed linearization is compared with the traditional APD-only or DPD-only methods in a real RoF transmission system experimentally. The experiment cases are similar with the simulation, and an RoF system is built up for the experiment.

5.1 Setup of the Experiments

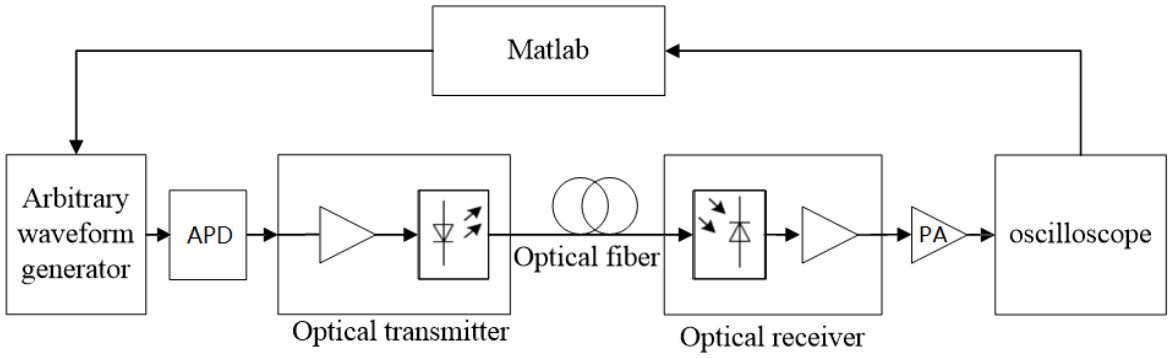

Figure 5-1 Experiment setup of the RoF transmission link

The original signal is generated in MATLAB and loaded into Arbitrary Waveform Generator (AWG). The original signal has the same setting with simulation, the details of LTE signals used in both simulation and experiment are demonstrated in Section 4.1. The AWG used in the experiment is Tektronix AWG7122B. The output signal is set to 17.7 dBm with a sampling rate of 10.32192 GS/s. A MITEQ SCM direct modulate optical transmitter and receiver is used in the optical link. Therefore, the optical power is directly modulated by RF signal. Then, the optical signal is transmitted by an eight-kilometer standard single mode optical fiber. The optical power is 7.12 dBm before transition and 1.82 dBm after transition. The optical signal is received by ORx and demodulated back to an RF signal with a power of -14.4 dBm. The SHF810 power amplifier has a 28 dB gain, which can amplified the signal to 12.7 dB. In the end, an Agilent DSO81204B

oscilloscope samples and records the final signal at 10.32192 GS/s. The signal is than processed by MATLAB in computer.

5.2 Optimal Memory Depth of Digital Pre-distortion

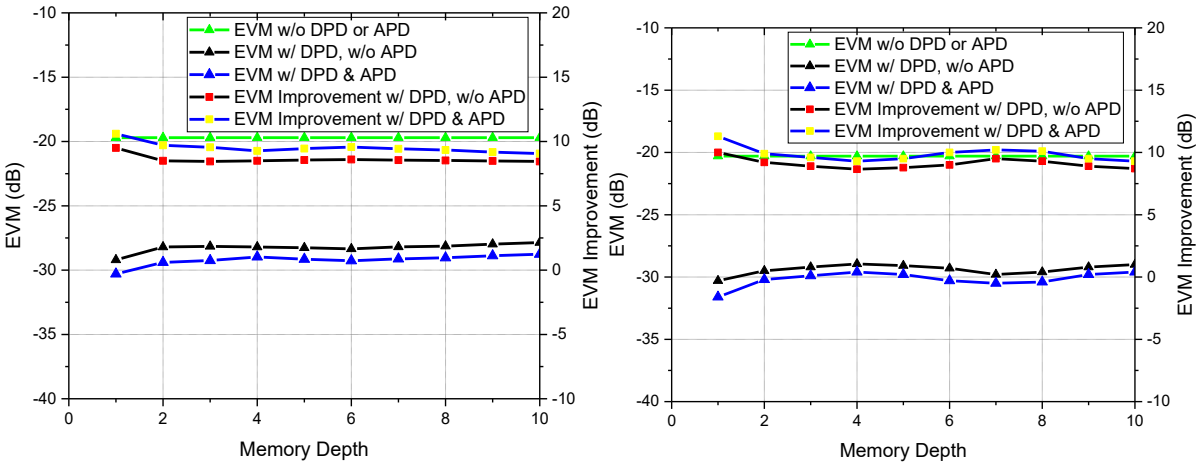

Figure 5-2 EVM vs base-band memory depth (Left: lower-band. Right: upper-band.)

Same to the simulation, the optimal memory depth of DPD should be found before the experiment. As shown in Figure 5-2, the EVM improvement achieve best performance when 2D-DPD memory depth is one. So, in the experiment, the memory depth is set to one.

Similar procedure is also applied to RF DPD. And the memory depth of RF DPD is set to three.

5.3 Optimal Input Power

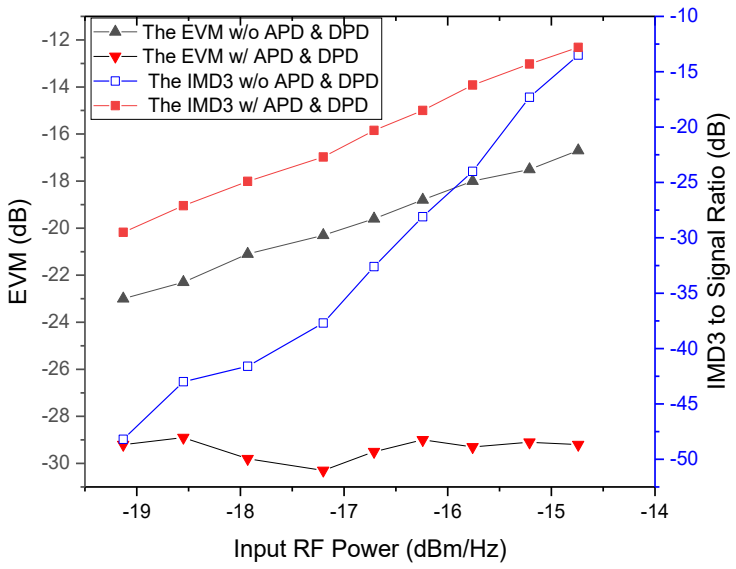

Figure 5-3 EVM and IMD3 vs input RF power in proposed linearization

Figure 5-3 shows the relationship between EVM and IMD3 versus input RF power in proposed linearization method with two-band LTE signal. The EVM improvement is mainly achieved by DPD method. The performance of DPD methods are power spectrum density related. The best performance achieves at 17.4 dBm/Hz. Different from DPD methods, the APD circuits are total power related. The changes of bandwidth or band number will influence the performance of APD. The Figure 5-3 shows that the performance of IMD3 improvement is decreased while the RF power is increasing. As for LTE system, the EVM of signals is much more important than the IMD3. Therefore, in the experiment, the RF power is set to 17.4 dBm/Hz to achieve higher EVM improvement.

Besides, the APD circuit can be designed to adapt specific circumstances. As a fabricated APD circuit [29] is applied in experiment, the performance of APD in case three is poor, which will be explained in Section 5.4.3.

5.4 Experiment Results

5.4.1 Case One: LTE 1 @800 MHz and LTE 2 @900 MHz

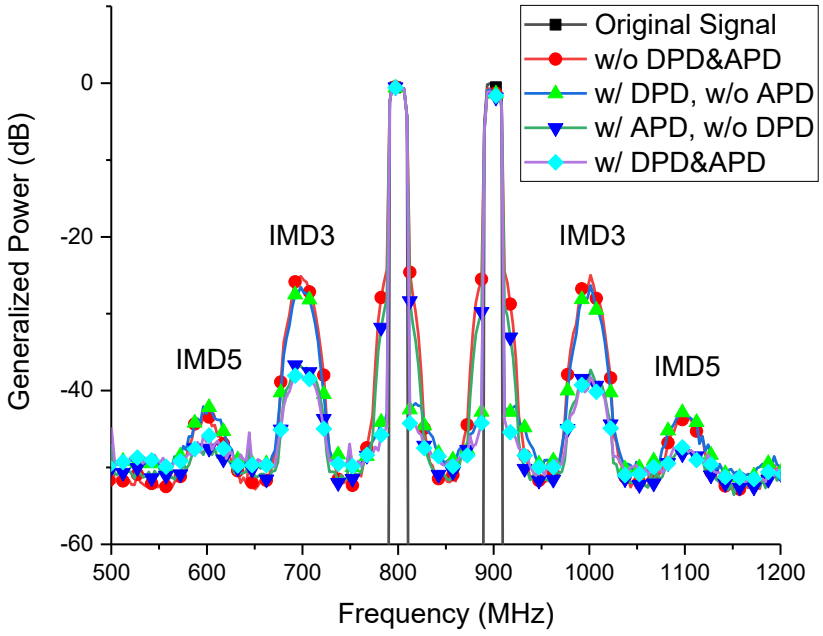

Figure 5-4 Output spectrum from 500 MHz to 1200 MHz in experiment (case one)

Figure 5-4 shows the spectrum of the output signals from 500 MHz to 1200 MHz. The improvement of IMD3 is 15.0 with proposed linearization and 14.8 with only APD circuit. The 2D-DPD cannot compensate the IMD3.

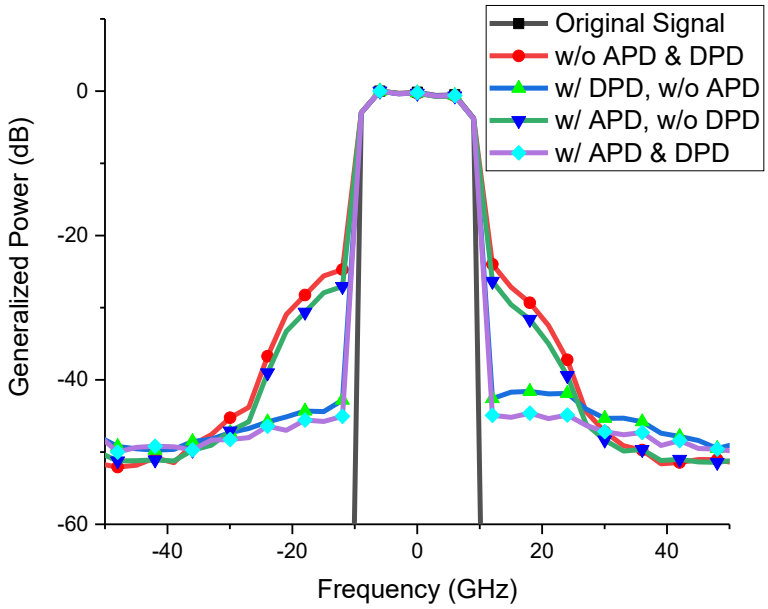

Figure 5-5 Spectrum around the lower band in experiment (case one)

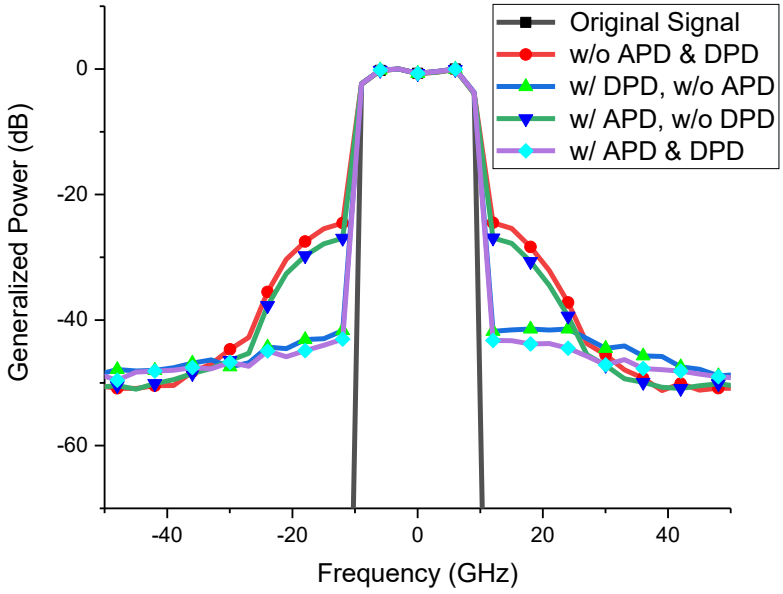

Figure 5-6 Spectrum around the lower band in experiment (case one)

The Figure 5-5 and Figure 5-6 shows that the ACPR is improved 1.8 dB by APD, 17.4 dB by 2D-DPD, and 19.4 dB by proposed linearization.

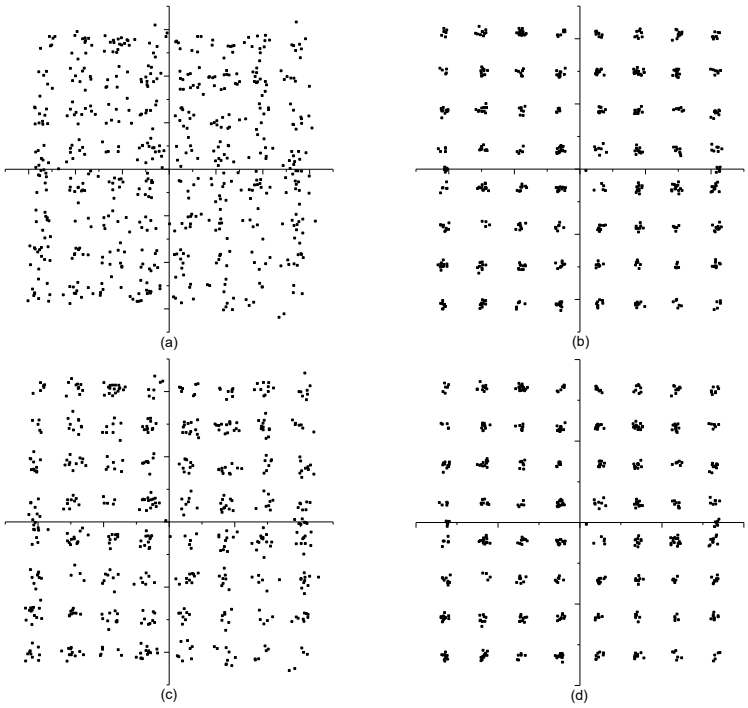

Figure 5-7 Constellation of signal in lower-band with (a) neither APD nor DPD, (b) with only 2D-DPD, (c) with only APD, (d) with proposed linearization (case one)

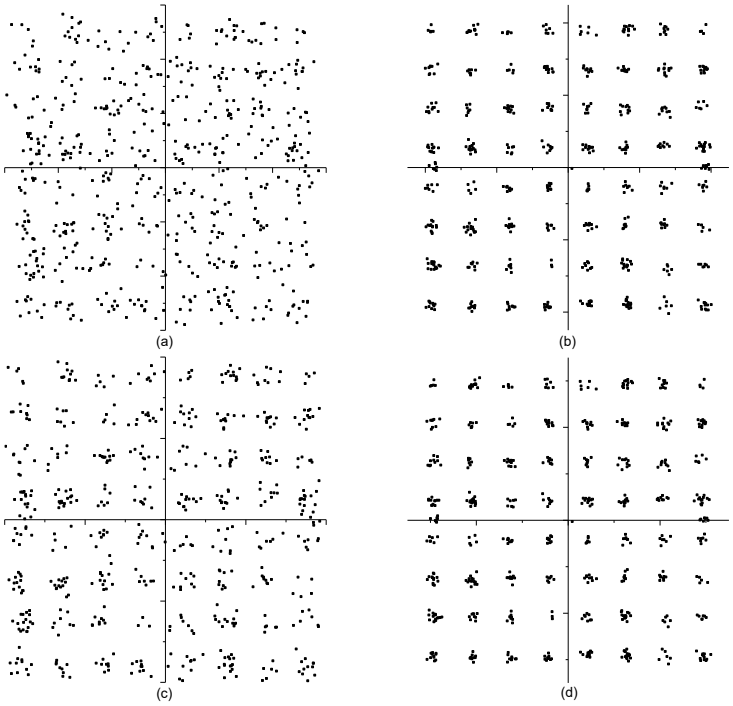

Figure 5-8 Constellation of signal in upper-band with (a) neither APD nor DPD, (b) with only 2D-DPD, (c) with only APD, (d) with proposed linearization (case one)

The Figure 5-7 and Figure 5-8 shows the constellation of the output signal. The EVM of lower-band is improved 10.2 dB with 2D-DPD, 2.0 dB with APD, and 11.3 dB with proposed linearization. The EVM of upper-band is improved 9.5 dB with 2D-DPD, 1.9 dB with APD, and 10.6 dB with proposed linearization.

5.4.2 Case Two: LTE 1 @800 MHz and LTE 2 @840 MHz

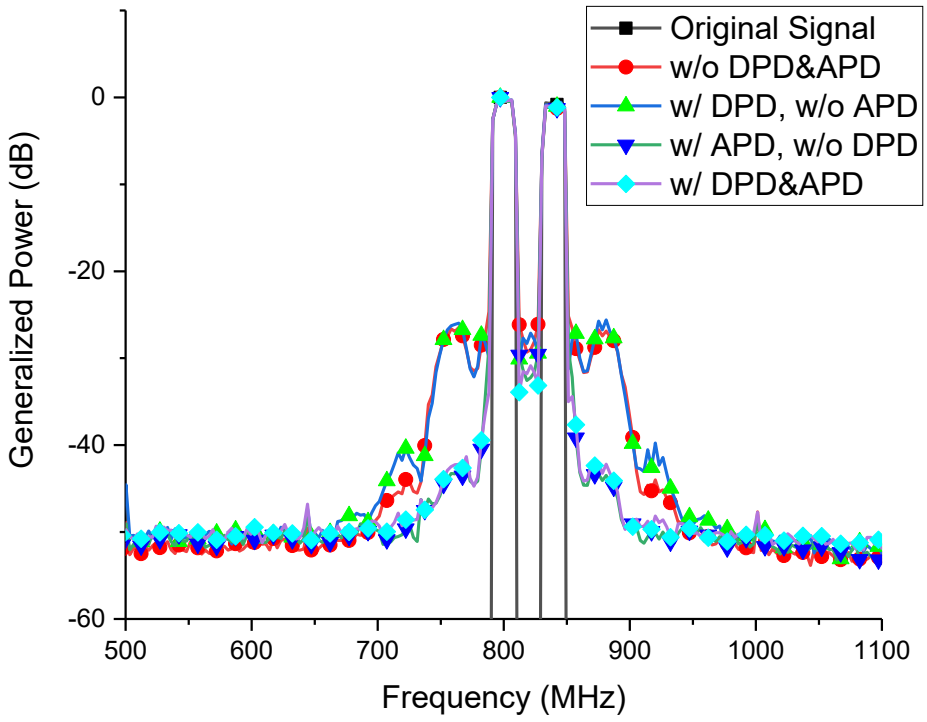

Figure 5-9 Output spectrum from 500 MHz to 1100 MHz (case two)

In case two, two LTE signals are located close to each other at 800 MHz and 840 MHz. The Figure 5-9 shows that the IMD3 is suppressed by 16.8 dB at 760 MHz and 17.2 dB at 880 MHz by APD. With the proposed linearization, the IMD3 is suppressed by 16.5 dB at 760 MHz and 16.9 dB at 880 MHz. The 2D-DPD even increases the IMD3 in this case.

The Figure 5-10 and Figure 5-11 shows an enlarged image around two LTE signals. The ACPR is decreased 4.7 dB by proposed linearization and 4.6 dB by APD. The 2D-DPD cannot suppress ACPR in this case as sampling bandwidth is limited.

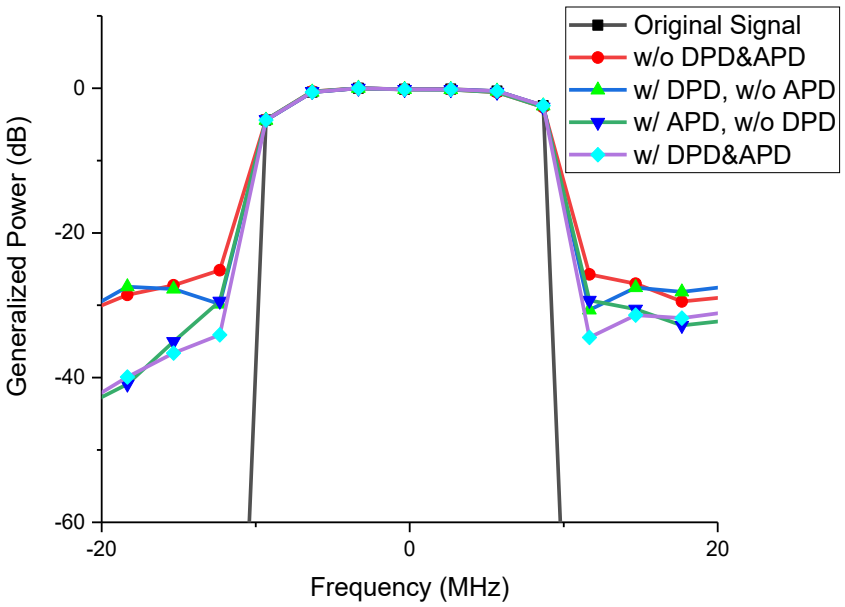

Figure 5-10 Spectrum around the lower-band in experiment (case two)

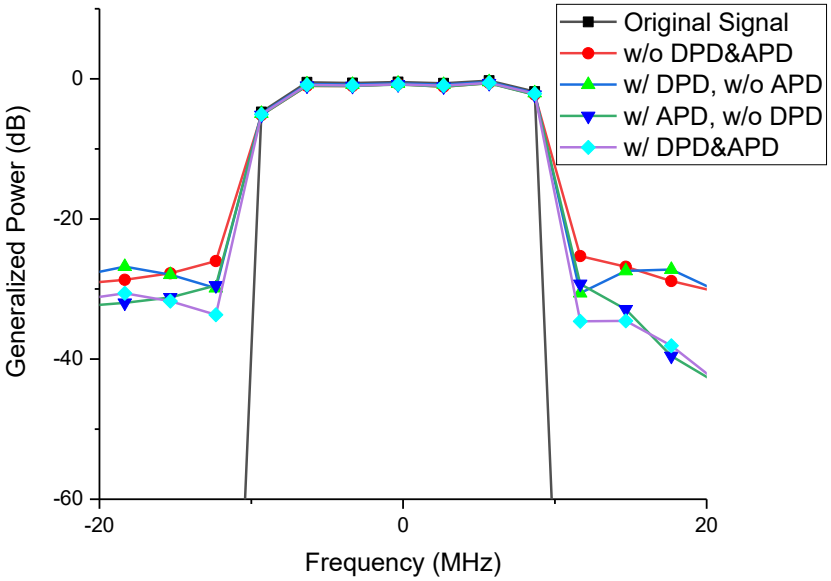

Figure 5-11 Spectrum around the upper-band in experiment (case two)

The constellation is given in Figure 5-12 and Figure 5-13. The EVM is improved 6.9 dB with 2D-DPD, 2.1 dB with APD, and 8.4 dB with proposed linearization in lower-band. In upper-band, the EVM is improved 7.0 dB with 2D-DPD, 2.2 dB with APD, and 8.2 dB with proposed linearization.

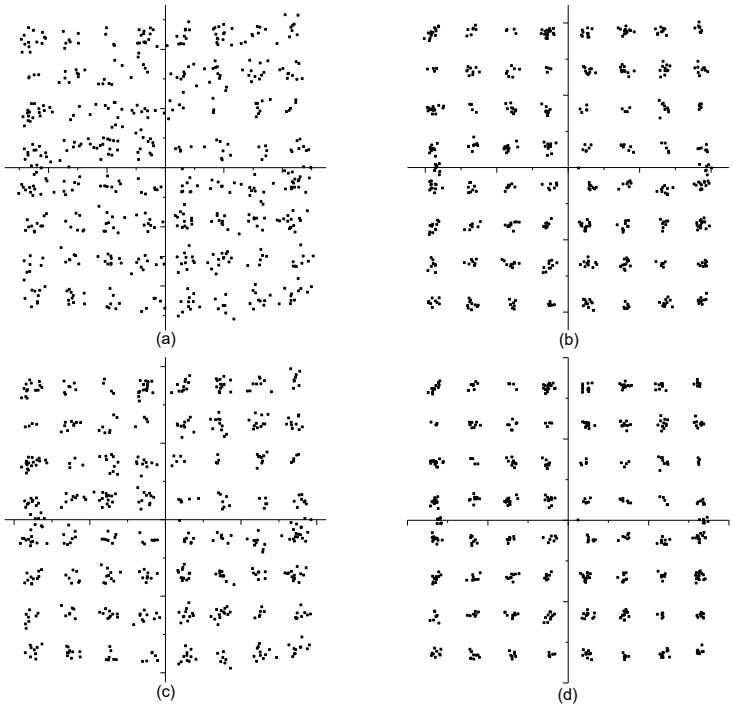

Figure 5-12 Constellation of signal in lower-band with (a) neither APD nor DPD, (b) with only 2D-DPD, (c) with only APD, (d) with proposed linearization (case two)

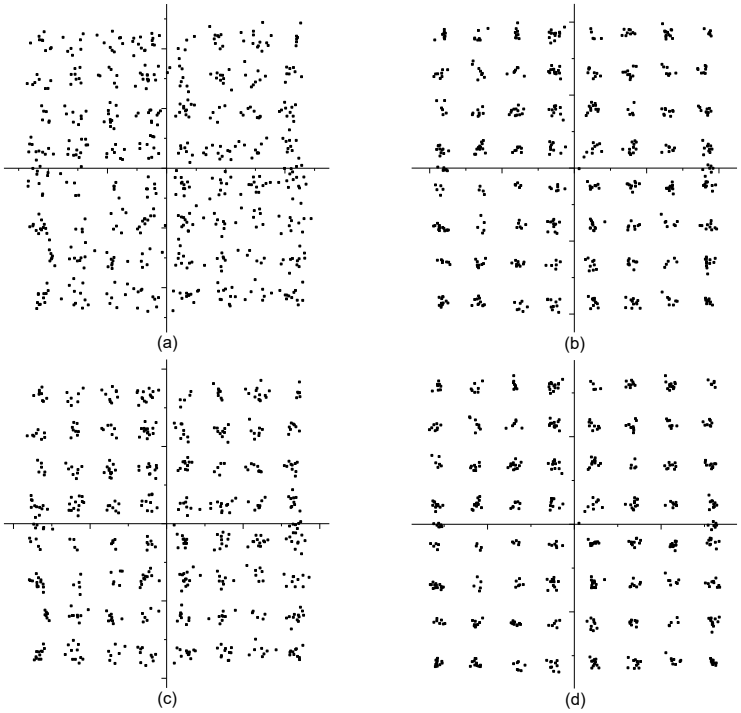

Figure 5-13 Constellation of signal in upper-band with (a) neither APD nor DPD, (b) with only 2D-DPD, (c) with only APD, (d) with proposed linearization (case two)

5.4.3 Case Three: LTE 1 @800 MHz, LTE 2 @850 MHz, and LTE 3 @900MHz

The 2D-DPD cannot deal with three-bands signal, so the RF DPD is adopted instead of 2D-DPD. Both RF DPD and APD can compensate IMD3 as shown in Figure 5-14. The improvement of IMD3 is 3.6 dB with APD, 14.3 dB with RF DPD, and 14.4 dB with proposed linearization method at 700 MHz. At 750 MHz, the improvement of IMD3 is 3.8 dB with APD, 17.5 dB with RF DPD, and 17.9 dB with proposed linearization method. At 950 MHz, the improvement of IMD3 is 3.7 dB with APD, 17.7 dB with RF DPD, and 17.7 dB with proposed linearization method. The IMD3 is improved 3.8 dB by APD, 14.6 dB by RF DPD, and 14.5 dB by proposed linearization method.

As the total power of the original signal in case three is higher than two-band tests, the improvement of APD is limited. In order to achieve the best performance of DPD, the APD is not working at its best input power. A specific designed APD circuit which can process higher input power may solve this problem.

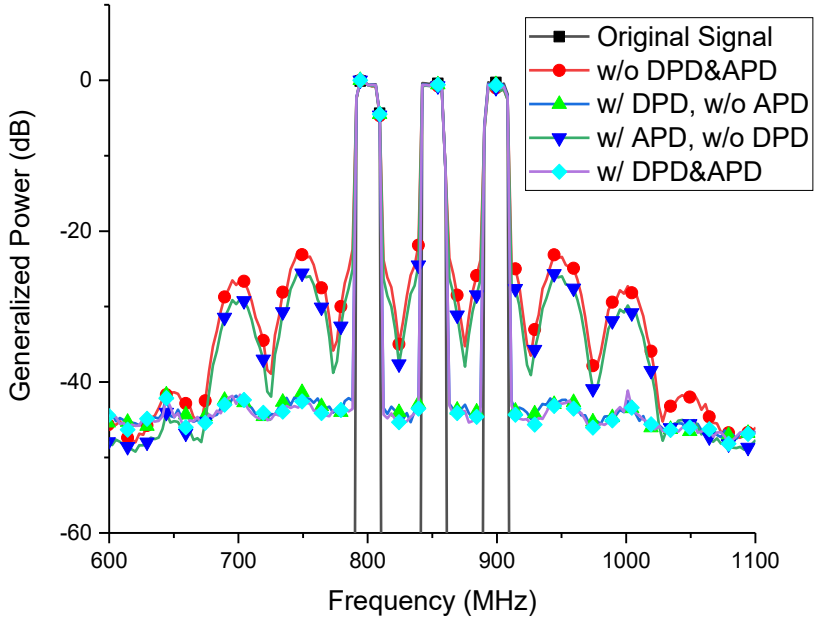

Figure 5-14 Output spectrum from 600 MHz to 1100 MHz in experiment (case three)

In Figure 5-15,Figure 5-16, and Figure 5-17, the ACPR is decreased by 3.4 dB, 3.3 dB, and

3.4 dB with APD in three bands. With RF DPD, the ACPR is improved by 8.7 dB, 8.5 dB, and 7.9 dB. With proposed linearization, the ACPR is improved by 8.9 dB, 8.5 dB, and 8.1 dB.

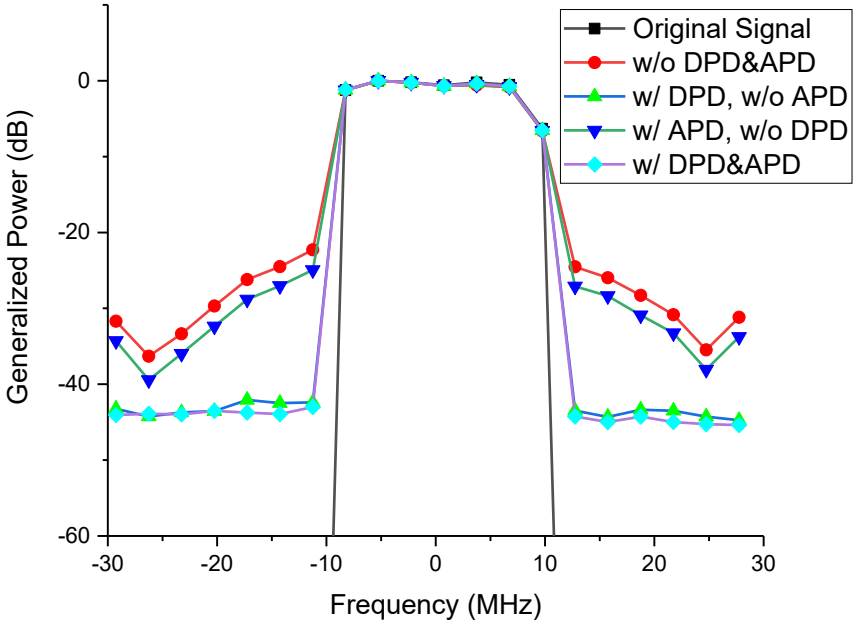

Figure 5-15 Spectrum around the lower-band in experiment (case three)

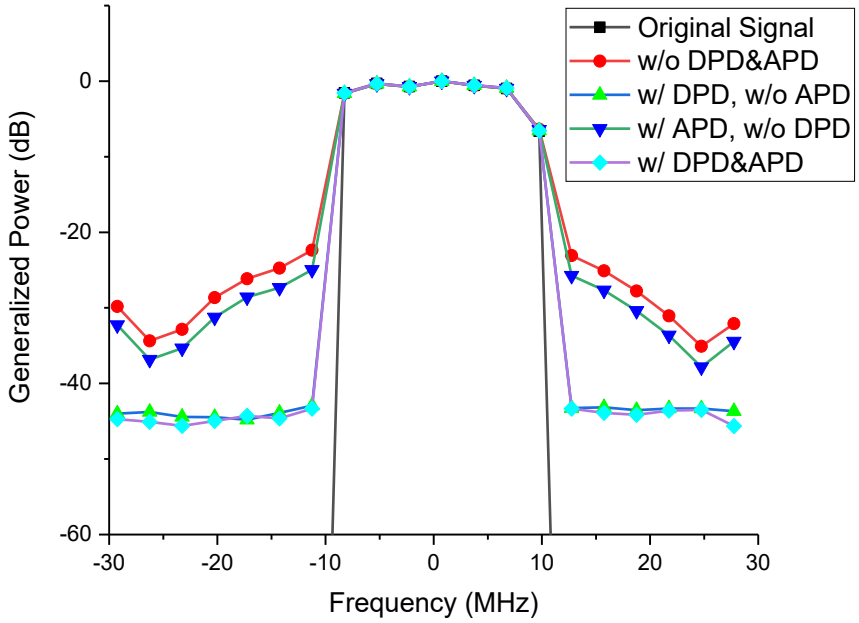

Figure 5-16 Spectrum around the middle-band in experiment (case three)

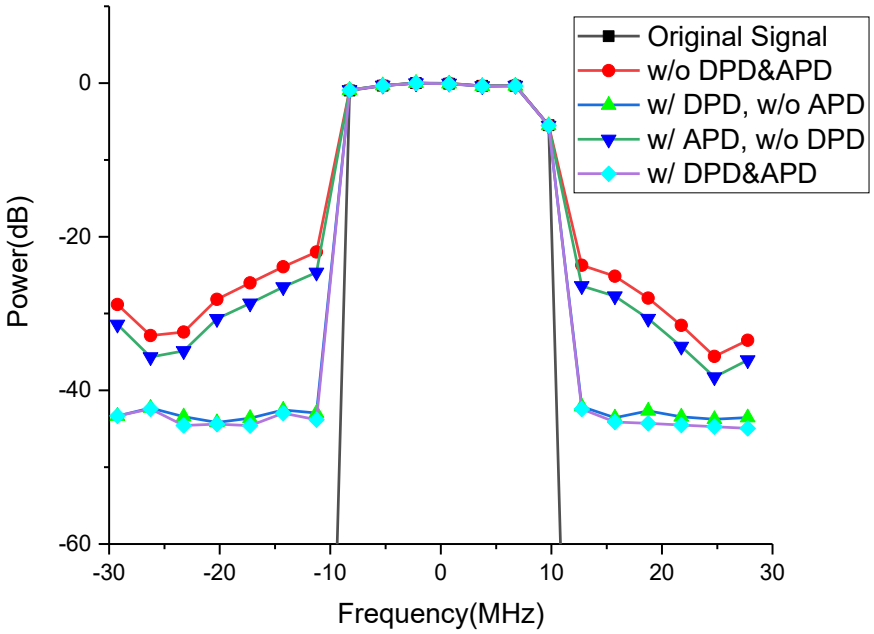

Figure 5-17 Spectrum around the upper-band in experiment (case three)

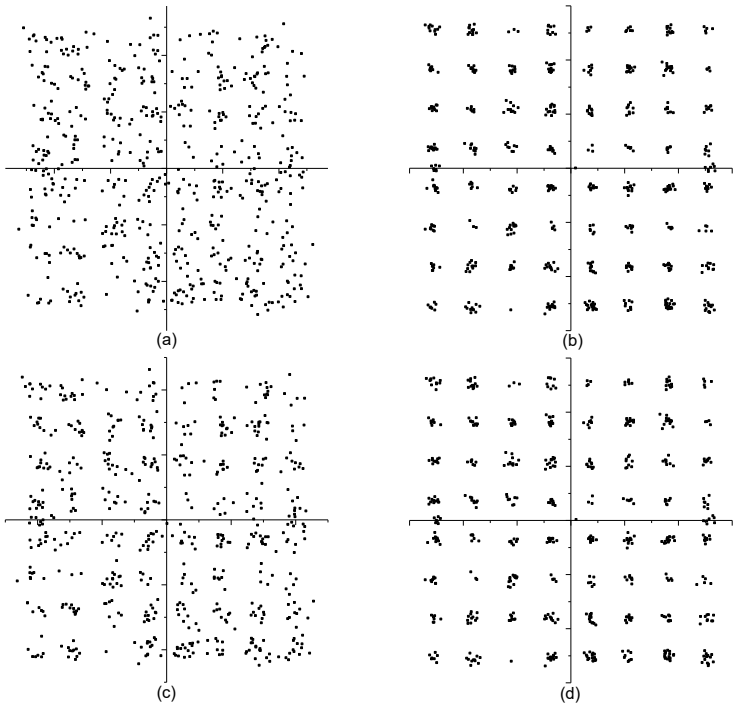

Figure 5-18 Constellation of signal in lower-band with (a) neither APD nor DPD, (b) with only 2D-DPD, (c) with only APD, (d) with proposed linearization (case three)

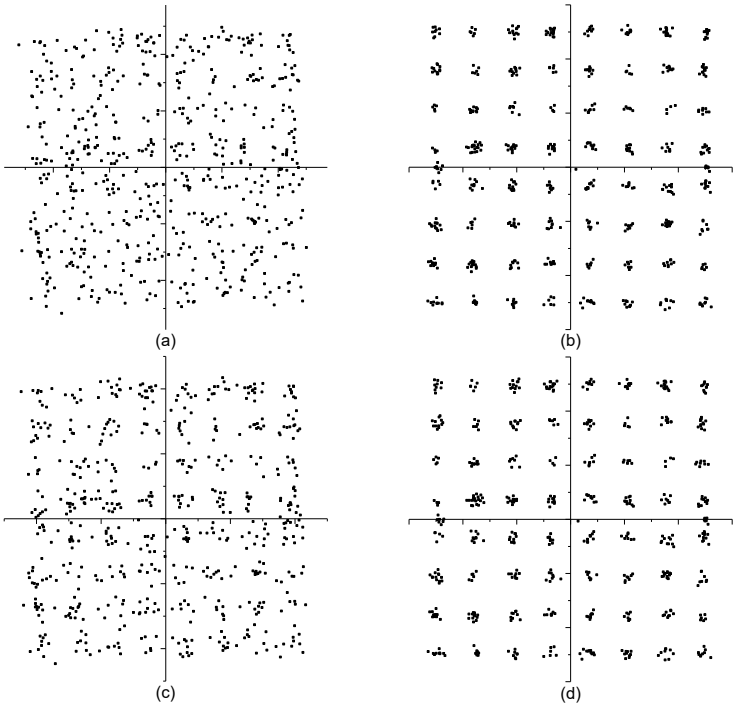

Figure 5-19 Constellation of signal in middle-band with (a) neither APD nor DPD, (b) with only 2D-DPD, (c) with only APD, (d) with proposed linearization (case three)

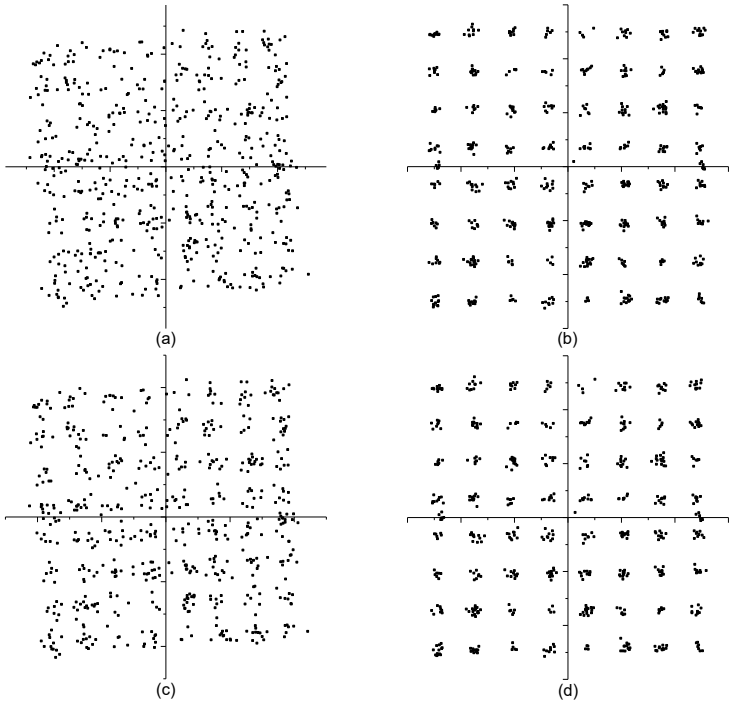

Figure 5-20 Constellation of signal in upper-band with (a) neither APD nor DPD, (b) with only 2D-DPD, (c) with only APD, (d) with proposed linearization (case three)

As shown in Figure 5-18, Figure 5-19, and Figure 5-20, the improvement of EVM of lower-band is 3.7 dB with APD, 9.1 dB with RF DPD, and 12.4 dB with proposed linearization. In middle-band, the improvement of EVM is 1.2 dB with APD, 10.5 dB with RF DPD, and 11.4 dB with proposed linearization. In upper-band, the improvement of EVM is 2.6 dB with APD, 8.8 dB with RF DPD, and 10.8 dB with proposed linearization.

5.5 Experiment Summary

As shown in Table 5-1, Table 5-2, and Table 5-3, the results of experiment agree with the simulation. The proposed linearization can improve the EVM, ACPR, and IMD3 in all cases.

Table 5-1 The experiment results in case one

PD Method	EVM Improvement	ACPR Improvement	IMD3 Improvement
w/ APD, w/o DPD	2.0 dB	1.8 dB	14.9 dB
w/o APD, w/ DPD	9.9 dB	17.5 dB	0.3 dB
w/ APD & DPD	11.0 dB	19.4 dB	15.0 dB

Table 5-2 The experiment results in case two

PD Method	EVM Improvement	ACPR Improvement	IMD3 Improvement
w/ APD, w/o DPD	2.2 dB	4.7 dB	17.0 dB
w/o APD, w/ DPD	7.0 dB	-0.3dB	-1.1 dB
w/ APD & DPD	8.2 dB	4.6 dB	16.8 dB

Table 5-3 The experiment results in case three

PD Method	EVM Improvement	ACPR Improvement	IMD3 Improvement
w/ APD, w/o DPD	2.4 dB	3.3 dB	3.7 dB
w/o APD, w/ DPD	9.3 dB	8.2 dB	16.5 dB
w/ APD & DPD	10.1 dB	8.6 dB	16.9 dB

The influence of memory depth and input power is also studied. In the experiment, the memory depth and input power is chosen to minimize the EVM, rather than IMD3.

5.6 Comparison Between Simulation and Experimentation Results

Although in both simulation and experiment, the proposed linearization method has the best performance in improving EVM, ACPR, and IMD3. There are some differences between the results of simulation and experiment. They will explain in detail.

Fist, in the simulation Case One and Two, if only 2D-DPD technique is applicated, the IMD3 and IMD5 is increased. This is different from the experimentation. The reason is that the nonlinearity in the simulated PA model is too severe. Therefore, the signal power is reduced higher than IMD3 power. This phenomenon does not occur in the experiment, because the nonlinearity of the devices is slitter than simulation models.

Second, in the third cased of experiment, the improvement of IMD3 and ACPR of proposed linearization method is not significantly larger than DPD-only method. The reason is that the performance of APD circuits are total power related while the DPD is power density related. The Figure 5-3 shows that the performance of IMD3 improvement is decreased while the RF power is increasing. The changes of bandwidth or band number will influence the performance of APD. Naturally, three-band signal has much stronger power than two-band signal. This is the reason why the improvement of ACPR and IMD3 in the third case of experiment is unbearably low with APD circuit. But in the simulation, the signal will be generalized several times within the whole

simulation. Therefore, the power is first generalized to fit the APD circuit, and then generalized to fit the DPD method. The overall improvement of APD circuit in the third case is similar with the first and second cases.

Chapter 6 An Evolved 2D-DPD Linearization

The 2D-DPD can significantly reduce the EVM of two-band signals. But the complexity of 2D-DPD is very high. As some components like high order memory effects are very small in the real system, they can be ignored to reduce the complexity.

A further evolved 2D-DPD is proposed based on formula (3.23). The (3.23) is the overall function of combined DPD and APD model. The basic idea of evolved 2D-DPD is to turn the APD part in (3.23) into digital domain. The formula of proposed evolved 2D-DPD is:

$$y_1(n) = \sum_{m=0}^{M-1}\sum_{k=0}^{N_1}\sum_{j=0}^{k} c_{k,j,m}^{(1)} x_1(n-m) * |x_1(n-m)|^{k-j}|x_2(n-m)|^j + \sum_{k=0}^{N_2}\sum_{j=0}^{k} d_{k,j}^{(1)} x_1(n) * |x_1(n)|^{k-j}|x_2(n)|^j$$

$$y_2(n) = \sum_{m=0}^{M-1}\sum_{k=0}^{N_1}\sum_{j=0}^{k} c_{k,j,m}^{(2)} x_2(n-m) * |x_1(n-m)|^{k-j}|x_2(n-m)|^j + \sum_{k=0}^{N_2}\sum_{j=0}^{k} d_{k,j}^{(2)} x_2(n) * |x_1(n)|^{k-j}|x_2(n)|^j \quad (6.1)$$

where M is the memory depth, N_1 is the nonlinearity order of memory effect, N_2 is the nonlinearity order of quiescent nonlinearity. In the real system N_2 is larger than N_1. So, we can reduce the coefficients number by reducing the N_1.

Evolved 2D-DPD formula contains two terms. The first one is traditional 2D-DPD model, which is:

$$\sum_{m=0}^{M-1}\sum_{k=0}^{N_1}\sum_{j=0}^{k} c_{k,j,m}^{(1)} x_1(n-m) * |x_1(n-m)|^{k-j}|x_2(n-m)|^j \quad (6.2)$$

This term is used to compensate the lower order memory effect and lower order quiescent nonlinearity. The second term is a memoryless polynomial with cross effect between two bands.

It can compensate high order quiescent nonlinearity. These two terms are added together. Therefore, the high-order memory effect is ignored. The complexity of evolved 2D-DPD is significantly reduced while the performance remains similar.

A simple simulation is done where M is equal to 4, N_1 is equal to 3 and N_2 is equal to 5. The simulation is same with Case One in Section 4.2.1. In Figure 6-1, the result shows that the EVM improvement of evolved 2D-DPD is 20.8 dB in lower-band and 20.5 dB in upper-band, which is 0.5 dB worse than traditional 2D-DPD. But evolved 2D-DPD can reduce the coefficients by 23, from 84 of 2D-DPD to 61 of evolved 2D-DPD.

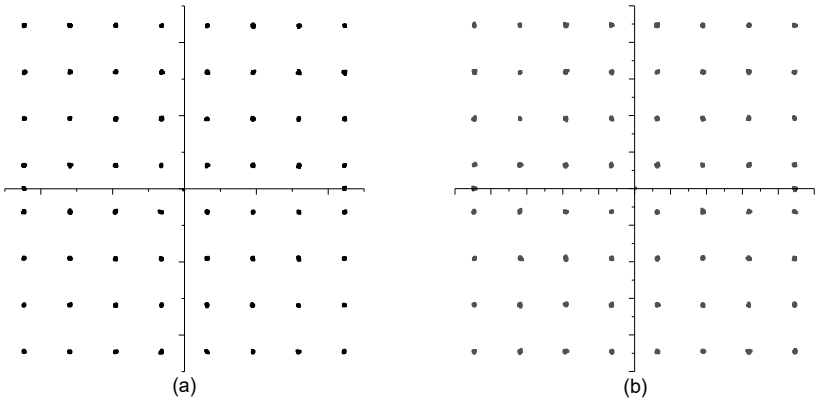

Figure 6-1 The simulation results of evolved 2D-DPD in (a) lower-band, (b) upper-band

The relationship between coefficients number and nonlinearity degree is shown in Table 6-1. When the memory depth is very low, the evolved 2D-DPD cannot reduce the coefficients umber. But when the memory depth is larger than three, the number of coefficients is reduced by evolved 2D-DPD.

Table 6-1 Number of coefficients vs memory depth

Memory Depth	**1**	**2**	**3**	**4**	**5**	**6**	**7**	**8**
2D DPD*	21	42	63	84	105	126	147	168
Evolved 2D-DPD**	31	41	51	61	71	81	91	101

* Suppose nonlinearity degree is 5.

** Suppose quiescent nonlinearity degree is 5, memory effect nonlinearity degree is 3.

Chapter 7 Conclusion

7.1 Thesis Conclusion

With the increasing of the transmission rate, the RoF system is developed and used in the communication systems. RoF systems are ultra-wideband transmission systems with low cost and high security. However, RoF link suffers from the high distortion induced by the optical transmitter and power amplifier. Therefore, several linearization methods have been proposed to suppress the quiescent nonlinearity and memory effect in RoF systems. One of the state-of-art linearization technique is pre-distortion technique. Pre-distortion methods can be divided into two branches, the APD and DPD. Both APD and DPD have their own advantages and disadvantages, they are complementary. Therefore, a combined analog and digital linearization method is proposed in this thesis.

The proposed combined APD and DPD linearization method combines the advantages from both digital and analog pre-distortion. In the proposed linearization, the APD is used to compensate quiescent nonlinearity. Therefore, IMDs, and ACPR can be improved. Also, minor EVM improvement is presented. As 2D-DPD is used in a two-band transmission system, the EVM is significantly reduced. The ACPR is also reduced in some cases. In three-band system, the RF DPD can reduce IMDs, ACPR, and EVM. The mathematic model proves that the proposed linearization makes the together of reducing the quiescent and memory effect simultaneously. Different DPD methods like 2D-DPD and RF DPD can work with APD to further improve the performance of the RoF system.

The simulations system was built up according to real devices. The model of RoF system and the model of PA is used in the simulation system in MATLAB. The model of APD circuit is designed in ADS. Therefore, the performance of proposed linearization can be evaluated with co-simulation between MATLAB and ADS. The optimal memory depth of both 2D-DPD and RF

DPD is found. The tests took place in three cases. The first case was a two-band general test. The second one was a two-band close-located test. The third test was a three-band close-located test. The DPD method used in first and second test was 2D-DPD and in third test was RF DPD. The simulation results agreed with the mathematical analysis. The improvement of EVM, ACPR, and IMD3 was 21.6 dB, 23.8 dB, and 4.6 dB in case one. In case two, the improvements were 11.3 dB, 9.3 dB, and 9.8 dB. In the third test, the improvements were 16.7 dB, 18.4 dB, and 21.8 dB. Compared with ordinary DPD or APD linearization, the proposed linearization can achieve higher improvement in an RoF system in all circumstances. So, a better pre-distortion method in ultra-wideband transmission system like 4G or 5G has been proposed.

The proposed linearization was tested with a real RoF link in the lab. The optimal RF power and optimal memory depth was found at the beginning. The experiment results agreed with the simulation. In first case, the EVM, ACPR, and IMD3 were improved by 11.0 dB, 19.4 dB and 15.0 dB. In second case, they were improved by 8.2 dB, 4.6 dB, and 16.8 dB. In third case, they were improved by 10.1 dB, 8.6 dB and 16.9 dB. In first and second cases, the 2D-DPD is applied as the DPD method. An ordinary 2D-DPD can deal with in-band nonlinearity only, but with the help of APD, it can improve EVM, ACPR, and IMD3 simultaneously in the proposed linearization method. Similar performances can also be achieved by RF DPD in first and second cases, but the improvement of EVM in RF DPD was lower. Additionally, the RF DPD required a higher sampling rate which means a high cost. In third case, the RF DPD was adopted as DPD method. The APD and RF DPD made a together in proposed linearization to further improve the performance of the RoF system.

Based on the simulation and the experiment, the proposed linearization can linearize the quiescent nonlinearity and memory effect simultaneously, and compensate both the in-band distortion and out-of-band distortion. The proposed linearization can also be used in three or more bands transmission systems with the RF DPD being adopted. Therefore, proposed linearization is a good choice in modern ultra-wideband multiplexed transmission systems.

After the combined APD and DPD nonlinearization method is proposed, an evolved 2D-DPD method is also proposed based on the mathematical model of combined APD and DPD method. The evolved 2D-DPD method ignores the high order memory effect by introducing a memoryless polynomial. The high order memory effect is very small in the RoF system. Therefore, the coefficient number is reduced, but the performance remains similar. The EVM of evolved 2D-DPD is only 0.5 dB worse than ordinary 2D-DPD in the simulation. With evolved 2D-DPD, the complexity is reduced considerably.

7.2 Future Works

In the experiment, the APD circuit is not fitful for three-band test, an APD circuit specifically for that circumstances should be designed.

The RF DPD adopted in case three still needs a high sampling rate. It can be reduced by intermediate frequency DPD (IF DPD). Thus, the DPD can focus on in-band distortion, and leave the out-of-band distortion to APD.

The evolved 2D-DPD is still at the very early stages of the design. Several improvements can be added to evolved 2D-DPD. Further experiment should be done with the evolved 2D-DPD.

Reference

[1] H. Jin, J. Chen, H. Ji and C. Feng, Principles of Mordern Switching, Beijing, China: Publishing House of Electronics Industry, 2011.

[2] T. Ojanpera and R. Prasad, "An overview of air interface multiple access for IMT-2000/UMTS," *IEEE Communications Magazine,* vol. 36, no. 9, pp. 82-86, Sep. 1998.

[3] H. Xu, "Towards an all-IP / flat architecture, LTE / SAE lifted a new revolution in mobile networks," Comunication components magazine, [Online]. Available: http://www.2cm.com.tw/technologyshow_content.asp?sn=0909030005.

[4] A. J. Cooper, "'Fibre/radio' for the provision of cordless/mobile telephony services in the access network," *IEEE Communications Magazine,* vol. 36, no. 9, pp. 2054-2056, Sep. 1990.

[5] A. Ng'oma, Radio-over-fiber technology for broadband wireless communication systems, Eindhoven, Netherlands: Ph.D. thesis, Dept. Elect. Eng., Eindhoven Technology Univ., 2005.

[6] S. Kumar and M. J. Deen, Fiber optic communications: fundamentals and applications 1st ed,, Chichster, United Kingdom: John Wiley & Sons, Ltd., 2014.

[7] X. Zhang, D. Shen and T. Liu, "Review of linearization techniques for fiber-wireless systems," in *IEEE International Wireless Symposium*, Xi'an, China, 2014.

[8] T. Yamamoto, "High-speed directly modulated lasers," in *OFC/NFOEC*, Los Angeles, CA, USA, 2012.

[9] K. Nishimura, R. Inohara, M. Tsurusawa and M. Usami, "80 Gbit/s wavelength conversion by MQW electroabsorption modulator with delayed-interferometer," *OFC 2003 Optical Fiber Communications Conference,* vol. 1, pp. 271-273, 2003.

[10] C. Sui, B. Hraimel, X. Zhang, L. Wu, Y. Shen, K. Wu, T. Liu, T. Xu and Q. Nie, "Impact of electro-absorption modulator combined laser on MB-OFDM ultra-wideband signals sver fiber systems," *Journal of Lightwave Technology,* vol. 28, no. 24, pp. 3548-3555, 2010.

[11] S. Højfeldt and J. Mørk, "Modeling of carrier dynamics in quantum-well electroabsorption modulators," *IEEE Journal of Selected Topics in Quantum Electronics,* vol. 8, no. 6, pp. 1265-1276, Nov/Dec 2002.

[12] R. Zhu, Broadband linearization technologies for broadband radio-over-fiber transmission system, Montrea, Canada: Ph.D. Thesis, Dept. Elect. and Comp. Eng., Concordia Univ.,

2015.

[13] H. Zhou, Selection of junior electronics, Beijing, China: Posts and Telecom Press, 2001.

[14] J. Domokos, "A power amplifier system". Patent WO2004019486, 2004.

[15] M. P. Wilson, "High efficiency amplification". Patent WO2005057769, 2005.

[16] S. Alihisa and K. Kunihiko, "Power amplifier for radio transmitter". Patent JP9064757, 1997.

[17] L. Larson, D. Kimball and P. Asbeck, "Wideband envelope tracking power amplifiers for wireless communications," in *2014 IEEE 14th Topical Meeting on Silicon Monolithic Combined Circuits in Rf Systems*, Newport Beach, CA, USA, 2014.

[18] H. HE, T. Ge and J. Chang, "A review on supply modulators for envelope-tracking power amplifiers," in *2016 International Symposium on Combined Circuits (ISIC)*, Singapore, 2016.

[19] A. Festoe and K. Onarheim, "Efficient power supply for rapidly changing power requirements". Patent WO2005041404, 2005.

[20] I. Bar-David, "Method and apparatus for improving the efficiency of power amplifiers operating under a large peak-to-average ratio". Patent US20006437641(Paragon), 2001.

[21] J. Wood, Behavioral modeling and linearization of RF power amplifiers, Norwood, MA, USA: Artech House, 2014.

[22] European Telecommunications Standards Institute, "Universal Mobile Telecommunications System (UMTS)," [Online]. Available: http://www.etsi.org/deliver/etsi_ts/125100_125199/125123/03.01.01_60/ts_125123v030101p.pdf.

[23] J. Liu, Practical behavioral modeling technique of power amplifiers based on loadpull measurements, Tempa, FL, USA: Ph.D. thesis, Dept. Elect. Eng., Univ. of South Florida, 2005.

[24] H. S. Black, "Stablized feed-back amplifier," *Electrical Engineering,* Vols. 53, No. 1, pp. 114-120, 1934.

[25] B. Harimel, X. Zhang, T. Liu, T. Xu, Q. Nie and D. Shen, "Performance enhancement of an OFDM ultra-wideband transmission-over-fiber link using a linearized mixed-polarization single-drive X-cut Mach–Zehnder modulator," *IEEE Transactions on Microwave Theory and Techniques,* vol. 60, no. 10, pp. 3328-3338, Oct. 2012.

[26] B. Hraimel and X. Zhang, "Suppression of radio over fiber system nonlinearity using a semiconductor optical amplifier and mixed polarization," in *2013 Optical Fiber Communication Conference and Exposition and the National Fiber Optic Engineers Conference (OFC/NFOEC)*, Anaheim, CA, USA, 2013.

[27] K. K. Loi, J. H. Hodiak, X. B. Mei, C. W. Tu and W. S. C. Chang, "Linearization of 1.3-/spl mu/m MQW electroabsorption modulators using an all-optical frequency-insensitive technique," *IEEE Photonics Technology Letters,* vol. 10, no. 7, pp. 964-966, July 1998.

[28] Z. Wu, K. Xu, J. Niu, Q. Lv, Y. Dai and J. Lin, "Third-order intermodulation distortion improvement radio-over-fiber link using dual-wavelength intensity modulation," in *2012 4th International High Speed Intelligent Communication Forum*, Nanjing, Jiangsu, China, 2012.

[29] S. Saha, Analog pre-distortion circuit for simultaneous suppression of third and fifth order intermodulation distortion in broadband radio-over-fiber systems, Montreal, QC, Canada: Ma.Sc. Thesis, Dept. Elect. and Comp. Engi., Concordia Univ., 2016.

[30] R. B. Ellis and M. H. Capstick, "Feedback control of a linearised Mach-Zehnder modulator for SCM applications," in *IEEE MTT/ED/AP/LEO Societies Joint Chapter. United Kingdom and Republic of Ireland Section. 1996 2nd High Frequency Postgraduate Student Colloquium*, Manchester, United Kingdom, 1996.

[31] G. C. Wilson, T. H. Wood, M. Gans, J. L. Zyskind, J. W. Sulhoff, J. E. Johnson, T. Tanbun-Ek and P. A. Morton, "Predistortion of electroabsorption modulators for analog CATV systems at 1.55 μm," *Journal of Lightwave Technology,* vol. 15, no. 9, pp. 1654-1662, Sep. 1997.

[32] H. Matsubara, K. Ishihara, N. Miyadai and T. Nojima, "A novel 3rd-and-5th-order predistortion circuit for 2 GHz band W-CDMA amplifier," in *2007 Asia-Pacific Microwave Conference*, Bangkok, Thailand, Dec. 2007.

[33] A. Katz, R. Gray and R. Dorval, "Truly wideband linearization," *IEEE Microwave Magazine,* vol. 10, no. 7, pp. 20-27, Dec. 2009.

[34] Y. Shen, B. Hraimel, X. Zhang, G. E. R. Cowan, K. Wu and T. Liu, "A novel analog broadband RF predistortion circuit to linearize electro-absorption modulators in multiband OFDM radio-over-fiber systems," *IEEE Transactions on Microwave Theory and Techniques,* vol. 58, no. 11, pp. 3327-3335, 2010.

[35] A. Katz, J. Wood and D. chokola, "The evolution of PA linearization: from classic feedforward and feedback through analog and digital predistortion," *IEEE Microwave Magazine,* vol. 17, no. 2, pp. 32-40, Feb. 2016.

[36] J. S. Kenney and P. Fedorenko, "Identification of RF power amplifier memory effect origins using third-order intermodulation distortion amplitude and phase asymmetry," in *2006 IEEE MTT-S International Microwave Symposium Digest*, San Francisco, CA, USA, 2006.

[37] M. Schetzen, The Volterra and Wiener theories of nonlinear systems, New York, NY, USA: Wiley, 1980.

[38] D. R. Morgan, Z. Ma, J. Kim, M. G. Zierdt and J. Pastalan, "A generalized memory polynomial model for digital predistortion of RF power amplifiers," *IEEE Transactions on Signal Processing,* vol. 54, no. 10, pp. 3852-3860, 2006.

[39] S. Boyd, L. O. Chua and C. A. Desoer, "Analytical foundations of Volterra series," *IMA Journal of Mathematical Control and Information,* vol. 1, no. 3, pp. 243-282, 1984.

[40] L. Ding, T. G. Zhou, D. R. Morgan, Z. Ma, J. S. Kenney, J. Kim and C. R. Giardina, "Memory polynomial predistorter based on the indirect learning architecture," in *Global Telecommunications Conference, 2002. GLOBECOM '02. IEEE*, 2002.

[41] S. A. Bassam, M. Helaoui and F. M. Ghannouchi, "2-D digital predistortion (2-D-DPD) architecture for concurrent dual-band transmitters," *IEEE Transactions on Microwave Theory and Techniques,* vol. 29, no. 10, pp. 2547-2553, 2011.

[42] W. Tang, Envilope-assisted RF digital predistortion for broadband radio-over-fiber system with RF power amplifier, Montreal, QC, Canada: Ma.Sc. Thesis, Dept. Elect. and Comp. Engi., Concordia Univ., 2017.

[43] D. Psaltis, A. Sideris and A. A. Yamamura, "A multilayered neural network controller," *IEEE Control Systems Magazine,* vol. 8, no. 2, pp. 17-21, April 1988.

[44] Avago Technologies, "Avago HSCH-5314 Datasheet," [Online]. Available: http://www.avagotech.com/docs/AV01-0484EN.